HEAT TRANSFER BY CONVECTION

TO A MOVING BED

A thesis submitted to
The University of Aston in Birmingham
for the degree of
Doctor of Philosophy.

John Bernard Akers
Department of Chemical Engineering
January, 1967.

Summary

A critical review of the literature pertaining to melting and moving beds has been made. The amount of reliable information is shown to be limited. A general review of fixed bed heat transfer literature is also given to illustrate intraparticle temperature distribution and wall effects, and to indicate the different problems in fixed and moving bed heat transfer.

Following Ross's work (1) on melting beds of granular solids, an apparatus was designed and built as a tower melter. Experiments on this apparatus showed two heat transfer regions, the preheating and melting zones.

The preheating zone has been studied theoretically and experimentally as a moving bed. In the experimental studies, glass ballotini of 12 mm. and 6 mm. diameter, and $\frac{1}{2}$ inch alumina ceramic spheres were made to flow in a regular manner down 3 inch and 4 inch diameter columns, being supported by a bed of fine ballotini draining through an orifice. Gas flow rates of 268 to 3,608 lb/hr ft^2 have been used in conjunction with solids flow rates of 518 to 4,516 lb/hr ft^2.

Analysis of results showed that intraparticle temperature distribution is present to a significant degree. A theoretical model has been developed, and an analogue computer programme used to determine the gas film heat transfer coefficients. It is shown that Ross's suggested correlation of $h_g a$ with G_g/d_p does not take sufficient account of particle diameter. Correlation of the Nusselt number with modified Reynolds number is seen to be more satisfactory.

The problem of calculating the thermophysical properties of glass and alumina ceramic is considered in some detail and experimental values are shown to agree well with theoretical predictions.

TABLE OF CONTENTS

TABLE OF CONTENTS contd.

TABLE OF CONTENTS contd.

ACKNOWLEDGEMENTS

The author wishes to express his sincere thanks to the following:

Professor W.G.S. Parker, Head of the Chemistry Department, where this research began.

Professor G.V. Jeffreys, for his help and encouragement.

Dr. B. Gay, for his advice, encouragement and supervision.

Mr. N. Roberts and his technical staff for their help in workshop matters.

Miss J. Preston and Mr. W.D. Fowler, for their help in using the PDS 1020 and Hybrid TR48 computers.

Miss A.C. Berryman and Miss J.M. Morris for their diligent typing.

INTRODUCTION

Research by Ross (1) on the melting of granular solids stimulated this study of convection heating in a moving bed. Ross classified three methods of melting low melting point solids; namely, mix melting, contact melting, and convection melting.

Mix melting occurs in a continuous stirred vessel. Heating is provided by means of a heating jacket or coils. The melt in the heating vessel covers the heating jacket or coil, and granular solid is added at the same rate as the melting rate. Hixon and Baum (2) give a correlation between the heat transfer coefficient h and the relevant physical variables governing the heat transfer from melt to solid:

$$\frac{h_L d_v}{k_L} = 0.20 \left[\frac{N d_p^2 \rho_L}{\mu_L}\right]^{0.63} \left[\frac{C_L \mu_L}{k_L}\right]^{0.5} \quad \ldots\ldots\ldots 1$$

Good design practice decrees that the jacket or coil heat transfer coefficient should be much greater than the melt heat transfer coefficient. Therefore, the heat transfer coefficient as given by equation 1 is equal to:

$$h_L = \frac{\lambda + c_s (T_m - T_{si}) + C_L (T_L - T_m)}{A_s (T_L - T_m)} \quad \ldots\ldots\ldots 2$$

The vessel diameter and stirrer speed can be selected from equations 1 and 2.

With the vessel diameter and stirrer speed chosen, the heat transfer coefficient is determined for the vessel jacket or coil from equation 3 or 4, after the work of Chilton, Drew and Jebens (3).

$$\frac{h_j d_j}{k_L} = 0.36 \left[\frac{N d_j^2 \rho_L}{\mu_L}\right]^{0.66} \left[\frac{C_L \mu_L}{k_L}\right]^{0.33} \quad \ldots\ldots\ldots 3$$

$$\frac{h_c d_c}{k_L} = 0.87 \left[\frac{N d_c^2 \rho_L}{\mu_L}\right]^{0.63} \left[\frac{C_L \mu_L}{k_L}\right]^{0.33} \quad \ldots\ldots\ldots 4$$

The total jacket or coil area is now calculable, and hence the depth of melt in the vessel can be found. Ross (1) points out that mix melters have a high hold up of melt and a poor rate of melting.

Theoretical and experimental work by Ross (1, 4) has led to good correlation of contact melting results. Ross studied the feeding of low melting point granular solids under gravity or pressure against a hot surface. For an inclined plane contact surface, Ross expressed his results for the viscous flow of melt by the equation:

$$h_m = 0.667 \left[\frac{k_L^3 \rho_L g \lambda}{\mu_L}\right]^{0.25} \left[\frac{\left[1 + c_s/\lambda \ (T_m - T_{si}) \ \sigma + \rho_L \cos \phi\right]}{H \ (T_w - T_m)}\right]^{0.25} \quad \ldots\ldots\ldots 5$$

Similarly, for a tube bundle contact surface, Ross's equation is:

$$h_m = 0.710 \left[\frac{k_L^3 \rho_L g \lambda}{\mu_L}\right]^{0.25} \left[\frac{\left[1 + c_s/\lambda \ (T_m - T_{si}) \ \sigma + \rho_L\right]}{d_o \ (T_w - T_m)}\right]^{0.25} \quad \ldots\ldots\ldots 6$$

The heating side heat transfer coefficient is usually large enough for the melt film coefficient to be considered equal to the overall heat transfer coefficient. Whilst having the advantage of a low melt hold up, high temperatures of the hot surface can cause decomposition and discolouration of the melt.

Ross's work on convection melting led to a process in which a packed column of granular solids received convective heat transfer from hot air flowing through the bed. The experimental results of this work led Ross to conclude that convection melting was a more controllable and flexible method of melting than mix or contact melting.

Further work by Watson and Glen(5) and Glen (6) showed that forced convection melting could have significance where the rapid melting of metals was needed. Forced convection melting offered the advantage of high thermal efficiency and heat transfer coefficients together with rapid start up and shut down of operation. The process has possible uses in foundry work for example, where the conventional methods of melting lack high thermal efficiency and require longer periods of warm up and a large melt hold up.

Convection melting offers a new approach to melting, but a review in Section A of the work of Ross, Watson and Glen, and Glen suggests that further development of the process is necessary. Practical and academic problems of fluid flow and heat transfer pertaining to the process development present interesting topics for further investigation.

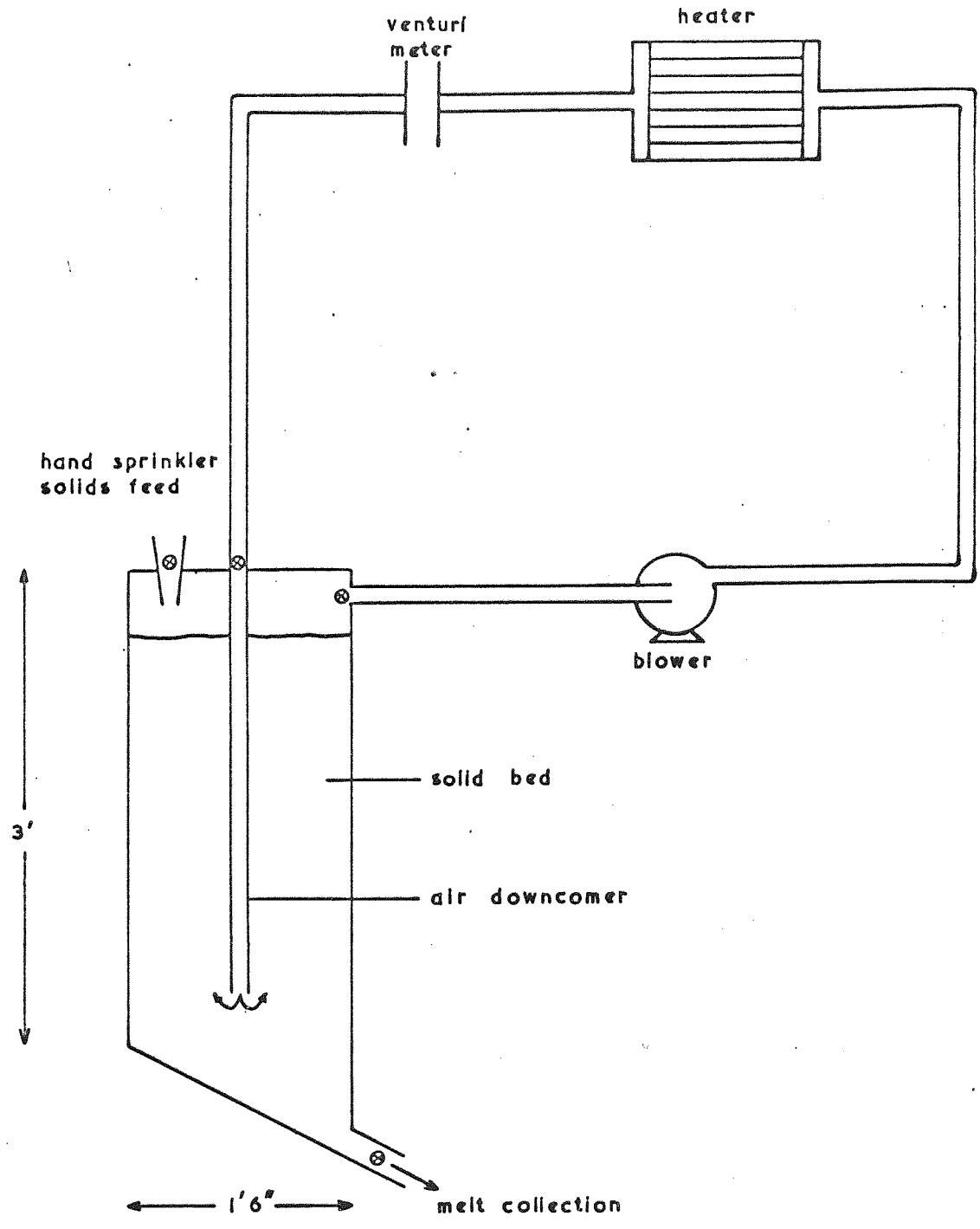

FIGURE 1. SIMPLIFIED DIAGRAM OF ROSS'S APPARATUS FOR THE MELTING OF GRANULAR SOLIDS BY FORCED CONVECTION.

Section A. Previous work on Melting Beds

(i) Low Melting Point Solids

Ross investigated the melting of organic solids by forced convection (1). Hot air was used to melt cubes and spheres of lauric acid, paraffin wax, phenol, cetyl alcohol and naphthalene. Fig. 1 shows the arrangement of Ross's apparatus.

Air was introduced to the bottom of the bed by a downcomer. Recirculation of air was used so that loss of solid through sublimation would be minimal. Solid was introduced into the bed by hand sprinkling to maintain constant bed height. The bed was charged with solid before heating began. Steady state inlet temperatures of gas and solid and exit temperatures of gas and melt were recorded. The overall heat transfer coefficient for the entire bed, Ua, was calculated as:

$$Ua = \frac{W\left[\lambda + c_s\ (T_m - T_{si})\right]}{A_x L\ \ (\Delta T_{g,s})_{l.m.}} \qquad \text{.....A 1}$$

By calculating the overall heat transfer coefficient on a logarithmic mean temperature difference basis, Ross assumed there was no temperature distribution in the particles. (see Section D)

The overall heat transfer coefficient is composed of the gas film and melt film heat transfer coefficients. The following approximation may be written:

$$\frac{1}{Ua} = \frac{1}{h_g a} + \frac{1}{h_m a} \qquad \text{.....A 2}$$

At low air flow rates and low melting rates Ross considered that the gas film heat transfer coefficient was controlling. In the range $10^2 < \frac{G_g}{d_p} < 10^4$ lb/hr. ft^2

Ross, therefore, correlated his experimental results by the equation:

$$h_g a = Ua = 0.15\left[\frac{G_g}{d_p}\right]^{0.66} \qquad \text{.....A 3}$$

assuming $h_m a$ is very much greater than $h_g a$.

For experimental results in the range $10^4 < \frac{G_g}{d_p} < 10^7$, equation A 3 did not correlate the results.

By plotting a logarithmic graph of overall heat transfer coefficient Ua against the ratio $\frac{G_g}{d_p}$, Ross noted that the results seemed to be approaching maxima. Before maxima could be reached, Ross suggested the beds would be fluidised.

Ross examined the relation between the gas and melt film heat transfer coefficients at the theoretical maximum overall heat transfer coefficient. He let both film transfer coefficients be represented by equations A 4 and A 5:

$$h_g a = C_1 (G_g)^x \qquad \text{.....A 4}$$

$$h_m a = C_2 (G_g)^{-y} \qquad \text{.....A 5}$$

where C_1 and C_2 are constants.

That is, the film transfer coefficients are dependent on the gas mass flow rate for a given solid gas system. Substituting into equation A 2 and finding the maximum value of Ua, that is $\frac{dUa}{dG} = 0$, Ross obtained equation A 6:

$$x\, h_m a = y h_g a \qquad \text{.....A 6}$$

By comparing the melting of particles to Nusselt's theory of condensing films on vertical surfaces (7,8), Ross (1) obtained a further relationship between the melt and melt film heat transfer coefficient. This is written:

$$h_m a = \left[\frac{k_L^3 \rho_L^2 g A_x a^4}{\mu_L W} \right]^{0.33} \qquad \text{.....A 7}$$

In steady state operation, the melting rate may be expressed by:

$$W = \frac{h_g a A_x L \ (\Delta T_g')_{l.m}}{\lambda + c_s (T_m - T_{si})} \qquad \text{.....A 8}$$

Combining equations A 7 and A 8:

$$h_m a = \left[\frac{k_L^3 \rho_L^2 g a^4 \left[\lambda + c_s (T_m - T_{si}) \right]}{h_g a \mu_L L \qquad (\Delta T_g')_{l.m.}} \right]^{0.33} \qquad \text{.....A 9}$$

or,

$$h_m a \propto (h_g a)^{-1/3} \qquad \text{.....A 10}$$

If equation A 3 is applied to the limit, then:

$$h_g a \propto G_g^{2/3} \qquad \text{.....A 11}$$

Therefore, equation A 10 becomes:

$$h_m a \propto G_g^{-2/9} \qquad \text{.....A 12}$$

Comparing equations A 11 and A 12 with A 4, A 5 and A 6, Ross obtained

$$3\, h_m a = h_g a \qquad \text{.....A 13}$$

Flooding of the column and serious bed displacement would occur well below values of G_g required for equation A 13 to apply. Therefore, Ross set an arbitrary limiting value of 80% of the value of the gas film coefficient, as predicted by equation A 3. Putting $(Ua)_{lim} = 0.8 h_g a$ into equation A 2:

$$h_m a = 4\, h_g a \qquad \text{.....A 14}$$

also

$$(\Delta T_g')_{l.m.} = 0.8\, (\Delta T_{g,s.})_{l.m.} \qquad \text{.....A 15}$$

Putting equations A 14 and A 15 into equation A 9:

$$Ua_{lim} = 0.299a \left[\frac{k_L^3 \rho_L^2\, g\, \lambda}{\mu_L} \right]^{0.25} \left[\frac{1 + c_s/\lambda\, (T_m - T_{si})}{L\, (\Delta T_{g,s})_{l.m.}} \right]^{0.25} \qquad \text{..... A 16}$$

The surface area was regarded as being inversely proportional to the mean diameter of the feed particles. The proportionality was evaluated from the experimental results to give the following correlation:

$$Ua_{lim} = 1.35 \left[\frac{k_L^3 \rho_L^2 g \lambda}{\mu_L}\right]^{0.25} \left[\frac{1 + c_s/\lambda \ (T_m - T_{si})}{d_p^4 L \ (\Delta T_{g,s})_{l.m.}}\right]^{0.25} \qquad \ldots\ldots A\ 17$$

Equation A 17 fits Ross's experimental data quite closely. The results do suggest that the theoretical exponent 0.25 may be slightly low.

Ross's theoretical approach to melting is supported by the work of Skelland on contact melting (9). Skelland considered earlier work by Ross (4) on contact melting of solids to Newtonian liquids. That is, the melting of solids against a hot inclined plane. A general mathematical theory of melting is developed by Skelland for non-Newtonian melts. This theory is based closely on Nusselt's theory of condensing films (7.8) but with several simplifying assumptions.

Skelland's general equation reduces to Ross's particular case for solid melting to Newtonian liquids on an inclined plane.. The equation due to Ross is:-

$$h_m = 0.667 \left[\frac{k_L^3 \rho_L \ g \ \lambda}{\mu_L}\right]^{0.25} \left[\frac{[1 + c_s/\lambda \ (T_m - T_{si})][\sigma + \rho_L \cos \phi]}{H \ (T_w - T_m)}\right]^{0.25} \qquad \ldots\ldots A\ 18$$

Equation A 18 was given as equation 5 in the introduction.

If, for convective heat transfer, $h_g a$ is eliminated from equation A 9 using equation equation A 13, we have:

$$h_m a = 0.760\, a \left[\frac{k_L^3 \rho_L^2 g \lambda}{\mu_L}\right]^{0.25} \left[\frac{1 + c_s/\lambda\ (T_m - T_{si})}{L\ (\Delta T_g')_{l.m.}}\right]^{0.25} \qquad \text{.....A 19}$$

The main difference between equations A 18 and A 19 is in the pressure gradient term σ. This term does not occur in Ross's convection analysis (1). The area term a is complex, and strictly should represent entirely vertical surfaces.

It is desirable to include the area term with the melt heat transfer coefficient in equation A 19 as Ross's final correlation given by equation A 17 includes a with the overall heat transfer coefficient.

It may be observed that Ross considered the entire bed to be the region of melting. This is only true for very short beds. A pre-heating zone and a melting zone have been visually observed both in the present research and in Glen's work. (6). The use of Ross's correlation as given by equation A 17 should be confined to the lower or melting region of the bed.

Equation A 17 may be criticised for its limited use, when $Ua = 0.8\, h_g a$. Ua would be better evaluated by substituting equations A 7 and A 3 into equation A 2. This would give the equation:

$$\frac{1}{Ua} = 0.667 \left[\frac{G_g}{d_p}\right]^{0.66} + \left[\frac{\mu_L G_L}{k_L^3 \rho_L^2 g a^4}\right]^{0.33} \qquad \text{.....A 20}$$

where $G_L = \frac{W}{A_x}$ = mass flow rate of melt

From experimental results the melting rate W would be known. Ua may be calculated from equation A 1 and compared to the value of Ua

calculated from the physical properties of the system as given by equation A 20.

Expressing a d_p by a constant, the constant can be evaluated by fitting experimental data to equation A 20. Ross did not compare the results for the cubic and spherical particles used in his experiments. The surface area for heat transfer is a function of the shape factor of the particles used. This relationship must be investigated further if the ultimate aim of melting solids of irregular shapes and sizes is to be achieved.

Criticism of Ross's method of introducing hot gas into the packed bed through a downcomer can be made. Firstly, some heat transfer from the walls of the downcomer to the packed bed is inevitable. Secondly, a downcomer causes difficulty in predicting hydrodynamic conditions from one apparatus to another. This has been demonstrated experimentally by Palmer (10) and Trollope (11) in studies of Oslo cooling crystallisers Introducing supersaturated liquor through a downcomer was found to create non-size classifying fluidised beds of crystals. This may be attributed in part to liquor flow pattern disturbances due to possible off centre positioning of the downcomer and vortices caused by a sudden 180° change of direction in liquor flow. Hot air inlet through a downcomer to the melting bed is therefore undesirable, as analysis of the problem becomes more complicated.

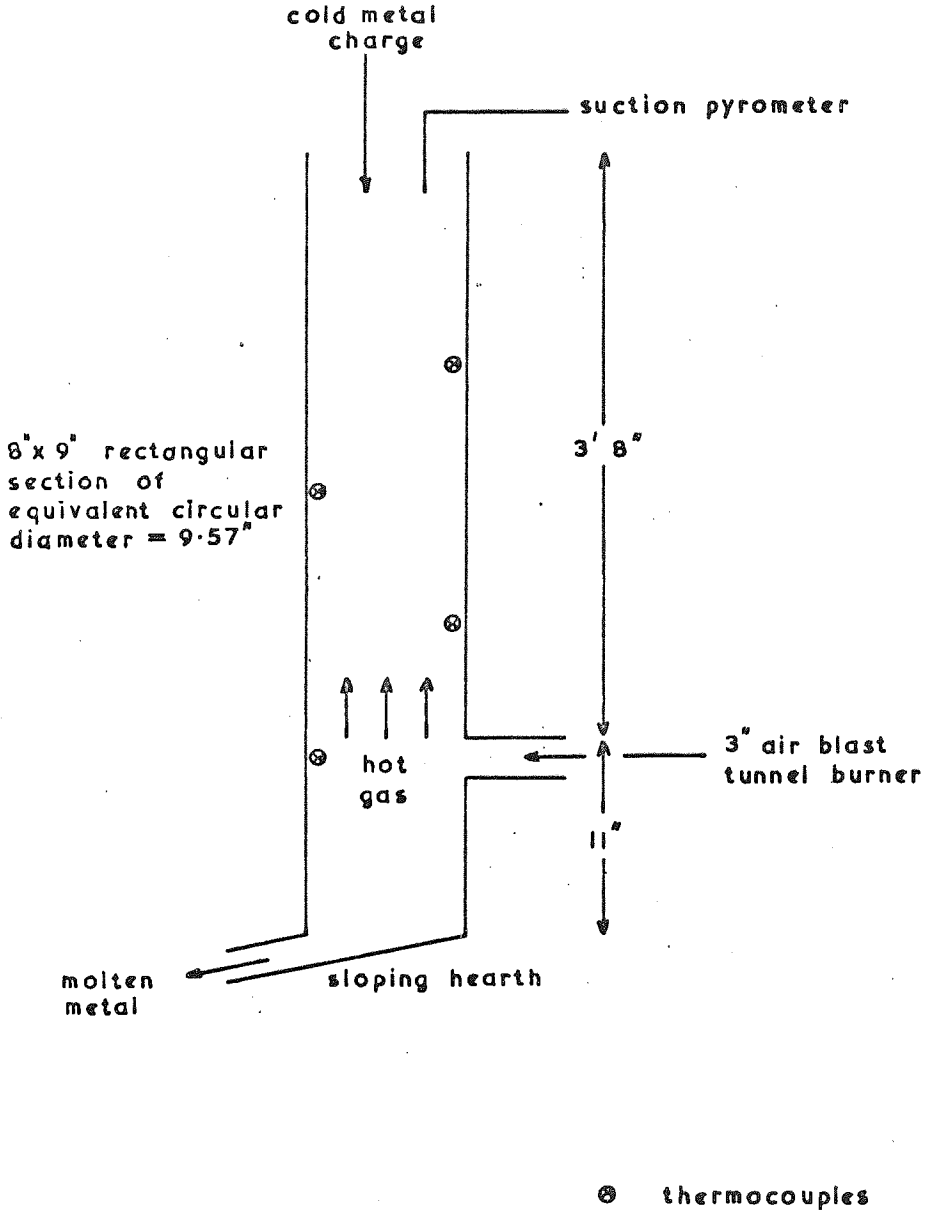

FIGURE 2. SIMPLIFIED DIAGRAM OF WATSON AND GLEN'S CONVECTION MELTING APPARATUS.

(ii) Melting of Metals

The interest of Watson and Glen (5) has been in the rapid melting of metals. In foundry work it is economically desirable to melt only the required amount of metal for casting processes. Melting larger amounts of metal can result in excessive surface oxidation of the metal due to prolonged contact with the atmosphere. It is also physiologically undesirable to have larger than necessary sources of heat in a place or work.

Watson and Glen report that the thermal efficiencies of conventional crucible and reverbatory furnaces are about 20% and 40% respectively. Experimental atmosphere controlled rapid melting furnaces, A.C.R.M.s, are also considered by Watson and Glen for rapid metal melting. In A.C.R.M. furnaces, a town gas-rich air mixture is burned in the furnace. The furnace atmosphere is controlled by additional air jets set up the height of the furnace wall. Watson and Glen report thermal efficiencies for A.C.R.M. furnaces of about 40%.

Watson and Glen carried out a comparative study of a radiation method and a forced convection method of melting. Figure 2 is a diagrammatic representation of Watson and Glen's convection melting apparatus. Three sizes of aluminium ingot were melted, having equivalent spherical diameters of 1.72, 2.96 and 3.56 inches. Hence furnace equivalent diameters to ingot equivalent diameters used were 5.57, 3.23 and 2.69.

Watson and Glen hoped to correlate their results by the commonly used relationship for convective heat transfer.

$$j_h = M\, Re_p^n \qquad \text{A 21}$$

Equation A 21 was re-expressed to give:

$$h_g \propto (\rho_g V_g)^{1+n}\, d_p^n \qquad \text{A 22}$$

The gas film heat transfer coefficient was calculated by Watson and Glen on a logarithmic mean temperature basis, that is, using equation A 1. The entire bed was assumed to be the melting zone.

Watson and Glen considered the melt film and solid metal to offer very little resistance to heat transfer because of the high thermal conductivities of liquid and solid aluminium. Therefore, the gas film heat transfer coefficient was equated to the overall heat transfer coefficient. The basis for calculating a, the specific surface for heat transfer was taken as the surface area of unmelted ingots per unit volume of bed. The results of Watson and Glen showed an appreciable scatter when plotted in the form of equation A 21. Watson and Glen concluded that the exponent n in equation A 22 was positive with respect to particle diameter. That is, increasing ingot size increases the heat transfer coefficient. The dependence of the heat transfer coefficient on the gas flow rate G_g was found to be approximately linear.

In a later paper (6) Glen used Watson and Glen's apparatus (5) shown in Figure 2 to melt copper ingots of equivalent spherical diameters 3.48 and 1.97 inches; that is, $\frac{d_v}{d_p}$ ratios of 3.48 and 1.97.

A second convection melter was built, having a 4 inch square cross-section. The equivalent diameter of the second furnace was, therefore, 4.51 inches. The bed height above the gas burner was 3 feet 8 inches, as in the first apparatus (5). Copper, brass and two sizes of aluminium ingots of equivalent spherical diameters 0.82, 0.80, 0.37 and 1.33 inches respectively were melted. The $\frac{d_v}{d_p}$ ratios were 5.50, 5.64, 12.20 and 3.39 respectively for the copper, brass and two sizes of aluminium ingots.

Glen divided the melting bed into preheating and melting zones. An approximate melting zone height of 4 inches was taken in all calculations for both melters for all runs. Watson and Glen's results were recalculated on the two zone basis and included in Glen's paper. A further correction was applied to the results of Watson and Glen, and Glen. Assuming a 2% heat loss from the column walls, it was assumed

that the remaining discrepancy in the thermal efficiency was due to gas escaping from the bottom of the column with the melt. The volume of gas going up the column was corrected accordingly. The gas flow rate used was calculated as the velocity of the products of combustion in the empty stack and ranged from 16,000 to 88,000 ft/hr. Gas exit temperatures ranged from 400 to 1,300°F. The flame temperature was about 3,200°F. Melting rates, given for Watson and Glen's results only (5), vary from 5.2 to 22.1 lb/min. of aluminium.

On the basis of equation A 21, Glen (6) correlated the experimental results for the preheater section by:

$$h_g = 0.00039\ V d_p^{0.2} + 1.18 \qquad \text{A 23}$$

Glen used the method of least mean squares to fit equation A 23 to the wide scatter of his results. Neglecting melt film resistance and temperature distribution in the ingots, the difference in heat transfer coefficients between the melting and preheating zones was attributed to an increase in the specific surface for heat transfer in the melting zone. For calculation, Glen's specific surface for heat transfer was the surface area of unmelted ingots per unit volume of bed for both melting and preheating zones.

Precise correlation of melting zone heat transfer coefficients was not possible for Watson and Glen (5) and Glen's (6) results. Glen plotted ingot equivalent diameter against γ, the ratio of the melting zone heat transfer coefficient to preheating zone heat transfer coefficient. A wide scatter of points was evident from the results, but Glen considered a curve could be drawn through the points.

Glen describes how a tower melter may be designed using his correlation of ingot equivalent diameter with the ratio of melting zone to preheating zone gas film heat transfer coefficients.

One explanation for the scatter and poor correlation of Watson and Glen, and Glen's results is the low ratio of equivalent stack diameter to equivalent ingot diameter $\frac{d_v}{d_p}$. As discussed in Section C. Denton (32,33)

found from expérimental results that increasing the ratio $\frac{d_v}{d_p}$ increased the heat transfer coefficient until a ratio of 17.5 was used.

Considerable deviations from the ideal uniform velocity and temperature profiles would occur across a horizontal plane in the column. This could mean gas by-passing through high void irregularities in the bed of ingots. High void irregularities occur mainly at the walls, hence the name, wall effects, which is given to such disturbances.

A temperature scan of the outlet gas across the top of the column could have been made by Watson and Glen, and Glen. This would have detected temperature irregularities due to wall effects and other high void irregularities. A suction pyrometer was used by Watson and Glen and Glen to measure outlet gas temperatures. No systematic gas outlet temperature irregularities due to high void irregularities were detected.

Radiation at the bottom of the column is considered by Watson and Glen, and Glen to be another factor contributing to poor correlation. Watson and Glen, and Glen suggest that at the flame temperatures used a significant amount of heat transfer occurs by radiation from the gas and column walls to the melting ingots. Decreasing heat transfer coefficients with increasing bed heights for otherwise similar runs were considered by Glen to be evidence of radiation at the bottom of the column.

Further criticism of the gas entry and melt outlet conditions can be made. With up to 15% of the inlet gas escaping through the melt outlet, a significant amount of very hot gas moves concurrently with the bed. It is a design feature of Watson and Glen's melter (5) that the non-melted ingots at the bottom of the melter and below the gas inlet help to reduce the amount of escaping gas.

For the purpose of theoretical analysis, the conditions at the base of Watson and Glen, and Glen's melters make the measurement of bed height unreliable. The melting zone was taken to be 4 inches high in all cases, whereas the distance from the bottom of the bed

to the burner was 11 inches in Watson and Glen's melter and 6 inches in Glen's later melter. It is incorrect to take the flame temperature as the gas inlet temperature for use in the logarithmic mean temperature distribution. This is because the gas escaping from the melt outlet will be at a lower temperature. The flame temperature is therefore too high for use in the logarithmic mean temperature distribution.

Glen states a figure of 2% for the heat lost from the column walls. This is an arbitrary average loss, but no calculation is submitted by Glen to substantiate the figure.

Glen tabulates the heat flow to the metal, heat lost in the flue gases, and heat lost from the walls and in the gas escaping through the melt outlet. This is apparently a complete heat balance but Glen's figures for each run show deficiencies of 7.7 to 1.1%. In an interim report on tower melters, Knight, Manuel, and Randle (12) present a specimen heat balance calculation exactly similar to Glen's (6). No deficiency is present in Knight et al's figures. There is no obvious explanation why Glen's heat balance deficiencies occur and no clue is given by the work of Knight et al. In a private communication, Glen was not able to offer an explanation for his heat balance deficiencies (13).

It is not possible to estimate here the true heat loss from the column walls in Glen's work (6) as no outside wall surface temperatures were measured by Glen. Watson and Glen indicate how the heat lost from the walls is used to calculate the heat lost by escaping gas from the melt outlet. Hence the gas flow rate up the column is calculated, knowing the heat transferred to the metal in heating and melting. Therefore, the heat lost from the column walls may have an appreciable effect on the gas flow rate used in correlating data.

The work of Watson and Glen, and Glen proves a very useful starting point for further development. It has not been the intention of the present work to develop convection melting of metals, but it will be useful to note certain interesting points that have arisen. Glen discovered from his experiments that the probability of the metal

charge sticking to the sides of the column was greater when the metal melted over a range of temperatures.

This problem of range of melting point will be met with alloys, and where ferrous metals are to be re-melted. Scrap iron together with runs of pig-iron from casting can represent a large proportion of the column's charge (5). Such a charge may soften considerably before melting. Watson and Glen suggest a tapered column to overcome such problems (5).

In the work of Knight et al (12) a slight taper was built into their aluminium melting tower. The tower had a circular cross section, approximately equal to that of Watson and Glen's apparatus (5). Aluminium ingots of approximately a 2 inch cube in shape and scrap castings of irregular shape were found to bridge across the column of Knight et al. Long ingots of approximately 2 x 2½ x 22 inches in size and scrap casting runners 5 to 7 inches long were found to move down the column quite readily. This suggests that tower melters for metal melting are limited in the charges that can be used.

Convection melting of metals was found by Watson and Glen, and Glen to be a flexible process. From ignition of the inlet gases to the commencement of melting depended on the heat input rate, but was of the order of 30 seconds. On stopping the supply of heat, Watson and Glen found melting continued for approximately one minute. A change in the heat input to the convection melter has, therefore, a quick response.

The degree of superheat, that is, temperature above the melting point of the metal, was low in Watson and Glen, and Glen's melter. Suspending the bed on a water-cooled grate or refractory lumps increased the superheat to between 100°C and 160°C.

Knight et al (12) found it preferable to add superheat to aluminium melt in an external crucible holding furnace. This method was found to reduce oxidation and slag formation. A similar apparatus was built for the melting and superheating of copper for use in continuous casting. In this apparatus a superheat chamber with additional gas burner was provided below the melt outlet. Pure copper could be superheated

from 1083°C to 1200°C with little oxidation by reducing the air to gas ratio below stoichiometric proportions.

Metal loss by oxidation and slag formation was found by Watson and Glen, and Glen to be somewhat more than desirable. Up to about 4% of metal could be lost by oxidation of the melt. This loss was more predominant for beds supported to give superheat. In an experimental run, using brass, zinc was found to be selectively oxidised.

Knight et al (12) found that metal oxidation was influenced by the burner position. In Watson and Glen's apparatus, Figure 2, the burner faced the melt outlet. Knight et al placed their burner diametrically opposite to Watson and Glen's burner. An additional small burner was placed near the bottom of the melt outlet. By this means the melt temperature was raised slightly, allowing the melt to run more freely. Knight et al claimed less oxidation and dissolution of gas in melt occurred because the melt and gas were in contact for a shorter period. Metal loss was reduced from 4% in Glen's apparatus (5) to less than 1%.

The quality of molten metal from a tower melter needs closer investigation. If a metal holding furnace has to be incorporated into a continuously operating tower melter for superheating or degassing purposes, the overall process efficiency will suffer. Knight et al suggest metal holding is desirable for intermittent use in casting. In this instance, a more controllable melt casting temperature is claimed.

Section B. Moving Bed Heat Transfer

It has been seen in Section A that the preheating zone of the tower melter has been considered solely by Glen (6). The correlation of Glen showed a first order dependence of the gas film heat transfer coefficient on the gas velocity. This is shown in equation B 1:

$$h_g = 0.00039\ V_g d_p^{0.2} + 1.18 \quad \text{.....B1}$$

This correlation has been fully discussed in Section A. Equation B1 is unsatisfactory for the present work, as high temperatures and void fractions were encountered in the work of Watson and Glen, and Glen. Radiation and wall effects therefore cause a wide scatter of results and make equation B1 suspect, even for the melting of large ingots of metal by forced convection in melters similar to those of Watson and Glen, and Glen (5,6)

Ross's work (1) on melting beds at low melting rates was seen in Section A to give the correlation:

$$h_g a = 0.15 \left[\frac{G_g}{d_p} \right]^{0.66} \quad \text{.....B2}$$

Ross equated the value of the gas film coefficient $h_g a$ given by equation B2 to the overall heat transfer coefficient in a bed at low melting rates over the range

$$10^2 < \frac{G_g}{d_p} < 10^4 \quad \text{lb/hrft}^2$$

Ross uses equation B2 to calculate gas film heat transfer coefficients for rapidly melting beds. Therefore, equation B2 is a relationship for heat trnasfer in the preheating zone of a tower melter. The specific area for

heat transfer can, by definition, be written:

$$a = \frac{6 A_x (1 - e)}{d_p} \qquad \text{.....B3}$$

Substitution into equation B2 gives:

$$h_g = \frac{0.025}{A_x (1 - e)} \; d_p^{0.33} \; G_g^{0.66} \qquad \text{.....B4}$$

Equation B 2 was found by Ross (1) to describe his results quite closely. It is partly the aim of the present work to discover from experimental work whether equation B 4 does describe heat transfer in the preheater zone.

One of the earliest papers relevant to the preheating section concerns pebble bed heaters (14). Norton was concerned with the heating or firing of refractory pellets in a moving bed heater. Only eight experiments were made using air, hydrogen, methane and steam as the gaseous phase, and $\frac{1}{2}$" and 5/16" pebbles as the solid phase. The results are shown in Table 1, Appendix 1. The overall heat transfer coefficients were calculated using the following equation:

$$U = \frac{Q}{a A_x L \Delta T_m} \qquad \text{.....B5}$$

Kilpatrick et al gave details (15, 16, 17) of the industrial use of a pebble bed heater for the thermal cracking of light hydrocarbons. A moving bed of pebbles was heated, using fuel gas burnt in a jacket round the vessel. The hot pebbles then passed into a reactor where n - butane or an ethan-propane mixture was cracked. The results of Kilpatrick et al are presented in terms of the yield of cracked gases.

Insufficient results are given to calculate heat transfer coefficients for the pebble bed heater. Due to the endothermic chemical reactions taking place in the reactor, its heat transfer analysis becomes much more difficult than for a simple moving bed.

Bowers and Reintjes (18) gave details of their work on the calcination of anthracite briquettes. In an attempt to derive general correlations for moving bed heat transfer, they included Norton's data with their results. Bowers and Reintjes expressed the j_h factor solely as a function of the Reynolds number, as shown in equation B 6:

$$j_h = \frac{h_g}{c_g G_g} \left[\frac{c_g \mu_g}{k_g} \right]^{2/3} = M \, Re_p^{-0.41} \qquad \text{.....B 6}$$

The Reynolds number exponent was taken from the work of Gamson et al (20) on heat and mass transfer between gases and solids in fixed beds. Gamson et al quote

$$M = 1.064 \quad \text{for} \quad Re > 350$$

Using equation B 6, Bowers and Reintjes tried to express the constant M as a function of particle diameter, gas mass flow rate and gas temperature. The results of Bowers and Reintjes, and Norton were described by equation B 7:

$$M = 0.54 \, d_p^{0.396} \qquad \text{.....B 7}$$

Equation B7 was taken to show that M was independent of G_g over the range

$$250 < G_g < 1{,}200 \text{ lb/hr.ft}^2$$

for gas temperatures between 900°F and 1000°F.

Norton's results (14), used to determine equation B 7, are shown in Appendix 1, Table 1 from 1 to 6. These results were at a mean gas inlet-outlet temperature of 1000°F.

The results of Bowers and Reintjes, shown in the same table as 9 and 10. were at 900°F. Norton's results for methane, at an average gas temperature of 1000°F (7 and 8 in Table 1) were not mentioned by Bowers and Reintjes. A further result, shown under 12 in Table 1, was used to derive equation B 7 and is credited to Norton by Bowers and Reintjes. No such result is evident in Norton's published results (14).

A repeat of the plot of Bowers and Reintjes, corresponding to equation B 7, has been made. The data plotted were those given in Table 1, results 1 to 11. M values for Norton's methane results (7 and 8) have been calculated, but M values calculated by Bowers and Reintjes have not been recalculated. The plot of these data are shown in Graph 1, Appendix 1. Bowers and Reintjes's plot of the same data does not shown results 1 to 3 or 6 to 8. Bowers and Reintjes did not consider result 11, presumably as it fell outside the limits specified for equation B 7, having a gas mass flow rate of 166 lb/hr.ft^2 and an average gas temperature of 600°F. It is evident from Graph 1 that Bowers and Reintjes'correlation of M with d_p should be treated with reservation.

The theoretical use of equation B 7 is questionable. No dependence of M on G_g is evident, and this may obscure the dependence of the heat transfer coefficient h_g on G_g. Substituting equation B 6 into B 7 we have:

$$h_g = 0.54 \frac{C_g^{1/3} k_g^{2/3}}{\mu^{0.25}} d_p^{-0.014} G_g^{0.59} \qquad \text{.....B 8}$$

Equation B 8 reveals little dependence of h_g on the particle diameter, and a dependence on the gas mass flow rate, as dictated by the work of Gamson et al.

A least mean squares analysis of the results used by Bowers and Reintjes (1 to 6, 9, 10 and 12 in Table 1 Appendix 1) shows:

$$h_g = 86.60 \, d_p^{-0.705} G_g^{-0.751} \qquad \text{.....B 9}$$

Equation B 9 may be compared directly with equation B 8. It is apparent that Bowers and Reintjes's treatment of the data does not take sufficient account of Norton's hydrogen results, i.e. results 5 and 6. This may be seen more clearly in Graph 2, Appendix 1. where h_g is plotted against G_g.

Bowers and Reintjes purport to show the effect of the gas mass flow rate using the data of Löf and Hawley (19) for fixed beds. These data should be considered in Section C, but are introduced in this section to develop the idea of the heat transfer coefficient being a function of gas mass flow rate and diameter. Löf and Hawley's data are given in Tables 2 to 5, Appendix 1. The heat transfer coefficients calculated by Löf and Hawley were on a volume basis, that is, $h_g a$. Using equation B 3, Löf and Hawley's heat transfer coefficients have been re-expressed on an area basis that is, h_g. For this case A_x equals 1.05 ft^2 in equation B 3.

Bowers and Reintjes appear to have recalculated the heat transfer coefficient on a similar basis. Their approximate values of the superficial area a are shown together with those used here for comparison in Tables 2 to 5. The calculations of Bower and Reintjes are neither accurate nor consistent. Only approximate values of the superficial areas used by Bowers and Reintjes can be estimated, and the ratio of their values to the ones calculated from equation B 3 are not consistent. The apparent value of a used by Bowers and Reintjes for results 18 and 19 in Table 5 is 85.0 ft^{-1}. Their calculated value of h_g for result 20 should be 3.43, not 3.81 Btu/hr.ft^2 ^oF.

Values of M against G_g as shown in Tables 2 to 5 were plotted by Bowers and Reintjes. These graphs are given as Graphs 3 and 4 in Appendix 1. Bowers and Reintjes's graph, equivalent to Graph 3, omits results 2, 3, and 13. The reason for this concerns the average gas temperature of the experiments. Results 2, 3 and 13 can be seen in Tables 2 and 3, Appendix 1, to vary from the majority of results at 150^oF. It is not clear how Bowers and Reintjes obtained their average gas temperatures, as Löf and Hawley give only gas inlet temperatures in their results. For this reason, all Löf and Hawley's results are replotted in the manner of Bowers and Reintjes.

It is not clear on what basis Bowers and Reintjes assume M tends to zero with G_g.

Gamson et al give the following equation to describe laminar flow conditions:

$$\frac{h_g}{c_g G_g}\left[\frac{c_g \mu_g}{k_s}\right]^{2/3}\left[\frac{d_p G_g}{\mu_g}\right] = M = 18.1 \qquad \ldots\ldots\ldots \text{B 10}$$

for Re < 40. This suggests that M tends to a non-zero value at low gas flow rates.

Graph 4 in Appendix 1 corresponds to Bowers and Reintjes's logarithmic plot of Graph 3. That is, the values of M and gas mass flow rates in Tables 2 to 5 are plotted on logarithmic coordinates. It is apparent that Bowers and Reintjes's correlating lines, shown on Graph 4, bear little relation to the points plotted. Their graph showed no plotted points only the correlating lines.

From Graph 4, Bowers and Reintjes derived the following general equation:

$$M = 0.66\, d_p^{0.25}\, G_g^{0.25} \qquad \ldots\ldots\ldots \text{B 11}$$

Eliminating M, using equation B 6:

$$h_g = 0.66\,\frac{c_g^{1/3}\, k_g^{2/3}}{\mu^{0.25}}\, d_p^{0.11}\, G_g^{0.84} \qquad \ldots\ldots\ldots \text{B 12}$$

For air at 200°F

$$h_g = 0.0592\, d_p^{0.11}\, G_g^{0.76} \qquad \ldots\ldots\ldots \text{B 13}$$

Löf and Hawley correlated their own results by the equation:

$$h_g a = 0.79 \left[\frac{G_g}{d_{(pv)}} \right]^{0.7} \qquad \text{.....B 14}$$

Using equation B 3, equation 14 may be rewritten

$$h_g = \frac{0.132}{A_x (1 - e)} \, d_{(pv)}^{0.3} \, G_g^{0.7} \qquad \text{.....B 15}$$

where $A_x = 1.05$

Least mean squares analysis of Löf and Halwey's results gives:

$$h_g = \frac{0.110}{A_x (1 - e)} \, d_{(pv)}^{0.289} \, G_g^{0.721} \qquad \text{..... B 16}$$

Results 7, 8 and 14 have been omitted from this analysis. Löf and Hawley considered these results to be in error and omitted them from the final correlation of results.

Equations B 11 and B 13 are less accurate descriptions of Löf and Hawley's results than their modified correlation, equation B 15. This comparison indicates that the data correlation of Bowers and Reintjes of heat transfer with the gas mass flow rate is inaccurate.

A comparison of equations B 16 and B 4, Ross's equation for slowly melting beds, is made in Section C.

Bowers and Reintjes present heat transfer data which purport to be calculated from the work of Kilpatrick et al (15, 16, 17). These data are given in Table 6 of Appendix 1, and apparently refer to the pebble heater, not the reactor. It will be recalled that, in the work of Kilpatrick et al, pebbles were heated in a jacketed vessel. No countercurrent flow of hot gas took place within the pebble heater. Kilpatrick et al give typical operating data for one run. Their data were incomplete and it is not understood how Bowers and Reintjes were able to calculate results for four runs, as given in Table 6.

An attempt was made by Bowers and Reintjes to relate M values to average gas temperatures at gas flow rates greater than 204.5 lb/hr.ft^2. They used their results, together with those of Norton (14), Löf and Hawley (19) and Kilpatrick et al (15, 16, 17). As Bowers and Reintjes's derivations of Löf and Hawley's average gas temperatures and Kilpatrick et al's results are questionable, this work of Bowers and Reintjes will not be considered further.

FIGURE 3. DIAGRAMS OF RAMASWAMY AND GERHARD'S APPARATUS (21)

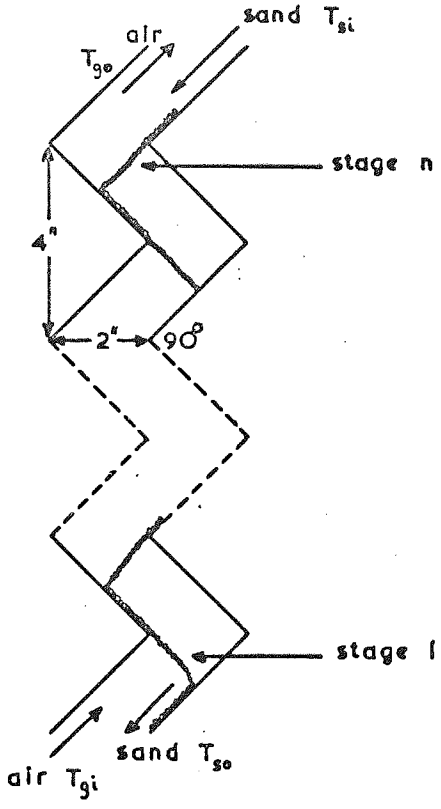

FIGURE 3A

Arrangement of stages.

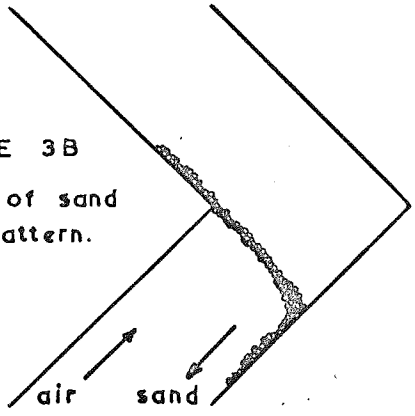

FIGURE 3B

Limits of sand flow pattern.

Low gas flow rate.

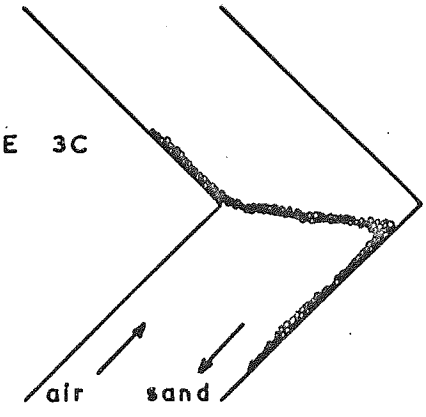

FIGURE 3C

High gas flow rate prior to solid transportation.

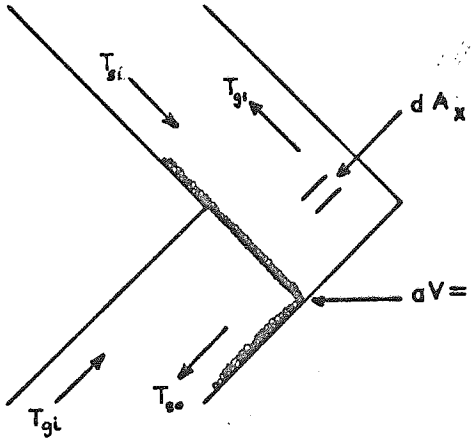

FIGURE 3D

First stage with symbols.

Gravity Flow Furnaces

Gravity flow furnaces are a class of moving bed heat exchanger, where solids fall rapidly under gravity. Forced convection heat transfer takes place between gas and solids due to countercurrent flow of hot air or the rapid movement of solids in stagnant gas.

Ramaswamy and Gerhard (21) have worked on a gas-granular solids heat transfer apparatus in which solids and hot gas pass countercurrently to each other in a zig-zag column. The arrangement is shown in Figure 3A. Heat is transferred from gas to solids in the cross-flow sections, as shown in Figures 3B, C and D. Resistance to heat transfer within the particles was considered negligible. Heat exchange was assumed to be negligible where the particles slide over the walls of the apparatus. The effect of the gas flow rate on the solids flow pattern is shown in Figures 3B and C. Referring to Figure 3D, for cross-sectional area of flow d A_x, the heat transfer model may be written mathematically as follows:

$$h_g(T_g - T_s)\, d\,(aV) = G_s c_s dT_s = G_g c_g dT_g \qquad \text{B 17}$$

where (aV) may be considered as the interfacial area for heat transfer per stage. Equation B 17 is rearranged by Ramaswamy and Gerhard to give:

$$aV = \int_0^{aV} d(aV) = \frac{G_s c_s}{h_g} \int_{T_{sl}}^{T_{so}} \frac{dT_s}{(T_{gi} - T_s)} \qquad \text{B 18}$$

The right hand side of equation B 18 was integrated with respect to solids temperature only. The gas outlet temperature was introduced through the heat balance for stage 1:

$$G_s c_s\, (T_{so} - T_{sl}) = G_g c_g\, (T_{gi}' - T_{gl}) \qquad \text{B 19}$$

By this means Ramaswamy and Gerhard obtained an equation for heat transfer over the first stage:

$$\frac{T_{gl} - T_{sl}}{T_{gi} - T_{so}} = \left[\left(1 - \frac{G_s c_s}{G_g c_g}\right) e^{\frac{haV}{G_s c_s}} + \frac{G_s c_s}{G_g c_g} \right] \qquad \text{B 20}$$

Hence for an apparatus of n stages:

$$\frac{T_{go} - T_{si}}{T_{gi} - T_{so}} = \left[\left(1 - \frac{G_s c_s}{G_g c_g}\right) e^{\frac{haV}{G_s c_s}} + \frac{G_s c_s}{G_g c_g} \right]^n \qquad \text{B 21}$$

Ramaswamy and Gerhard's analysis breaks down in the integration of equation B 18. For the integration of equation B 18 to be valid, Ramaswamy and Gerhard's model would have to be as follows. The sand phase would be mixed, and the gas phase at a unifrom temperature until it leaves the heat transfer zone. This model may be compared with that of a continuous stirred tank reactor, where the feed immediately assumes a constant temperature or concentration, equal to the outlet value, on entering the vessel.

A better model of Ramaswamy and Gerhard's heat transfer process is that of a crossflow heat exchanger. In this model it is more probable that the gas phase would be mixed, whilst the solids phase is unmixed. The general problem of cross-flow heat exchange with one mixed fluid has been mathematically analysed by Smith (22). As a result of his work, the following equation may be written for the first stage of the apparatus:

$$\left(\frac{T_{so} - T_{sl}}{T_{gl} - T_{sl}}\right) \ln \left[1 - \left(\frac{T_{gl} - T_{sl}}{T_{gi} - T_{so}}\right) \ln \left(\frac{T_{gi} - T_{sl}}{T_{so} - T_{sl}}\right) \right] = \frac{h_g aV}{G_s c_s} \qquad \text{B 22}$$

It is difficult to generalize equation B 22 to describe a process of n stages so that $h_g aV$ may be calculated from the inlet and outlet gas and solids temperatures. The problem is much more complicated than Ramaswamy and Gerhard's initial interpretation.

Ramaswamy and Gerhard plotted their heat transfer data from equation B 21 as $h_g aV$ against solids flow rate W lb/hr. Separate curves were obtained for several series of runs at one gas flow rate. Solids flow rates were in the range 50 to 300 lb/hr, for air rates of 60, 80, 100 and 120 lb/hr. Values of $h_g aV$ were calculated to be in the range 1 to 10 Btu/hr ^{o}F. No correlation is offered by Ramaswamy and Gerhard. Their data show $h_g aV$ to increase with gas and solids flow rate.

Some work has been done on heat transfer to particles by forced convection from furnace walls. That is, particles falling under gravity through stagnant gas. Johnstone, Pigford and Chapin (23) have developed Boussinesq's treatment (24) of heat transfer from a moving fluid to a submerged body. Johnstone et al (23) obtained the following general formula:

$$Nu = \sum_{o}^{n} \frac{1 + e^{-\pi b_i^2}}{1 + b_i^4} \qquad \text{B 23}$$

An overall heat transfer coefficient was calculated by Johnstone et al for the heating of particles in their furnace using a logarithmic mean temperature difference. After separating the heat transferred to the falling particles from the furnace walls by radiation, a forced convection heat transfer coefficient was calculated. Equation B 23 was found by Johnstone et al to agree with experimental heat transfer coefficients to within 20%.

As Reynolds number approaches zero, equation B 23 gives Nusselt number of 2. This value is in agreement with Frosling's well-known work on convective heat transfer to small spheres in quiescent fluids (25). At Peclet numbers greater than 200, equation B 23 was expressed more simply by:

$$h_g = 0.714 \sqrt{\frac{k_f V_s \rho_f c_g}{d_p}} \qquad \text{B 24}$$

or: $St = 0.714 \; Re_s^{-\frac{1}{2}} \; Pr^{-\frac{1}{2}}$ B 25

where $Re_s = \frac{d_p V_s \rho_g}{\mu_g}$

Adamski (26) has reported brief trials of gravity flow furnaces similar to those used by Johnstone et al (23). Adamski assumed a Biot number of unity to describe convectional heat transfer to solids in his furnace. The Biot number, $h_g \, d_p / k_s$ may be considered as the ratio of the thermal resistance to conduction inside and convection to a sphere. Knowing typical residence times of particles in the furnace, Adamski calculated the centre temperature of the solid particles. This was done using Gurney and Lurie charts (27) for unsteady state heat transfer to a sphere.

Adamski found from his calculations that the centre temperature of the particles reached 90% of the furnace temperature in fractions of a second. Therefore, temperature distribution in the particles was thought not present. One value of 18.62 Btu/hr ft^2 ^oF for a heat transfer coefficient is reported by Adamski. Adamski states neither the nature nor the diameter of the particles to which this heat transfer coefficient applies. It is not possible, therefore, to check Adamski's assumed value of unity for the Biot number.

Adamski's work is of limited value to the present study of moving bed heat transfer for two reasons. Firstly, no discussion of radiation effects on the total rate of heat transfer is made. Secondly, insufficient particle data are given to enable Adamski's results to be reworked and plotted in terms of Johnstone et al's equation B 24 for comparison purposes. Adamski does point out that materials of high thermal conductivity allow coarse-grained particles to be used without lowering the heat transfer rate. Under these conditions, temperature distribution in the falling particles is not significant.

FIGURE 4. SCHUMANN'S MODEL OF HEAT TRANSFER BETWEEN FLUID AND PARTICLES IN A PACKED BED (28)

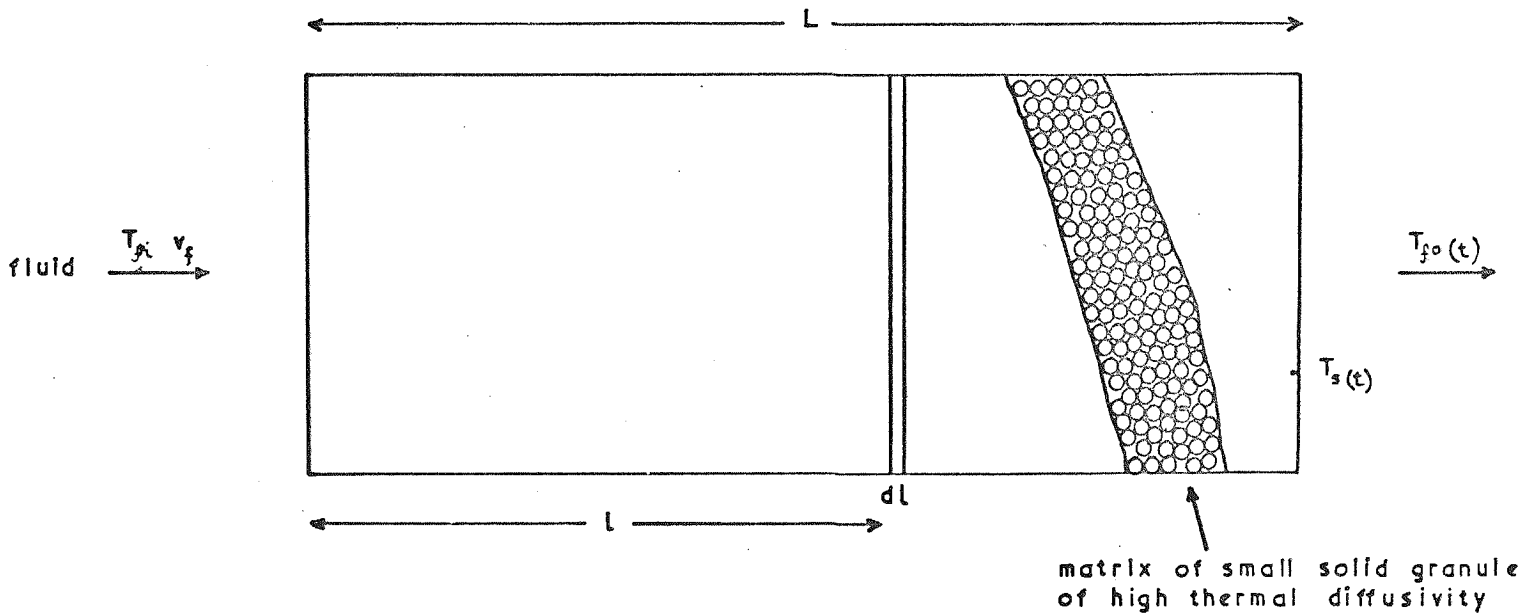

SECTION C Heat Transfer Between a Gas and Solids in a Packed Bed

(i) Single Blow Technique

Schumann (28) was one of the first research workers to attempt a mathematical treatment of heat transfer between a stationary packed bed and a fluid flowing through it. The problem is inherently one of unsteady states, and therefore will present a complex solution. Several assumptions were made by Schumann, as follows. Firstly, particles of solid were of high thermal diffusivity, that is, each particle was at a uniform temperature. Secondly, conduction of heat in the fluid or solid was small compared to the heat transferred by convection. Thirdly, changes in temperature produced negligible change in the thermophysical properties or volume of the fluid.

For the system shown in Figure 4, Schumann formulated the equations:

$$\frac{\partial T_f}{\partial t} + V_f \frac{\partial T_f}{\partial l} = \frac{h_f a (T_s - T_f)}{e \rho_f c_f} \qquad \text{.....C 1}$$

and

$$\frac{\partial T_s}{\partial t} = \left[\frac{h_f a}{c_s \rho_s (1 - e)} \right] (T_f - T_s) \qquad \text{.....C 2}$$

The necessary boundary conditions were:

$$\text{at } l = 0, \quad T_f = T_{fi} \quad \text{for all values of } T$$

$$T_s = T_{si} \quad \text{for } t = 0$$

$$\text{at } l = L, \quad T_s = T_{si} \quad \text{for } t = 0$$

Three dimensionless variables arose from Schumann's solution.
The dimensionless gas or solids temperature variable $\theta = \dfrac{T - T_{si}}{T_{fi} - T_{si}}$

Schumann's variable Y was $h_f a l / G_f c_f$.

The variable Z was $\dfrac{h_f a \ (t - l/v_f)}{c_s \rho_s \ (1 - e)}$ or $\dfrac{h_f a t}{c_s \rho'_s \ (1 - e)}$

as l/v_f is usually negligible.

Schumann's solutions to equations C 1 and C 2 which take the form of an infinite series of Bessel functions were represented by a series of sigmoidal curves of θ against Z with Y as parameter. Values of θ for fluid and solid were given on separate graphs. Schumann's work was intended to apply to liquid flow, as varying physical properties of air with large temperature changes are not accommodated in Schumann's solution. Nevertheless, Schumann's graphs have found application in the calculation of the gas film heat transfer coefficient $h_g a$ from a gas and solids temperature history of a packed bed subjected to a step change in the gas inlet temperature. This method is called the single blow technique.

Schumann's curves are for values of θ_s and θ_g from 0 to 1, and Y and Z values from 0 to 10. Young (29) recalculated Schumann's work by computer, and found that his curves were slightly in error. This may be attributed to the improved accuracy of Young's calculations. Furnas (30, 31), using a method of graphical integration to compute Schumann's series solution, has extended Schumann's curves up to a Y value of 500.

The usual technique for using Schumann's curves to determine the gas film heat transfer coefficient is as follows. The gas temperature history curve, θ_g against t, is plotted on tracing paper and compared to the shape of Schumann's curves. The heat transfer coefficient $h_g a$ is then estimated by interpolating the experimental Y value. This value of $h_g a$ should compare with the values given by the Z variable for the corresponding experimental time values of t. The advantage of this method of determining $h_g a$ is that gas-solids temperature differences are not measured. In the transient state, this measurement is difficult to make accurately.

Furnas (30, 31) was the first person to apply Schumann's curves to packed bed heat transfer. After determining the heat transfer coefficient $h_g a$ from Schumann's Y variable, Furnas used the Z variable to calculate the solid specific heat.

There are other limitations, of an experimental nature, to the work of Furnas. Furnas used beds of crushed iron ore, coke, coal and limestone. Particle sizes ranged from 0.4 to 7.3 cm. in beds of 15 and 23 cm. diameter. To overcome gas temperature measuring difficulties due to wall effects (32, 33), Furnas provided for inlet and outlet gas from the bed to pass through orifices. Whilst this arrangement allows for an average gas outlet temperature to be measured, serious inlet disturbances are caused. Saunders and Ford (34) point out that Furnas's gas inlet arrangement would cause non-uniform gas distribution at the bottom of the bed. Denton(32, 33) believed that Furnas's gas inlet distribution would tend to offset the errors due to wall effect.

A further criticism of Furnas's experimental work is made by Saunders and Ford. The columns used by Furnas were of "extra heavy pipe", having a greater heat capacity and thermal conductivity than the contained bed. The effect of high wall thermal conductivity on the wall temperature will be to closely follow the temperature response of the packed solid to the changing gas temperature. Such a response is necessary for unsteady state operation (11). The large wall heat content is undesirable, as a significant proportion of heat transferred from the gas is to the column walls. It is doubtful whether Furnas's results are applicable, except in the particular circumstances of his experiments.

Löf and Hawley (19) used Furnas's extension of Schumann's curves to determine their experimental results by the single blow technique. Their packed bed matrix was 3 feet long, and had approximately a square cross-section of area 0.77 ft^2. The matrix was contained in a well-lagged wooden box. Air inlets and outlets to the wooden box were through small pipes, in which multi-thermocouples were situated for temperature measurement. This arrangement is similar to that shown in Figure 4.

It has been shown in Section B that Löf and Hawley's results were described by the equation:

$$h_g = \frac{0.110}{A_x (1 - e)} \; d_{(pv)}^{0.289} \; G_g^{0.721} \qquad \text{.....C 3 and B 16}$$

Equation C 3 may be compared to Ross's equation (1).

$$h_g = \frac{0.025}{A_x (1 - e)} \; d_p^{0.33} \; G_g^{0.66} \qquad \text{.....C 4 and B 4}$$

There are several important differences between the work of Löf and Hawley, and Ross. The chief difference in Ross's bed was a moving and melting bed, whilst Löf and Hawley's bed was packed and stationary. It is not possible to infer how this difference will affect the two cases. An important difference lies in the definition of particle diameter. Ross (1) uses the ratio of particle volume to surface area, whilst Löf and Hawley use the expression:

$$d_{(pv)} = \sqrt[3]{\frac{6}{\pi}\left(\frac{\text{volume of particles}}{\text{number of particles}}\right)} \qquad \ldots\ldots\ldots C\ 5$$

It is not possible to draw any comparison between the two definitions of diameter without knowledge of Löf and Hawley's shape factor (35).

Coppage and London (36) make an additional criticism of Löf and Hawley's experiments. They believe that heat loss through the matrix wall may have been very high.

Perhaps the most important difference between the work of Ross and that of Löf and Hawley is in the measurement of heat transfer coefficient. It will be seen in Section D that moving bed heat transfer reduces to simple counter-current heat exchange for no intraparticle temperature distribution. This leads to calculation of the heat transfer coefficient using a logarithmic mean temperature distribution. Using the single blow technique with Schumann's curves is a very much more difficult problem, the accuracy of which is inherently questionable for large temperature changes.

Saunders and Ford (34) investigated experimentally the heating and cooling of fixed beds of lead, glass and steel spheres with air. Their work was carried out in beds of 2, 4, and 8 inches diameter, with a d_v/d_p ratio of 32. The single blow technique was used, but with an interesting modification to Schumann's curves. Schumann's z variable was

divided by

the Y variable to give the variable: $\frac{v_g}{\beta L} \frac{t}{(1 - e)}$. Curves of θ against this new variable were plotted for Y values from 4 to 500. Saunders and Ford's new variable was calculated form experimental results. Curves of θ_g against this new variable were plotted and compared to the corresponding Y values of Schumann's modified curves.

Saunders and Ford found the heat transfer coefficient h_g to be directly proportional to the gas velocity only. This is improbable. A possible reason for Saunders and Ford's unexpected result is their modification of Schumann's curves, which tends to bunch the curves together. This makes comparison of theoretical and experimental curves difficult. At values of Y about 4, comparison is good, but at values of 25, comparison is not close.

Saunders and Ford carried out a dimensional analysis of packed beds. The particle diameter was included in their analysis only to show the geometric similarity of different beds. Their analysis indicates that:

$$\frac{T_g - T_{si}}{T_{gi} - T_{si}} = f\left[\frac{V_g t c_g \rho_g}{d_p \; c_s \rho_s}, \frac{G_g c_g d_p}{k_s}, \frac{G_g c_g}{h_g}, \frac{L}{d_p}, \frac{d_v}{d_p}\right] \qquad \text{.....C 6}$$

Saunders and Ford stated that, for heat transfer between a fluid flowing in a tube and the tube walls, the following relationship may be written:

$$h \propto G_g^n \qquad \text{.....C 7}$$

where n lies between 0.8 and 1.0.

Assuming $n = 1$, Saunders and Ford wrote:

$$\frac{G_g c_g}{h_g} \propto (Re_p)^{1-n} Pr \qquad \text{.....C 8}$$

Using equation C 8, the heat transfer coefficient was eliminated from equation C 6. This analysis pre-supposes that experimental results will show the heat transfer coefficient to be directly proportional to the gas velocity.

It is of interest that Saunders and Ford found no difference in plots of θ_g against

$$\frac{V_g}{L} \qquad \frac{c_g \rho_g}{(1-e) c_s \rho_s}$$

for the heating and cooling of solids. Dimensional analysis led Saunders and Ford to believe that the group $\frac{G_g c_g d_p}{k_s}$ was the experimental variable that would indicate intraparticle temperature distribution. As a result of their experiments, Saunders and Ford ascribed an upper limit of 4 to their variable $\frac{G_g c_g d_p}{k_s}$. It is of interest to note that the Biot number $h_g d_p / k_s$ is more conventional in this context (27). Saunders and Ford could have come to this conclusion equally well from their dimensional analysis.

Coppage and London (36) have carried out fixed bed heat transfer by the single blow technique. The comparison between experimental and theoretical curves was accomplished by matching the maximum slope of the curves. Excellent correlation of experimental results was given by:

$$St = 0.738\ Re_p^{-0.31} \qquad C9$$

where $25 < Re_p < 550$

(ii) Cyclic Method

The measurement of heat transfer coefficients in fixed beds has been facilitated by the method of cyclic temperature variation. In this method, the inlet gas temperature is a sinusoidally varying function of time. Bell and Katz (37), Dayton et al (38), and Meek (39,40) have carried out extensive work in this field. They have shown that the solution of equations C1 and C2 can yield the heat transfer coefficient by measuring either attenuation or phase change between the inlet and outlet gas temperatures. The measurement of phase attenuation is more convenient than the temperature measurements of the single blow technique.

The cyclic method has another very important advantage over the single blow technique. Small variations of temperature fluctuations are necessary.

This obviates the difficulties of substantial changes in gas properties during the run. A criticism of the single blow technique is that it can only give an average value of heat transfer coefficient for a range of gas properties.

Dayton (38), Dingee and Chastain (41) evaluate the errors due to variations in gas velocity and longitudinal and axial gas mixing. Errors due to variations in heat transfer coefficient along the column axis were also assessed. Adjustments of gas temperature frequency variations readily minimise errors in the value of the heat transfer coefficient.

In Meek's published work (40) R. W. Bain has solved equations C1 and C2 for the case of intraparticle temperature distribution. Theoretical calculation shows that intraparticle temperature distribution becomes important at Biot numbers greater than 1.0. This problem will be discussed further, in relation to moving beds, in section D. Meek's results were not affected by this difficulty. It was noted that for fixed beds, increasing gas temperature frequencies would theoretically overcome problems of intra-particulate temperature distribution.

Meek eliminated wall effects from his matrix by setting each side of his square cross-sectional bed in epoxy-resin. It was concluded that low wall effects substantially increased Meek's heat transfer coefficient, as bypassing of gas was reduced. Meek also observed from his experiments that the packing arrangement of spheres in his matrix affected the heat transfer coefficient. Martin et al. (42) performed two separate friction factor experiemants, on one packing, with the gas flows at right angles. They report a wide separation of the two sets of results. As changing friction factor with gas flow rate closely parallels the Stanton number, $h_g/G_g c_g$, packing arrangement appears to have an effect on heat transfer beyond that measured simply by porosity.

(iii) Instrumentation of Individual Spheres

Denton (32,33) has carried out experiments on the convective heating of air passed through beds of glass spheres. Copper spheres of the same size as the glass spheres were distributed through the bed. Each copper test sphere generated its own heat by means of a small electrical element placed in the centre of the sphere. One junction of a thermocouple was soldered to the surface of a sphere, and the other junction suspended in the air stream.

Spheres adjacent to the test spheres were also heated, but were not instrumented for temperature measurement. By this means, air-solid temperature differences for the convective heating of air were made.

Point heat transfer coefficients over the entire surface of the sphere were found experimentally. These values were integrated over the surface area of the sphere to give a representative overall heat transfer coefficient. By this means, Denton concluded that wall effects were present in packed bed heat transfer until a $\frac{d_v}{d_p}$ ratio greater than 17.5 was used. Denton's results, for no wall effect, were described by the equation:

$$St = 0.72\ Re_p^{-0.30} \qquad C10$$

where $500 < Re_p < 53{,}000$

The close comparison between equations C9 and C10 must be noted.

Wadsworth (43,44) has made experiments similar to those of Denton. Wadsworth's work was mainly concerned with local variations in heat transfer coefficient for a single sphere in an extensive flowing fluid. A graph of overall Stanton number against Reynolds number was presented for a packed bed arrangement. Wadsworth's graph shows wall effect to reduce the overall heat transfer coefficient. No equation is presented by Wadsworth to describe his packed bed results. These results give heat transfer coefficients between 70% and 90% greater than those predicted by Denton's results, that is, equation C10. It is considered that heat transfer through point contact from the test copper sphere to adjacent unheated wooden spheres would cause elevated heat transfer coefficients to be measured.

An interesting point has been made by Rowe and Claxton (45), and Cornish (46), arising from the use of instrumented spheres. For a sphere being heated or cooled in infinite stagnant gas surroundings, the Nusselt number approaches a value of 2. This fact was mentioned in Section B (25). For the cooling of many spheres in an array, the heat sink is not infinite. This is the more usual practical case and it is expected that, under these conditions, the

Nusselt number would approach zero with the gas flow rate.

(iv) Mass Transfer Analogy

Gamson et al. (20) were the first researchers to investigate packed bed heat transfer using the heat transfer-mass transfer analogy. Their analogy was:

$$\frac{j_h}{j_d} = 1.08 \qquad \text{C11}$$

Experiments were made on the evaporation of moisture from particles in packed beds.

The following results were obtained:

$$j_h = 1.064\ Re_p^{-0.41} \qquad \text{C12 and B6}$$

for $Re_p > 350$

$$j_h = 18.1\ Re_p^{-1} \qquad \text{C13 and B10}$$

for $Re_p < 40$

Exactly similar experiments by Wilke and Hougen (47) give the equation:

$$j_h = 1.95\ Re_p^{-0.51} \qquad \text{C14}$$

for $40 < Re_p < 350$

The work of Gamson, and Wilke and Hougen suggests that there is a transition region of gas flow between particle Reynolds numbers of 40 to 350.

(v) General Correlation of Results

No attempt has been made here to compare in detail the results of different researchers. Denton (32) and Meek (39,40) have made extensive graphical comparisons of other results. In general, the results of Gamson et al. (20), Denton (32,33), Coppage and London (36), and Dayton et al. (38) are in fair agreement.

F. Yoshida (48) has compared a considerable amount of heat and mass transfer data to obtain the following general correlation:

$$j_h = 2.27\left(\frac{G_g d_p}{(1-e)\mu\psi_g}\right)^{-0.51} \psi \qquad C15$$

for $\left(\frac{G_g d_p}{(1-e)\mu\psi}\right) < 300$

and

$$j_h = 1.27\left(\frac{G_g d_p}{(1-e)\mu\psi_g}\right)^{-0.41} \psi \qquad C16$$

for $\left(\frac{G_g d_p}{(1-e)\mu\psi}\right) > 300$

where ψ is Gamson's empirical shape factor (35).

Equations C15 and C16 may be rewritten as :

$$h \propto G_g^{0.49}\left(\frac{d_p}{1-e}\right)^{-0.51} \qquad C17$$

and

$$h \propto G_g^{0.59}\left(\frac{d_p}{1-e}\right)^{-0.41} \qquad C18$$

Equations C17 and C18 do not compare closely to the equations of Löf and Hawley, C3, and Ross, C4. It is partly the intention of the present research to investigate further this discrepancy.

FIGURE 5. SCHEMATIC DIAGRAM OF A MOVING BED OF GRANULAR SOLIDS BEING HEATED BY GAS.

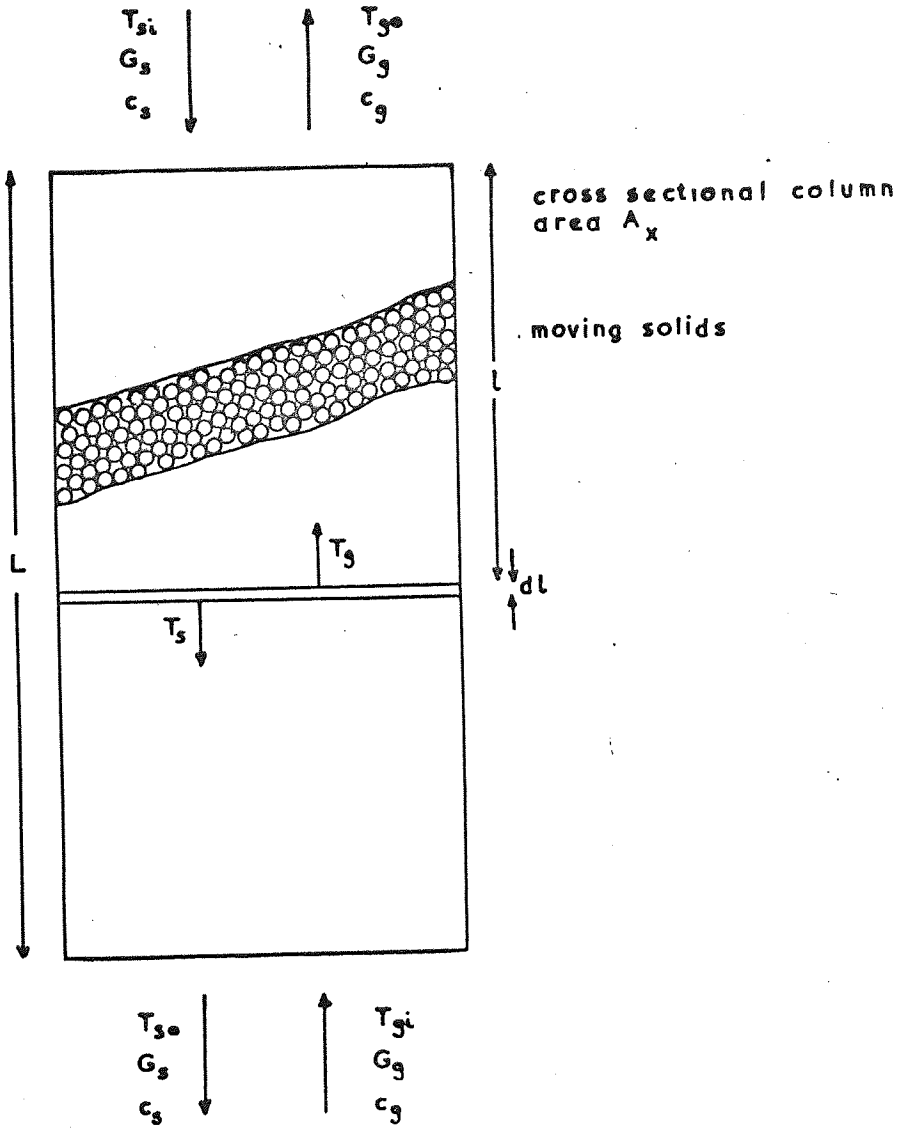

Section D. Theory.

(i) No Intraparticle Temperature Distribution in Moving Beds

Consider the moving bed shown in Figure 5. Granular solids, consisting of uniform spheres, enter at the top of the column. The solids addition is at a constant temperature and feed rate. Gas enters at the bottom of the column at constant temperature and flow rate. It is assumed that heat transfer takes place between the gas and solid only. That is, the bed is adiabatic. Further assumptions are that the gas has a uniform flat velocity profile, and that axial conduction and mixing are negligible. It is assumed in this analysis that there is no temperature distribution in the granular solids.

Over the element of column height, dl, heat balances for gas and solid are written:

$$G_g c_g A_x \frac{dT_g}{d\ell} - h_g a (T_g - T_s) = 0 \qquad D1$$

and $$G_s c_s A_x \frac{dT_s}{d\ell} - h_g a (T_g - T_s) = 0 \qquad D2$$

when $\ell = 0$, $T_g = T_{go}$ and $T_s = T_{si}$

and when $\ell = L$, $T_g = T_{gi}$ and $T_s = T_{so}$

Subtracting equation D2 from equation D1 and rearranging:

$$\int_{T_{gi}, T_{so}}^{T_{go}, T_{si}} \frac{d(T_g - T_s)}{T_g - T_s} = \int_0^L \frac{h_g a}{A_x} \left[\frac{1}{G_s c_s} - \frac{1}{G_g c_g}\right] \partial\ell \qquad D3$$

Integrating equation D3 gives:

$$\ln \left[\frac{T_{go} - T_{si}}{T_{gi} - T_{so}}\right] = \frac{h_g a L}{A_x G_g c_g} \left[\frac{1 - \beta}{\beta}\right] \qquad D4$$

By definition, $a = \dfrac{3 A_y (1-e)}{R_o}$ D5 and B3

Equation D4 becomes:

$$\ell n\left[\frac{T_{go} - T_{si}}{T_{gi} - T_{so}}\right] = \frac{h_g}{G_g c_g} \quad \frac{6(1-e)L}{d_p} \quad \left[\frac{1-\beta}{\beta}\right] \qquad \text{D6}$$

This is the usual expression for calculating the gas film heat transfer coefficient for steady state adiabatic counter-current or parallel flow heat exchanges. It is evident that constant heat capacities are required for equation D6 to hold true.

(ii) Previous Theoretical Work on Intraparticle Temperature Distribution in Moving Beds.

Where temperature distribution in the spheres is considered, the solution must be modified. Equation D2 is replaced by equation D7, in which the heat transferred from the gas by forced convection is equated to the heat conducted into the sphere:

$$-k_s \left(\frac{\partial T_s}{\partial r}\right)_{r = R_o} = h_g (T_s - T_g) \qquad \text{D7}$$

The equation for temperature distribution in a sphere being heated or cooled is:

$$\frac{\partial^2 T_s}{\partial r^2} + \frac{2}{r}\frac{\partial T_s}{\partial r} = \frac{c_s \rho_s}{k_s}\frac{\partial T_s}{\partial t} \qquad \text{D8}$$

It is convenient to change the time variable t by introducing the solids mass flow rate, G_s, and position in the column, ℓ:

$$G_s t = \ell \rho_s (1 - e) \qquad \text{D9}$$

Equation D8 becomes:

$$\frac{\partial^2 T_s}{\partial r^2} + \frac{2}{r}\frac{\partial T_s}{\partial r} = \frac{G_s c_s}{k_s (1-e)}\frac{\partial T_s}{\partial \ell} \qquad \text{D10}$$

It is required to solve equations D1, D7 and D10 for the following boundary conditions:

$\ell = 0$, $T_g = T_{go}$, and $T_s = T_{si}$

$\ell = L$, $T_g = T_{gi}$, and $T_s = T_{so}$

and $\left(\frac{\partial T_s}{\partial r}\right)_{r=0} = 0$ D11

Equation D11 is known as the sphere centre boundary condition. It is convenient at this point to let $\frac{k_s (1-e) \ell}{G_s c_s R_o^2}$ be a modified Fourier number, Fo_1.

Munro and Amundson (49) have solved equations D1, D7 and D10, so that the gas temperature at any position down a moving bed may be calculated, if the heat transfer coefficient is known. Their solution, for β not equal to 1, is:

$$\frac{T_g - T_{si}}{T_{go} - T_{si}} = 1 + 6\beta \sum_{n=1}^{n=\infty} \frac{1 - e^{-a_n^2 Fo_1}}{(3\beta + a_n^2/Bi)^2 - 3(3\beta + a_n^2/Bi) + a_n^2 (1+2/Bi)} \quad \text{D12}$$

For $\beta = 1$:

$$\frac{T_g - T_{si}}{T_{go} - T_{si}} = 1 + \frac{15\ Fo_1}{(1 + 5/Bi)}$$

$$+6 \sum_{n=1}^{n=\infty} \frac{1 - e^{-a_n^2 Fo_1}}{(3 + a_n^2/Bi)^2 - 3(3 + a_n^2/Bi) + a_n^2 (1+2/Bi)} \quad \text{D13}$$

The eigenvalues a_n in equations D12 and D 13 are given by the transcend--ental equation:

$$\left[(1-1/Bi)\ a_n^2 - 3\beta\right] \tan a_n + (3\beta + a_n^2/Bi)\ a_n = 0 \quad \text{D14}$$

It is apparent that Munro and Amundson's solution can not be used to calculate the heat transfer coefficient from the measurable variables of a moving bed. Equations D12 and D13 are difficult to apply, even when the heat transfer coefficient is known. Firstly, eigenvalues a_n have to be calculated from equation D14 and then substituted into equations D12 or D13 until the series converges.

Munro and Amundson extend their solution to cases involving the generation of heat in the granular solids. This is the case for the pebble bed hydrocarbon cracker of Kilpatrick et al. (15,16,17). Munro and Amundson's solution considers heat generation only as linear functions of time.

Leung and Quon (50) developed a numerical solution of equations D1, D7 and D10. Their solution is readily extended to cases involving non-linear generations of heat in moving beds. The partial differential equation D10 was reduced to an ordinary differential equation by finite difference approximations for the terms on the left hand side of equation D10. The finite difference approximations for discrete values of sphere radius were third-order correct. For this purpose, spheres were split into six increments. The difference equation corresponding to equation D10 was solved, together with equations D1 and D7, using the Runge-Kutta-Gill explicit finite difference method, by digital computation.

One advantage of Leung and Quon's (50) treatment over Munro and Amundson's analytical solution to moving bed heat transfer is that equation D14 is not solved for eigenvalues. The limitation of Leung and Quon's analysis, as with Munro and Amundson's, is that heat transfer coefficients cannot be calculated readily from the measured variables of a moving bed.

An analogue computer solution to equations D1, D7 and D10, is mentioned by Leung and Quon. There is no elaboration of this solution. The application of Leung and Quon's analyses to a problem where the solution may be calculated from Munro and Amundson's method is discussed in Part (iv) of this section.

FIGURE 6. CIRCUIT DIAGRAM FOR ANALOGUE COMPUTER SOLUTION OF UNSTEADY STATE HEAT TRANSFER TO A SPHERE.

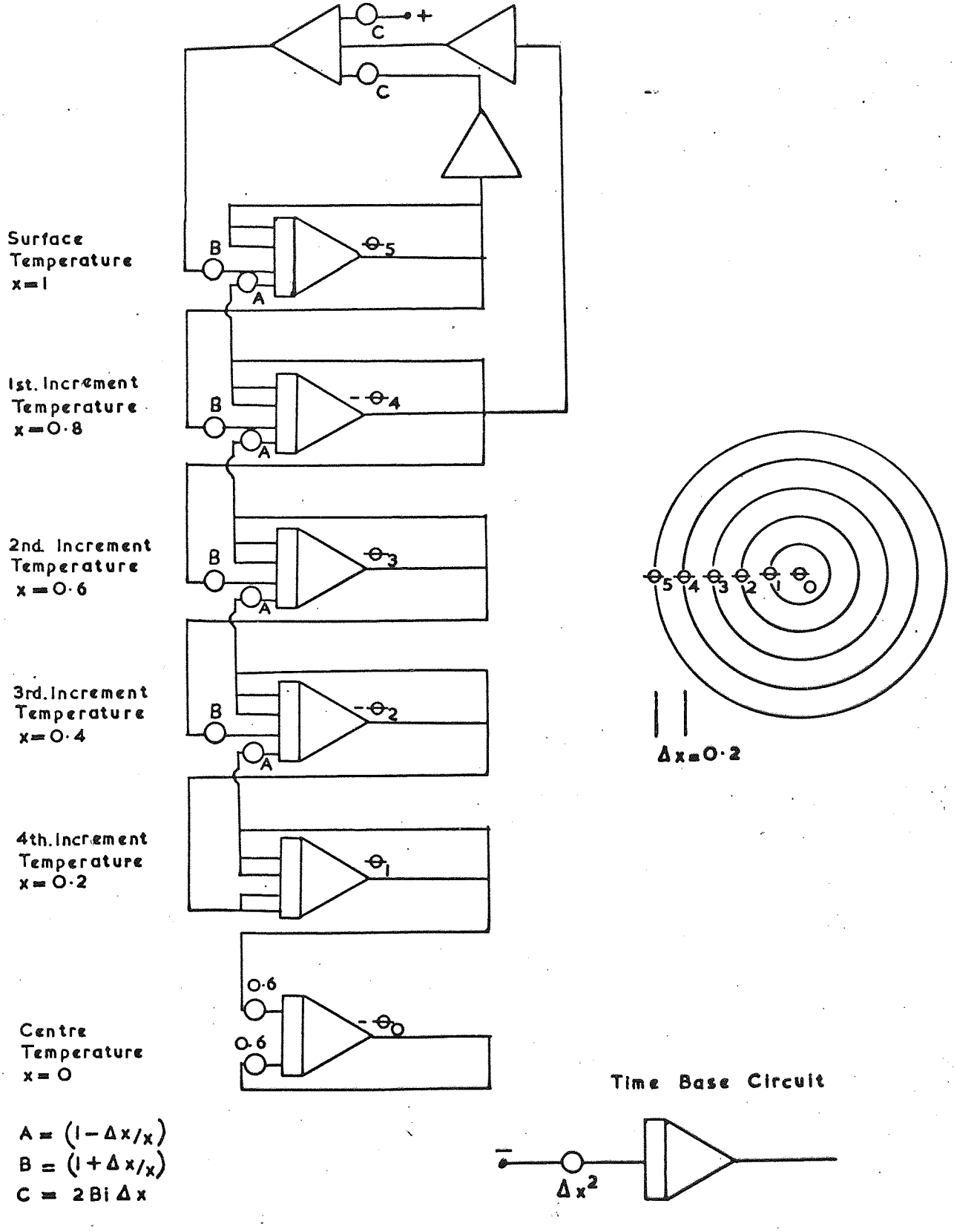

(iii) Calculation of Heat Transfer Coefficients for Intraparticle Temperature Distribution in Moving Bed Heat Transfer by Analogue Computation

It has been seen that no method exists for the calculation of gas film heat transfer coefficients where intraparticle temperature distribution is present. An analogue computer solution has been developed for this purpose. The development of this problem necessitated the solution of equation D8.

(a) Solution of heat transfer to a sphere by forced convection

It is convenient in an analogue computer solution to make equation D8 dimensionless. For a problem where the convective gas temperature is constant:

$$\frac{\partial^2 \theta_s}{\partial x^2} + \frac{2}{x}\frac{\partial \theta_s}{\partial x} = \frac{\partial \theta_s}{\partial \tau} \qquad \text{D15}$$

where $\theta_s = \dfrac{T_s - T_{si}}{T_g - T_{si}}$; $x = \dfrac{r}{R_o}$

and $\tau = \dfrac{k_s t}{c_s \rho_s R_o^2}$ = Fourier number.

Equation D15 is converted into ordinary differential form for analogue computer solution by means of finite difference substitutions. It is required to split the sphere into discrete spatial increments. This may be seen in Figure 6, where temperature nodes are coincident with spatial increments. Second order correct finite difference approximations were considered adequate for analogue computer accuracy. The necessary finite difference approximations for θ_s as a function of x may be derived from a Taylor expansion:

$$f'(x_n) = \frac{\partial \theta_s}{\partial x} = \frac{\theta_{n+1} - \theta_{n-1}}{2\Delta x} \qquad \text{D16}$$

$$\text{and } f''(x_n) = \frac{\partial^2 \theta_s}{\partial x^2} = \frac{\theta_{n+1} - 2\theta_n + \theta_{n-1}}{\Delta x^2} \qquad \text{D17}$$

where $\frac{1}{\Delta x}$ = number of spatial increments.

Substituting into equation D15:

$$\frac{\partial \theta_n}{\partial \tau} = \left[\left(1 + \frac{\Delta x}{x}\right) \theta_{n+1} - 2\theta_n + \left(1 - \frac{\Delta x}{x}\right) \theta_{n-1} \right] \Big/ \Delta x^2 \qquad \text{D18}$$

The initial values of equation D18 are:

$\tau = 0$, $\theta_s = \theta_{si} = 0$; $\theta_g = 1$.

The boundary conditions are:

(1) $$\left(\frac{\partial \theta_s}{\partial x}\right)_{x=0} = 0$$

(2) $$\left(\frac{\partial \theta_s}{\partial x}\right)_{x=1} = Bi\ (\theta_g - \theta_s) = Bi\ (1 - \theta_s),$$

that is, equation D7. Boundary condition (1) causes the second term in equation D15 to become indeterminate at the sphere centre. That is, $\frac{\partial \theta_s}{\partial x} \Big/ x = 0 \Big/ 0$. By L'Hôpital's rule, equation D15 becomes:

$$\frac{\partial^2 \theta_s}{\partial x^2} + \frac{2\partial^2 \theta_s}{\partial x^2} \Big/ 1 = \frac{\partial \theta_s}{\partial \tau} = 3 \frac{\partial^2 \theta_s}{\partial x^2} \qquad \text{D19}$$

Substituting D17 into D19:

$$\frac{\partial \theta_o}{\partial \tau} = 3 \left[\frac{\theta_1 - 2\theta_o + \theta_{-1}}{\Delta x^2} \right] = \frac{6\theta_1 - 6\theta_o}{\Delta x^2} \qquad \text{D20}$$

The surface boundary condition (2) generates an imaginary solids temperature θ_i when equation D16 is substituted into it. For a 5 - increment sphere problem (see Figure 6):

$$\frac{\theta_i - \theta_4}{2\Delta x} = Bi\ (\theta_g - \theta_5) \qquad D21$$

θ_i becomes θ_{n+1} in equation D18 when n = 5.

The circuit diagram for the analogue computer solution of equations D18, D20 and D21, is shown in Figure 6. A time-base circuit is required if the results are output to an X - Y plotter. It was found more convenient to follow the calculation on a digital voltmeter.

The problem requires no amplitude scaling, as the values of θ cannot exceed unity. Time scaling of the problem is effected by multiplying all integrator gains by the factor $1/\Delta x^2$. For a 5 - increment problem, $\Delta x = 0.2$, and the computation is slowed down by a factor of 25. If the time base potentiometer setting, also shown in Figure 6, is Δx^2, the computation takes $1/\Delta x^2$ seconds for τ to grow to unity. When the output of θ_s is by digital voltmeter, τ is recorded on an accurate stop-watch.

Calculations were made, assuming a Biot number of unity. This value was used because Meek (39,40) found intra-particle temperature distribution becoming important at a Biot number of unity.

To check the answers given by this solution to equation D15, the analytical solution was calculated. For the same initial and boundary conditions, the analytical solution may be written (51,52,53,54):

$$\theta_s = 1 - 2 \sum_{n=1}^{n=\infty} \left\{ \left[\frac{\sin a_n - a_n \cos a_n}{a_n - \sin a_n \cos a_n} \right] e^{-a_n^2 \tau} \frac{\sin a_n x}{a_n x} \right\} \qquad D22$$

The eigenvalues a_n are given by:

$$a_n = (1 - Bi) \tan a_n \qquad D23$$

FIGURE 7A. CIRCUIT DIAGRAM FOR THE ANALOGUE COMPUTER SOLUTION OF MOVING BED HEAT TRANSFER.

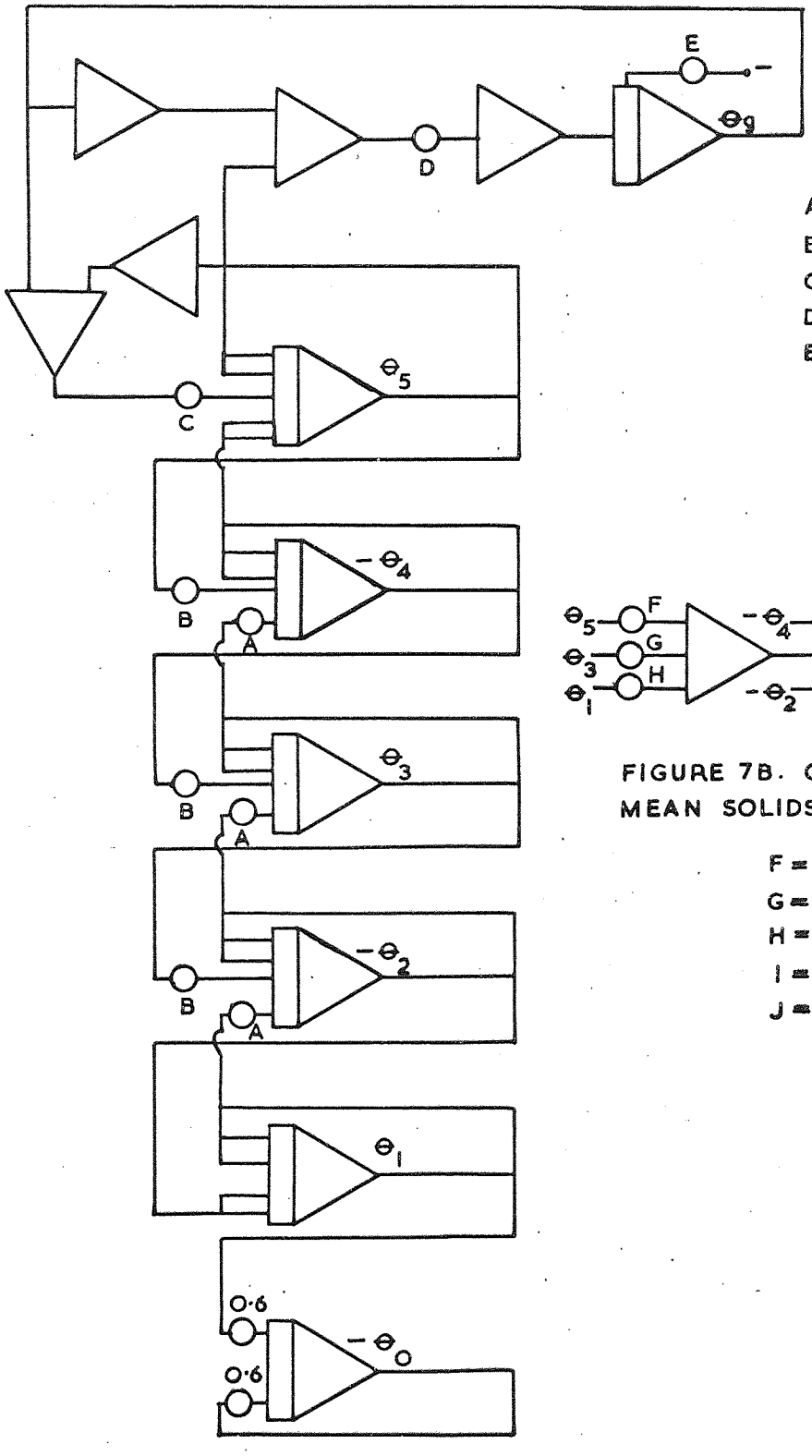

$A = (1 - \Delta x/x)$
$B = (1 + \Delta x/x)$
$C = 2Bi\,\Delta x\,(1 + \Delta x/x)$
$D = 3Bi\,\Delta x^2\beta$
$E = \theta_{go}$

FIGURE 7B. CALCULATION OF MEAN SOLIDS TEMPERATURE.

F = 0·198
G = 0·187
H = 0·031
I = 0·500
J = 0·083

Roots of equation D23 were found by Newton's method for Bi = 1. Five roots were required for the series in equation D22 to converge for values of τ equal to 0.1. Only two values of a were required when τ was greater than 1.0.

Calculations were carried out on a PDS 1020 computer. This machine is a small digital computer, with data input by keyboard or 8 - channel paper tape. Data output is by paper tape or typewriter. The programmes used to solve equations D22 and D23 are shown as Computer Programmes 1, 2 and 3 in Appendix 2.

Answers to the solution of equation D15 are given in Table 7 and Graphs 5 to 8, Appendix 2, where a comparison is made with Schneider's results (55). The analogue computer results were considered sufficiently accurate to proceed with the moving bed problem. Calculations were repeated using an 8 - increment spherical model. No significant improvement in accuracy was found.

(b) Analogue computer programme for moving bed heat transfer

Re-expressing equations D1 and D10, we have:

$$\frac{\partial \theta_g}{\partial z} = 3 \, Bi \, Fo_1 \, \beta \, (\theta_g - \theta_5) \qquad D24$$

and :

$$\frac{\partial^2 \theta_s}{\partial x^2} + \frac{2}{x} \frac{\partial \theta_s}{\partial x} = \frac{1}{Fo_1} \frac{\partial \theta_s}{\partial z} \qquad D25$$

where $z = \ell/L$.

It is apparent from equation D24 that the gas temperature θ_g as a function of column position z may be generated by electrical analogy. Using the sphere problem circuit as a base, the circuit diagram for the solution of moving bed heat transfer is shown in Figure 7A. The initial conditions are:

$$z = 0 \; ; \; \theta_g = \theta_{go} \; ; \; \theta_s = \theta_{si} = 0.$$

The computation proceeds until the final conditions are reached:

$$z = 1 \; ; \; \theta_g = \theta_{gi} = 1 \; ; \; \theta_s = \theta_{so}.$$

The computation is terminated when $\theta_g = 1$. Values of θ_g greater than unity have no significance to the problem. Using the time scaling constant $1/\Delta x^2$, the computation will have taken $\frac{k_s (1 - \varepsilon) L}{G_s c_s Ro^2 \Delta x^2}$ seconds of machine time.

The amplification of this analysis to calculate heat transfer coefficients will be discussed in part (v) of this section.

(iv) The Lovell and Karnofsky Problem.

Lovell and Karnofsky (56) gave an approximate solution to moving bed heat transfer, based on the Schmidt method (57) for unsteady state heat transfer to a slab. Lovell and Karnofsky's method of solution has been superseded by more accurate methods using computers; for example, Leung and Quon's analysis (50).

An interesting problem is stated by Lovell and Karnofsky: "Lime is calcined in a continuous countercurrent vertical lime kiln. $CaCO_3$ is fed from the top in 2" diameter pieces at a mass flow rate G_s of 2230 lb/hr ft^2. Gas rises through the bed at a mass flow rate, G_g, of 2500 lb/hr ft^2. If $CaCO_3$ is initially at 100°F and the flue gases leave at 200°F, at what level in the kiln is the gas temperature 400°F?"

Data:

c_g = 0.25 Btu/lb °F
c_s = 0.28 Btu/lb °F
k_s = 1.3 Btu/hr ft °F
h_g = 78 Btu/hr ft^2 °F
e = 0.5

The problem is to be treated as one of simple heat transfer.. Munro and Amundson(49), and Leung and Quon (50) have considered this problem. Their solutions will be compared to that given by the method proposed in part (iii) of this section.

Using the data given in Lovell and Karnofsky's problem, the following quantities are calculated:

$$\frac{G_s c_s}{G_g c_g} = \beta = 1,$$

$$Bi = \frac{h_g R_o}{k_s} = 5$$

The values for potentiometer settings C, D, and E, as shown in Figure 7A, were calculated:

Potentiometer C attenuation $= 2Bi\Delta x\ (1 + \Delta x/x) = 2.4$

Potentiometer D attenuation $= 3Bi\Delta x^2\beta = 0.6$

Potentiometer E attenuation $= \theta_{go} = 0.3333$

The results of the computation are shown in Table 8 and Graph 9, Appendix 2.

The calculated value of Fo_1, when θ_g was equal to 0.998, was 0.253. That is, a machine time of 6.33 seconds. Results for this computation were taken from an X - Y plotter, with a time base potentiometer attenuation of $\Delta x^2 = 0.04$.

The mean solids temperature was calculated to check that the problem fulfilled the heat balance. For a sphere, the mean solids temperature is given by:

$$\theta_m = \int_{x=0}^{x=1} \theta_s\, x^2 dx \qquad \text{.....D 26}$$

This calculation was made using a 6 - point closed end Newton-Coates quadrature (58). The analogue computer circuit to perform this calculation is shown in figure 7B. Writing the heat balance in dimensionless form:

$$(\theta_g - \theta_{go}) = \beta\,(\theta_s - \theta_{si}) \qquad \text{.....D 27}$$

The mean solids temperature θ_m checks with the gas temperature θ_g for all values of z. This is shown in Table 8B. The mean solids temperature, $\theta_m = 0.667$, corresponds to 300°F for a gas temperature of 400°F.

The results of this computation compare very favourably with those of Munro and Amundson, and Leung and Quon. This may be seen in Table 8A and Graph 9, Appendix 2. As Munro and Amundson did not tabulate the results of their calculations, equations D13 and D 14 were used to recompute their results. Leung and Quon state that their digital method took 28 minutes, and their analogue method less than 10 seconds. It is concluded, therefore, that the solution of this moving bed heat transfer problem by the analysis described in part (iii) of this section had an accuracy comparable to the analytical solution. Moreover, the analogue computer method was much simpler to apply than any method found in the literature.

To complete the calculation of Lovell and Karnofsky's problem, one may write:

$$\frac{k_s (1 - e)L}{G_s c_s R_o^2} = 0.253 = Fo_1$$

Inserting the data given in the problem, the length of bed is calculated as:

$$L = 1.69'$$

Munro and Amundson present a graph of their solution, and have to extrapolate their curve to obtain their answer. Their extrapolation is slightly in error, giving a bed length L of 1.63'.

(v) Proposed use of analogue computer method to calculate a moving bed gas film heat transfer coefficient

For the purposes of calculating a heat transfer coefficient, it is assumed that all the variables and constant measurements of the system are known. The only unknown is the heat transfer coefficient, which must be found by a process of trial and error.

A first approximation for the heat transfer coefficient may be found from equation D6. That is, an initial assumption that no resistance to heat transfer is provided by the particles. This first approximation will give a low value of heat transfer coefficient and Biot number. The value will be low because for a given heat flux, the gas-solid surface temperature difference will be smaller when intra-particle temperature distribution is present. This may be demonstrated by calculating the gas film heat transfer coefficient for Lovell and Karnofsky's problem from equation D 6.

When $\beta = 1$ as for Lovell and Karnofsky's problem, equation D 6 becomes indeterminate. This is a special case. By means of L' Hôpital's rule, equation D 6 may be written for $\beta = 1$:

$$\frac{1 - \theta_{go}}{\theta_{go}} = \frac{3h_g}{G_g c_g} \frac{L}{R_o} (1 - e) \qquad \text{.....D 28}$$

The gas film heat transfer coefficient is calculated to be 41.1 Btu/hr ft^2 ^oF for Lovell and Karnofsky's problem.

The technique for determining the gas film heat transfer coefficient will be to increase the Biot number, and compare the time of computation in seconds with that given by

$$\frac{k_s (1 - e) L}{G_s c_s R_o^2} \Big/ \Delta x^2$$

It will be seen in Section F that increasing the Biot number decreases the computation time. It will be appreciated that for a fixed θ_{go}, θ_m will be fixed by the heat balance, and will not vary with Biot number. The application of this technique to the present research work is discussed in Section F.

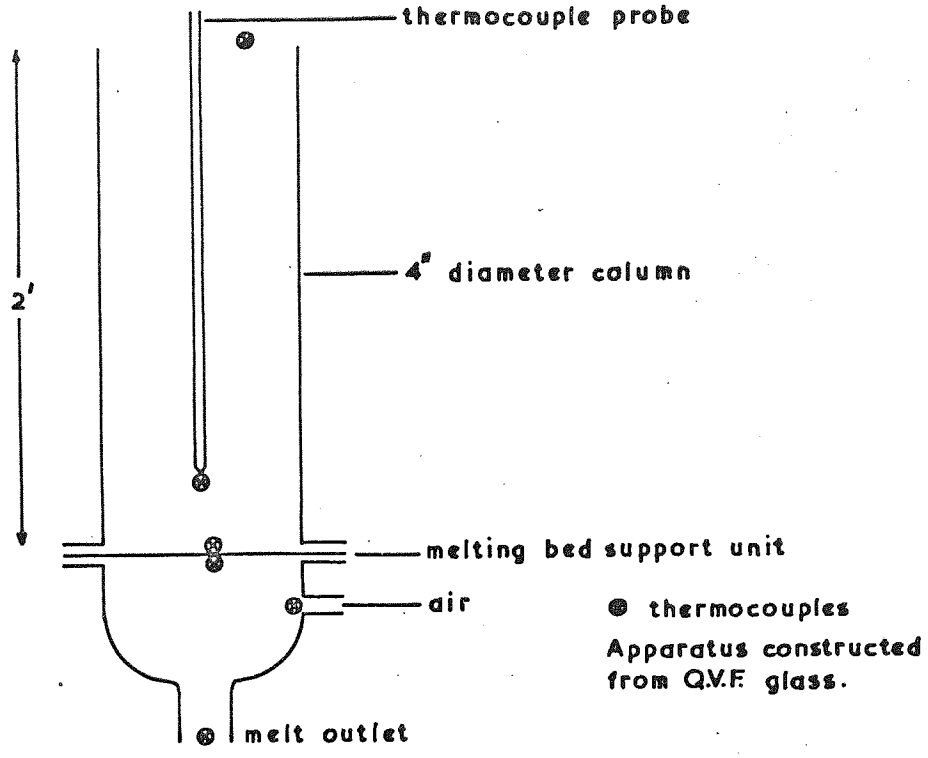

FIGURE 8A. DIAGRAMMATIC REPRESENTATION OF MELTING BED APPARATUS.

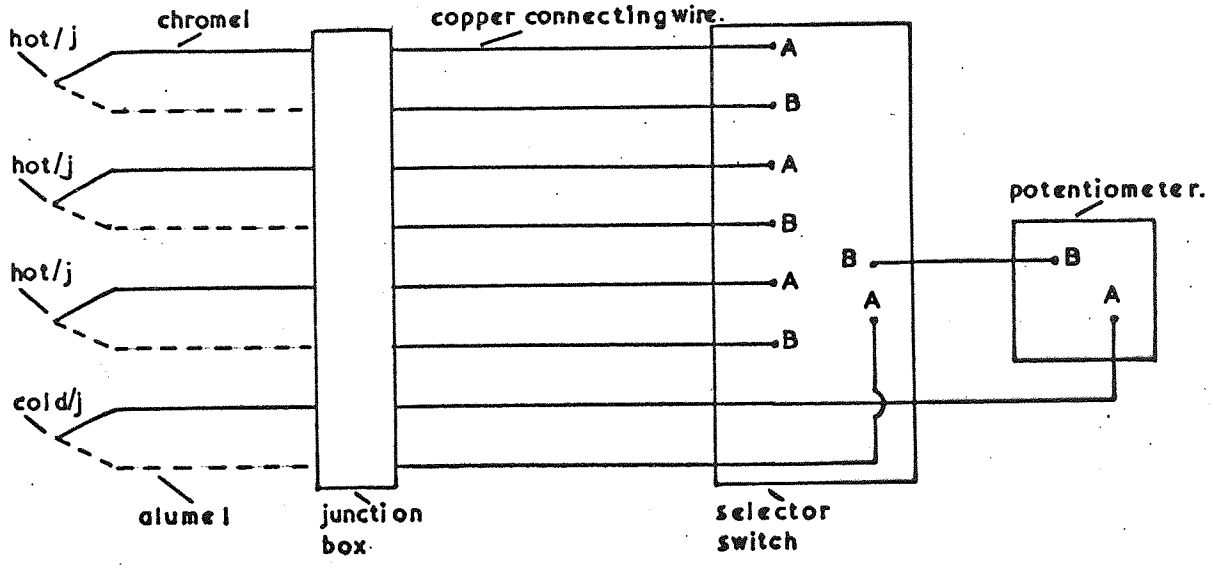

FIGURURE 8B. SIMPLIFIED THERMOCOUPLE DIAGRAM.

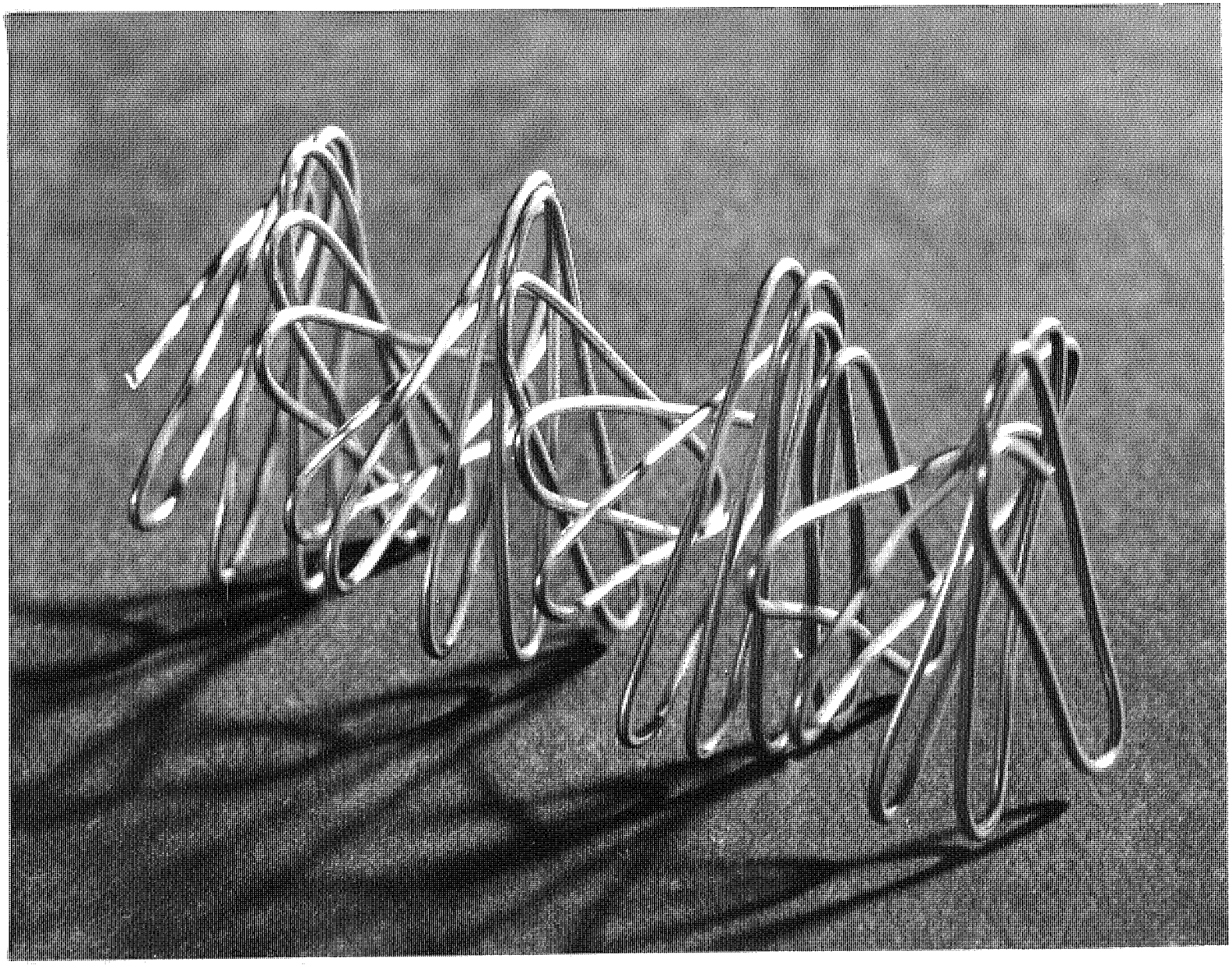

Plate 1 Heating Coil

SECTION E Experimental

(i) Melting Bed Apparatus

(a) Construction

The melting bed is shown diagrammatically in figure 8A. This apparatus was constructed from 4 inch diameter Q.V.F., with a column height of 2 feet. Air feed lines were of $1\frac{1}{2}$ inch diameter Q.V.F. The reason for using glassware for construction was to enable visual inspection of the melting bed to be made. That is, so that the division between melting and preheating zones might be detected.

The bed was supported on a stainless steel wire mesh. To ensure an effective air seal between the glass buttresses, the gauze was cast into a polyester resin annulus, reinforced with glass fibre strands. The bed support unit was cast on to a glass sheet so that a flat bottom surface was made. The top surface of the unit was made flat and parallel to the bottom surface by grinding on a revolving emery paper tape. The final unit had an internal diameter of 4 inches and was about $\frac{3}{8}$ inch thick.

Air heating was carried out electrically. Brightray C electrical heating wire (59) was wound on to an elliptical former. On drawing the wire off the former, the coils spiralled into what might be described as an ellipsoidal helix. A section of the coil is shown in Plate 1. This means of coiling the heating element provides an effective contact of air with the hot wire surface in a glass tube for a very low pressure drop (60).

The coil operating temperature should not exceed 500°C, the temperature at which borosilicate glass begins to soften. To ensure that 500°C was not exceeded, an electrical loading of 30 watts/inch^2 of wire was recommended for forced convection heating (61). In the absence of any available heat transfer coefficient data for the heating of air by electrical wires, the given loading was used in determining the dimensions of the coil wire.

The tower melter, for organic solids, was intended for use at temperatures of about 100°C. That is, an increase in temperature of about 80°C above ambient. Ross (1) does not state his maximum gas flow rate. It was calculated from Ross's graphs that his maximum air flow rate was about 800 lb/hr ft^2. An 80°C temperature rise for air in a 4 inch column requires a heat input of about 0.7 K.W. for an air flow rate of 800 lb/hr ft^2. An electric heater was made to have a power input of about 2.4 K.W. The high power rating was desired as the thermal efficiency of the electrical heater could not be estimated without experiment.

The electrical heater was constructed from about 55 feet of 19 S.W.G. Brightray C, to have an electrical resistance of 24 ohms. Heater control was effected through a variable transformer working from a 240 volt mains supply of electricity. Experiments have shown the heater to be more than 90% efficient.

FIGURE 9. AIR FLOW DIAGRAM.

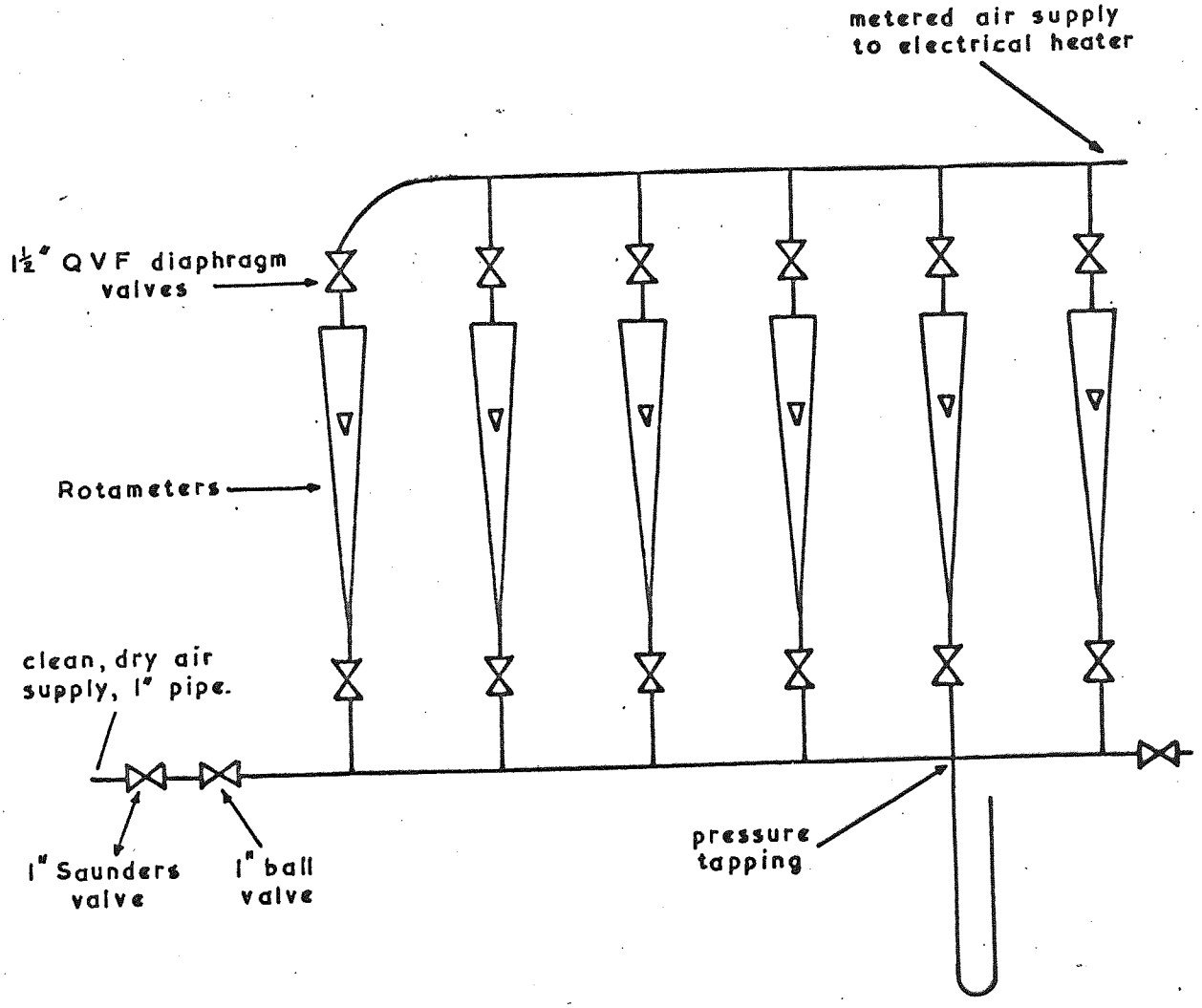

(b) Air Flow Rate Measurement

The gas supply was from an air compressor, having a maximum output of 200 ft^3/hr at 2 atmospheres pressure. The air flow rate was metered using a bank of rotameters in parallel. This is shown in Plate 2. Metric series rotameters 7, 14, 24, 35, 47 and 65 were used in conjunction with duralumin (A) floats. A Koranite float (K) was available also for rotameter 65.

Each rotameter could be separately isolated by 1½ inch bore Q.V.F. diaphragm valves upstream and downstream. Control of the flow rate was effected by a 1 inch bore Saunders diaphragm valve, upstream of the rotameter bank. It was not possible to control the air flow rate using Q.V.F. diaphragm valves, as an insufficiently long run of straight pipe was available between rotameters and valves. This caused the rotameter floats to rotate in a corkscrew manner, giving an elevated scale reading for the flow rate. A quick action ball valve was sited between the Saunders valve and the rotameter bank so that air could be turned on and off without readjustment of the flow rate, if required. A flow diagram of the apparatus is given in Figure 9.

Pressure measurement was made using a mercury U - tube. The pressure tapping was from a 5/16 inch glass tapping into a 1½ inch diameter Q.V.F. T - piece below the 47 rotameter. This arrangement was quite satisfactory. A T - piece was constructed out of 1½ inch bore copper, having three 1/16 inch pressure tappings upstream of the T stem. No difference in pressure measurement was found between the two T - pieces.

The Rotameter Manufacturing Company issue calibration charts for each rotameter. The charts show scale reading against flow rate at 76 cm. Hg and 15°C. To convert the flow rate at different operating pressures and temperatures, equation E 1 may be derived from the theoretical rotameter equation:

$$G_g = Q_F \sqrt{\frac{P_u}{76}} \left[\frac{288}{273 + T_g}\right] \left[\frac{0.17}{A_x}\right] \quad \text{lb/hr. ft}^2 \quad \ldots\ldots\text{E 1.}$$

A book of calibration data is also published by the Rotameter Manufacturing Company. This method of flow rate measurement gives the fluid flow rate Q under the operating or measured conditions. This involves a somewhat lengthy calculation. Firstly, the impedance of flow is calculated:

$$I = \log_{10} \left[K_1 \nu_f \frac{\sigma \rho_f}{\omega(\sigma - \rho_f)} \right] + 4 \quad \ldots\ldots\text{E 2.}$$

From theoretical charts of intensity against scale reading, values of f are interpolated linearly. Secondly, the fiducial flow F_T is calculated:

$$F_T = K_2 \sqrt{\frac{\omega (\sigma - \rho_f)}{\sigma \rho_f}} \quad \ldots\ldots\text{E 3.}$$

The flow rate Q at the operating conditions is given by the product $F_T f$.

A programme for the PDS 1020 computer was written so that G_g could be calculated directly for the 4 inch column. The programme, shown as Computer programme 4, Appendix 3, incorporates a calculation of ν_f and ρ_f for air under the operating conditions. The computer method of calculation very much simplifies the procedure for determining flow rates by this method.

To compare the accuracy of the two methods, an independent calibration was made with venturi meters. Two venturi meters accurately calibrated for flow rates from 0 to 8 and 0 to 50 $ft^3/min.$ at 60^oF and 30 inches w.g. were used in conjunction with inclined paraffin manometers. The comparison of this calibration with the rotameter calibration charts is shown in Graph 10, Table 8, Appendix 3.

No graphical comparison of flow rates calculated using equations E 2, E 3 and the f factor, with the venturi meter results, is made. Using B.S. 1042, the calibration of the venturi meters was calculated to be within the expected $\pm$ 3% tolerance. Rotameter flow rates compared closely, using equations E 2 and E 3, and were within the tolerance.

It was concluded that, for the 35 rotameter and larger rotameters, the calibration data gave more accurate results than the calibration charts. All air flow rate results presented in Section F were calculated by the calibration data method, using Computer programme 4.

(c) Temperature Measurement

The measurement of gas temperature is difficult. At high temperatures, the sensing element will receive heat by forced convection from the gas. Further heat transfer will occur by radiation to or from the containing walls of the system.

Gas temperatures encountered in experiments were of the order of 100°C. Gas velocities were relatively high, providing good convective heat transfer to the temperature sensing element. It was decided to use chromel-alumel thermocouples, with bare junctions exposed to the air stream. It was considered that radiation errors in temperature measurement by this method would be low because of the low temperatures encountered and the small area of the sensing element.

A diagrammatic representation of the thermocouple temperature recording circuit is given in Figure 8 B. It will be seen that this arrangement requires one cold junction only. To reduce the length of thermocouple wire between the temperature measurement position and the galvanometer, connections were made to single strand copper wire in a strip connector junction box. This box was thermally insulated with expanded polystyrene. This system ensures that the law of intermediate metals is obeyed, as the copper to thermocouple wire connections for hot and cold junctions are at the same temperature.

To ensure that no other spurious voltaic effects were present, the cold junction was sealed in a glass tube. As the cold junction was at the ice point, this was a necessary precaution to eliminate corrosion by water (63). Both hot and cold junction leads were electrically and thermally insulated with P.V.C. sheathing and brought side by side to the junction box and galvanometer. This reduces the possibility of the two wires from a thermocouple junction being at different temperatures.

Thermocouples were made by the method of electrical discharge. Comparison of thermocouple thermo-electric characteristics with those given for chromel-alumel thermocouples in B.S. 1827 showed the electrical discharge method to be a satisfactory method of making thermocouples. The probe thermocouple shown in Figure 8A was a proprietary mineral-insulated thermocouple of $\frac{1}{8}$ inch diameter. With the same cold junction thermocouple at the ice point, each hot junction thermocouple E.M.F. was measured at the ice point, the transition point of sodium sulphate decahydrate, and the boiling point of distilled water. The corresponding temperatures and E.M.Fs for chromel-alumel thermocouples are $0^{\circ}C$ and 0 m.v. ; $32.38^{\circ}C$ and 1.298 m.v. ; and $100^{\circ}C$ and 4.10 m.v. Each thermocouple was found to agree closely with the published results.

The measurement of thermocouple E.M.F. was made initially using a portable D.C. potentiometer; type P 3 by the Croydon Precision Instrument Company. This instrument enabled thermocouple E.M.F.s to be recorded to within 10 microvolts. In practice, it was found inconvenient to use this multipoint selector switch and potentiometer system as a high degree of dexterity was required to record temperatures and manipulate the melting bed.

Temperature measurement was made continuous, using a 16-point millivolt recorder by George Kent Limited. As thermocouple selection is automatic on a 2 minute cycle using the Kent recorder, modifications to the circuit diagram given in Figure 8B were required. The cold junction alumel lead was connected in parallel to the hot junction alumel leads at the junction box. Copper extension leads from the chromel leads of the cold junction and hot junctions were taken to the Kent recorder. The cold junction lead was connected in parallel to the negative terminals in the Kent recorder. Hot junction leads were connected to the positive terminals. To make use of all 16 points in the recorder cycle, hot junction leads may be connected in parallel in the Kent recorder.

Using a chart span of 0 to 3 m.v. with 0 or 50% zero suppression and a chart speed of 1 inch per minute, a point resolution of 0.01 m.v. or about $0.25^{\circ}C$ was possible. This accuracy was considered to be sufficiently high for the present experimental purposes.

(d) Manufacture of Granular Solids

To fill a 4 inch diameter column to a depth of 1 foot requires over 1,000 spheres of $\frac{1}{2}$ inch diameter, assuming a void fraction of about 0.4. A method of manufacturing large quantities of granular solids was therefore required.

Attempts at casting spheres of stearic acid using a split clay mould were unsuccessful. Spheres produced by this method were severely mis-shapen. To investigate the solidification of stearic acid further, a boiling tube containing stearic acid flakes was suspended in an oil bath at 90°C. The oil bath temperature was progressively reduced to room temperature over a period of 12 hours. It was found that large voids entered the stearic acid on shrinkage and solidification.

An attempt was made to manufacture spheres by barrelling. That is, pieces of stearic acid of irregular shape were placed into a cylindrical container, which was then rotated for a period of time. This method proved unsuccessful, as many hours were required to change the shape of the solids to a small degree. This method was considered of little value due to the length of time required and difficulty in producing uniformly sized solids. Inclusion of porcelain balls into the drum caused break-up of the solid.

Injection moulding was investigated to evaluate the plastic properties of stearic acid. This showed stearic acid to be insufficiently plastic on solidification to allow the manufacture of granular solids by injection moulding.

The only remaining method of granular solids manufacture is by pelleting. An evaluation of this method was attempted after the failure of other methods. The available pelleting machine was a 12 ton single impression horizontal hydraulic pelleter, manufactured by B.I.P.Engineering Limited. The machine was designed to shape phenolic resins into pellets of 1.1 inch diameter.

The principle of operation of the B.I.P.E.L. pelleter is as follows. The die is situated horizontally in a moving crosshead to which a powder hopper and reservoir are attached. A fixed punch projects into the powder reservoir. On the filling stroke, the crosshead moves towards the fixed punch, and a charge of powder is pushed into the die. The size of the powder charge may be changed experimentally by adjusting the hydraulic ram to alter the length of the moving punch. The distance between the fixed and moving punches governs the size of the powder charge admitted to the die, as the moving punch projects through the crosshead and die into the powder reservoir prior to the filling stroke.

After the die has been filled, the hydraulic ram exerts a pressure of up to 12 tons absolute on to the moving punch to compress the powder. The moving punch retreats to leave the pellet on the face of the fixed punch in the die. The crosshead and die then move further over the fixed punch, until the pellet is pushed out of the die. The pellet is then removed from the fixed punch face by an automatic doctor knife.

Using small spheres of pure stearic acid as representative of the fatty solids to be melted, pellets of 1.1 inch diameter were made. In general, the pellets were of a consistently high quality. Some tendency of the pellet to adhere to the moving punch was observed. This was attributable to blemishes on the punch face, as adhesion of pellet to punch was much reduced after polishing the punch face with jewellers' rouge.

It is necessary to reprocess the solid after melting into a pelletable form. Solid was broken up using a hammer mill. This was found to produce a powder containing lumps of up to $\frac{1}{4}$ inch diameter. It was found from experiment that unless a sieve fraction up to $\frac{1}{8}$ inch diameter was used, bridging of powder in the pelleter hopper occurred. The pellets made from solid reprocessed in the hammer mill were of a particulate consistency, coherent, but irregularly sized. Knacke and Pohl (64) state that the pellet strength decreases as the powder size increases . Jaffe and Foss (65) state that, apart from granular flow properties, the powder particle size has no bearing on its ability to form pellets. Visual observations of the present work tend to support Jaffe and Foss.

Figure 10.
Pellet Approximating To A 1/2 Inch Sphere.

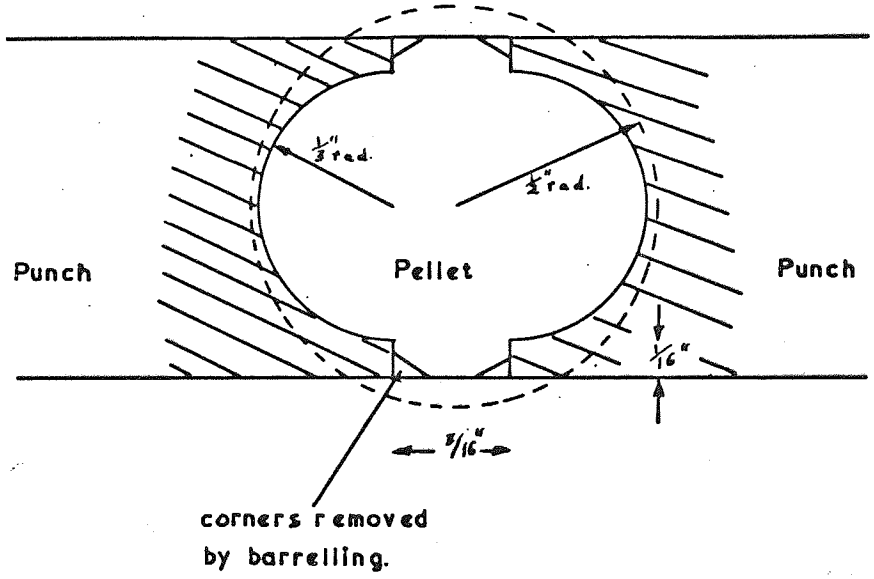

It was found from experiments that flakes of stearic acid flowed well in the hopper and produced agglomerate and cohesive particles. Entrained air in pellets was found to be about 3% by volume. A machine to produce flakes was developed from a machine designed to make milk flakes. It was necessary to operate the machine at atmospheric pressure, using cooling water in the rollers.

Bulk supplies of stearic acid and cetyl alcohol were obtained initially in flake form. Reprocessed flake pelleted well when warm, but produced pellets that did not cohere until cooled. It was discovered that stearic acid and cetyl alcohol flakes became moist when cooling in or simply exposed to open laboratory conditions. Slightly moist powder or flake caused irregular flow and eventual bridging of flow in the pelleter hopper, stopping the flow of powder or flake to the die. This is an unsatisfactory state, as irregularly sized pellets are produced, with the inevitable contact of the two punch faces when powder flow ceases. In consequence, reprocessed flake was hermetically sealed in polythene bags to cool.

It was considered that pelleting should be extended to the manufacture of spherical pellets. To make this type of pellet, the punch faces need to be deeply recessed. It is necessary to have the punch recess diameter less than the die diameter so that the punch tips are not excessively thin. The best pellet that may be made, approximating to a $\frac{1}{2}$ inch sphere, is shown in Figure 10. The sharp corners of the raised middle of the pellet may be smoothed down by barrelling.

Pelleting of stearic acid and similar fatty substances is not considered easy (66). The plate-like crystals of stearic acid are believed to be poor transmitters of radial energy. For this reason, the stearic acid exhibits poor flow properties at low compression, and does not form good tablets. Further difficulty is caused by internal strain in the pellets, produced by recessed punches (67). There is, therefore a tendency for pellets to fracture in a plane normal to the direction of compression. This has been found in the present experiments, and is more pronounced with so-called spherical pellets.

Using flakes, it was found experimentally that an operating pressure of about 2 tons absolute, for the $\frac{1}{2}$ inch spherical recessed punches, was the optimum operating pressure. Below that pressure, pellet fracture was common. Above 2 tons pressure, pelleting material extruded explosively between the punches and die. This extrusion tended to cause blockage of feed from the hopper to the die during subsequent pelleting cycles.

With pressures above 2 tons, further pellet fracture was caused by adhesion to the moving punch. The majority of the pellet remained in the die until pushed out by the die moving over the stationary punch. The pellet was not withdrawn entirely with the moving punch, as friction between the pellet and die was greater than the adhesion of the pellet to the moving punch.

Train (68) has observed from experiments that the transmission of a compressive force is lowest directly under the centre of the moving punch. Weak pellet bonding in this region, therefore, could be the cause of pellet capping; that is, part adhesion to the moving punch. Experiments have shown that when the adhered deposit on the moving punch builds up with repetitive pelleting, the deposit occasionally clears, becoming part of the pellet. This suggest that the region of low pressure transmission is no longer present.

A further difficulty was encountered in ejecting the pellet from the fixed punch recess. The doctor knife was not feasible, as the pellets fractured, being unable to escape from the recess. Various attempts at ejecting by attaching plastic and rubber cushioning materials to the doctor knife were unsuccessful. Whilst the pellet was released, it was prevented from falling free by the cushioning material on the ejector tip.

The doctor knife was replaced by an air jet. This was a good method of pellet ejection, as it removed the pellet rapidly. The major difficulty was excessive noise caused by the air jet impinging on the sharp edge of the stationary punch face.

It was decided to try to reduce the adhesion of the pellet to the punches so that a low pressure air jet ejector could be used. Silicones, such as Midland Silicone Releasil 7 and high vacuum grease, and I.C.I. Silicone fluid F111were successful for single compressions, but caused pellet contamination. Semi- permanent silicone preparations Releasils 86 and 2540 were used. These preparations required short curing periods at 100°C, using stannous octoate as catalyst. Some improvement was made in the number of pellets produced before the punch faces required further attention. The pelleter could operate for about 15 minutes. It was necessary then to disassemble and re-treat the punches. This represented a considerable expenditure of time for the production of relatively few pellets.

The recessed punch faces were coated with sintered P.T.F.E., a recognised non-stick surface. The sintered surface was apparently porous, as both stearic acid and cetyl alcohol compacted on to both punch faces. The P.T.F.E. coating came off the punch faces very quickly. Siegel et al (76) have used P.T.F.E. tipped punches, but found the tips permanently deformed under pressure.

Attempts were made to stick P.T.F.E. and polythene sheet to the $\frac{1}{2}$ inch flat-faced punches to make cylindrical pellets. The adhesives used were epoxy resin, various impact adhesives, and Midland Silicones Silastoseal A. It was not found possible to attach the edges of the sheet sufficiently strongly to the punch faces.

It has been observed by other workers (69, 70, 71) that the polar portions of long carbon-chain molecules, such as stearic acid and cetyl alcohol, adhere to metal surfaces. Strickland et al (72) observed that stearic acid, used as a lubricant to reduce pellet-die dynamic friction adheres strongly to metal surfaces.

In the pharmaceutical industry, when it is necessary to pellet difficult powders, it is usual to use punches tipped with phosphor bronze, having an amalgam on the pelleting faces (73, 74, 75). Punches with phosphor bronze tips were obtained in order to make ½ inch diameter spherical and cylindrical pellets. The flat-faced punches for cylindrical pellets were found to work very well. After a period of amalgam renewal, the phosphor bronze tips began to spread. This was undesirable as frequent disassembly of the pelleter was required to remachine the punch tips. The phosphor bronze tips of the recessed punches were unable to withstand the compressive forces applied during pelleting. The tip of the moving punch developed a slight crack, which encouraged a build-up of pelleting material.

It was considered that the amalgam presented a surface to which the polar portions of stearic acid and cetyl alcohol molecules did not adhere as easily as to the usual chromium-plated surface. The possible explanation for this is the low position of mercury in the electromotive series. Mercury will not readily form an oxide coating, as will the usual chromium-plated finish. The polar groups of the stearic acid and cetyl alcohol molecules may be expected to have less encouragement, therefore, to adhere to the punch faces.

The chromium plating on the original recessed ½ inch punches was removed by caustic soda solution, and the punches were copper-plated. Using an amalgam on the polished copper-plated faces of the punches proved to be an improvement over any other method that had been tried. The copper plating softened with continued renewal of amalgam and eventually came off the punch faces. The next logical step was to plate the punch faces with silver, which is lower than mercury in the electromotive series. The silver plated finish was poor, and came off the punch faces after about two hours of use.

This is the extent to which the pelleting of stearic acid and cetyl alcohol has been devleoped. Little and Mitchell(77) give a recipe for the convenient pelleting of stearic acid, using various inorganic binding materials. A pellet produced in this way would have unknown thermo-physical properties, would leave a solid residue on melting, and would be, therefore, of no value to the present research. About 1 cwt. each of stearic acid and cetyl alcohol have been passed through the B.I.P.E.L. pelleter. It is considered, after this work, that the use of silver plated punches with a smooth coherent finish, may be the best method of pelleting stearic acid and cetyl alcohol for the present purposes.

(e) Operation of the Melting Bed

The hot air supply was fed from the electrical heater to the empty column for several minutes. Mis-shapen pellets were fed by hand onto the bed support grid, as shown in Figure 8A. The pellets were added slowly, care being taken to ensure that the column walls were not hot enough to melt them. When melting is started in a warm column, it is essential that pellets must not melt due to heat transferred from the column walls, and then re-solidify as the column walls approach their steady state temperature. This warm start-up procedure was an attempt to reach equilibrium more quickly. Mis-shapen pellets were used in these initial stages due to the shortage of pellets caused by their time consuming manufacture. As equilibrium was reached, shown by steady temperature records, the column was filled to a height of 2 feet with pellets of acceptable shape.

The pool of melt at the melt outlet was maintained, using a Q.V.F. stop-cock valve for intermittent melt pool volume control. A pool of melt was considered to be an effective way of sealing the melt outlet against escaping gas. Solidification of melt invariably occurred in the valve, making this method of control unsatisfactory. A better procedure was found to be a swan's neck syphon outlet, to maintain a head of melt, and balance the column air inlet pressure against atmospheric pressure. By this means, a more constant discharge of melt is obtained. Solidification of melt in the syphon tube was overcome using a Bunsen burner flame. An improvement would be to use an electrical heating coil round the syphon tube outlet.

Considerable difficulty was found in maintaining movement of solid down the bed. This was attributed at first to excessive heat loss at the column walls, causing solidification of melt and the development of bridging across the bed. Frequent rodding down of the bed was required. Heating tape was wound round the column in an attempt to balance the heat loss and leave the contents of the bed visible through the column walls. This was unsuccessful, as the solids flow was not improved, and a thermocouple probe in the centre of the bed reflected a heat input from the heating tape through the column walls. The method of heat loss calculation from the column walls is indicated in Part (ii,b) of this

section.

The division between melting and preheating zones was readily visible through the column walls. It was observed also that the height of the preheating zone tended to increase as the experiment progressed. The thermocouple probe indicated temperatures in this region higher than the solids melting temperature. This method of temperature scanning the bed did not help to determine the extent of the melting zone. It was observed eventually that melt hold up was taking place on the bed support. The bed support wasmade from 8 mesh, 17 S.W.G. wire. Air, on entering the bed through the mesh, was entraining droplets of melt and transporting them up the bed. Such droplets solidified on reaching column walls or solid at temperatures below the melting point. Adhesion of the pellets to each other in this manner hindered their movement down the column, as they must descend as a solid unit under these conditions.

Melt droplets were transported up the interior of the bed, and not at the column walls. This was because the melt hold up was constrained at the centre of the support mesh. The reason for this constraint is probably that the air flow is lowest at the centre of the column, due to wall effect at the edges. Droplets, appearing at the column walls above the melting zone, solidified and prevented the bed from moving down the column as melting progressed.

To allow free drainage of melt the bed support was replaced by a $\frac{1}{4}$ inch clear mesh of 14 S.W.G. As melting progressed, there was a slight tendency for pellets to fall through the mesh. Movement of the bed was found to be intermittent, in steps of about 3 cms.

A total of 10 melting bed runs was made. No successful results were obtained. Runs failed mainly because of bed blockage. This occurred through transportation and solidification of melt droplets. At low gas flow rates the bed failed to reach equilibrium before the supply of pellets ceased. It is considered that melting beds in future could be successfully operated having the gas inlet above the bed support.

FIGURE II. DIAGRAMMATIC REPRESENTATION OF MOVING BED APPARATUS.

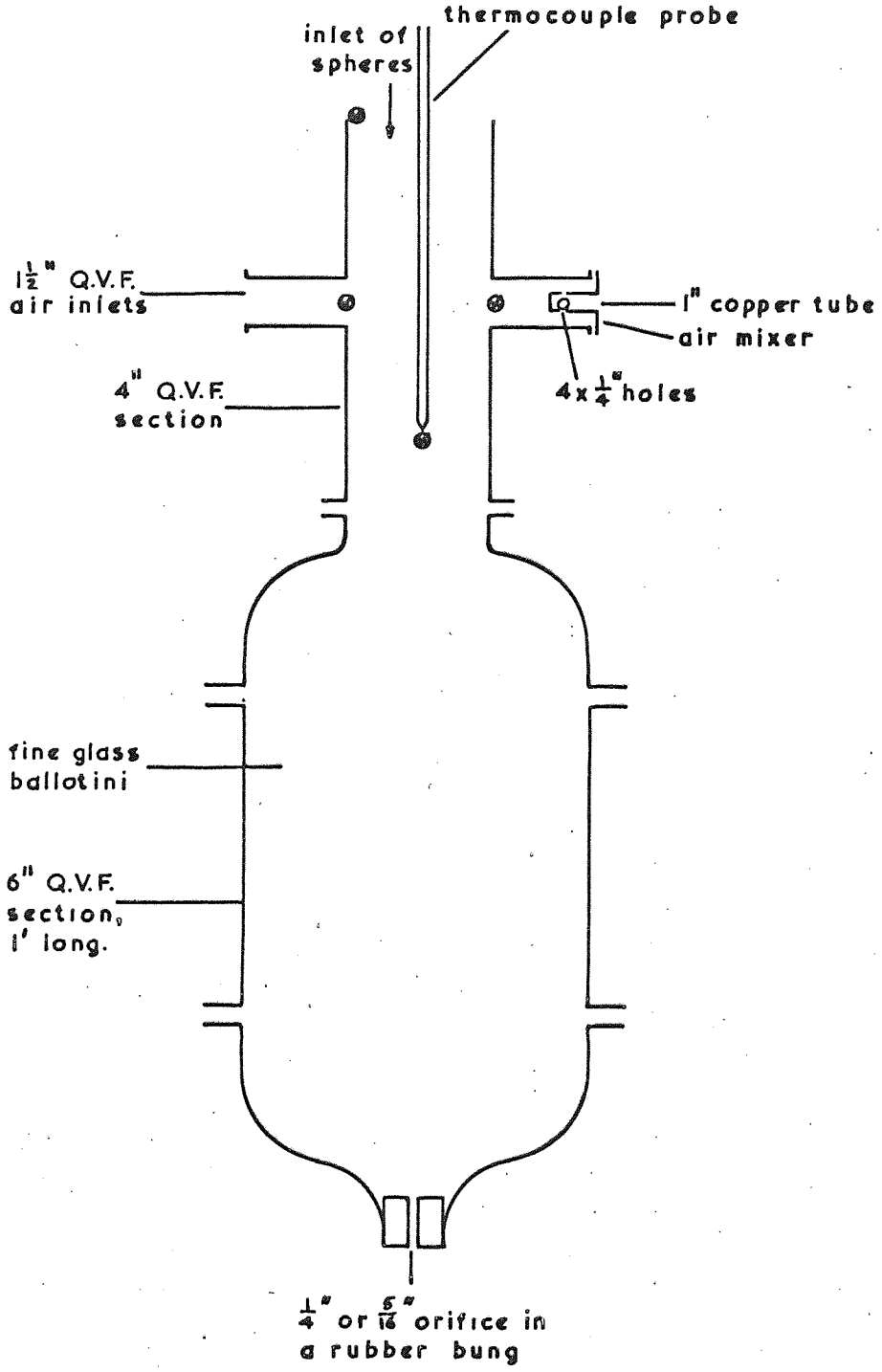

Plate 2 Moving Bed

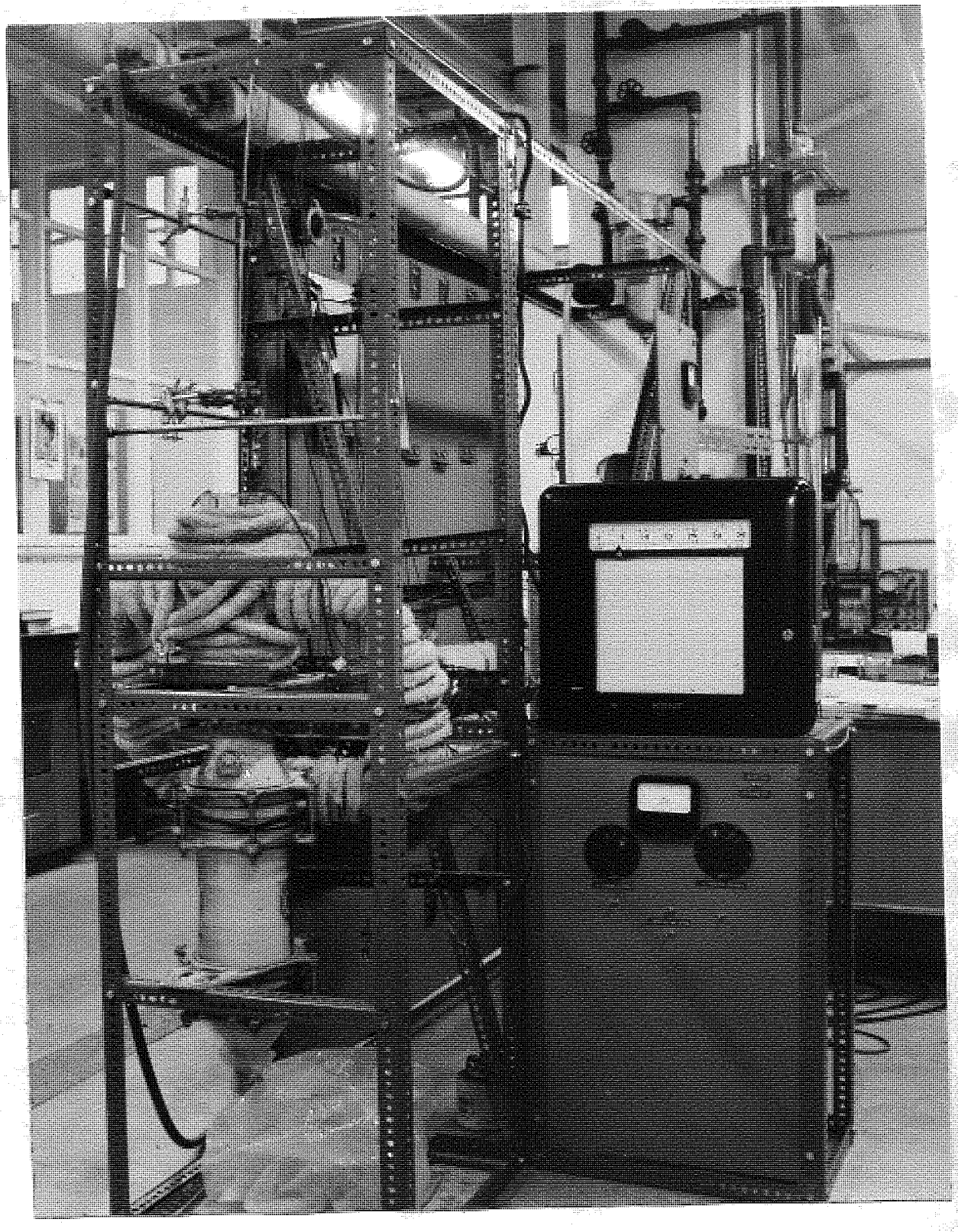

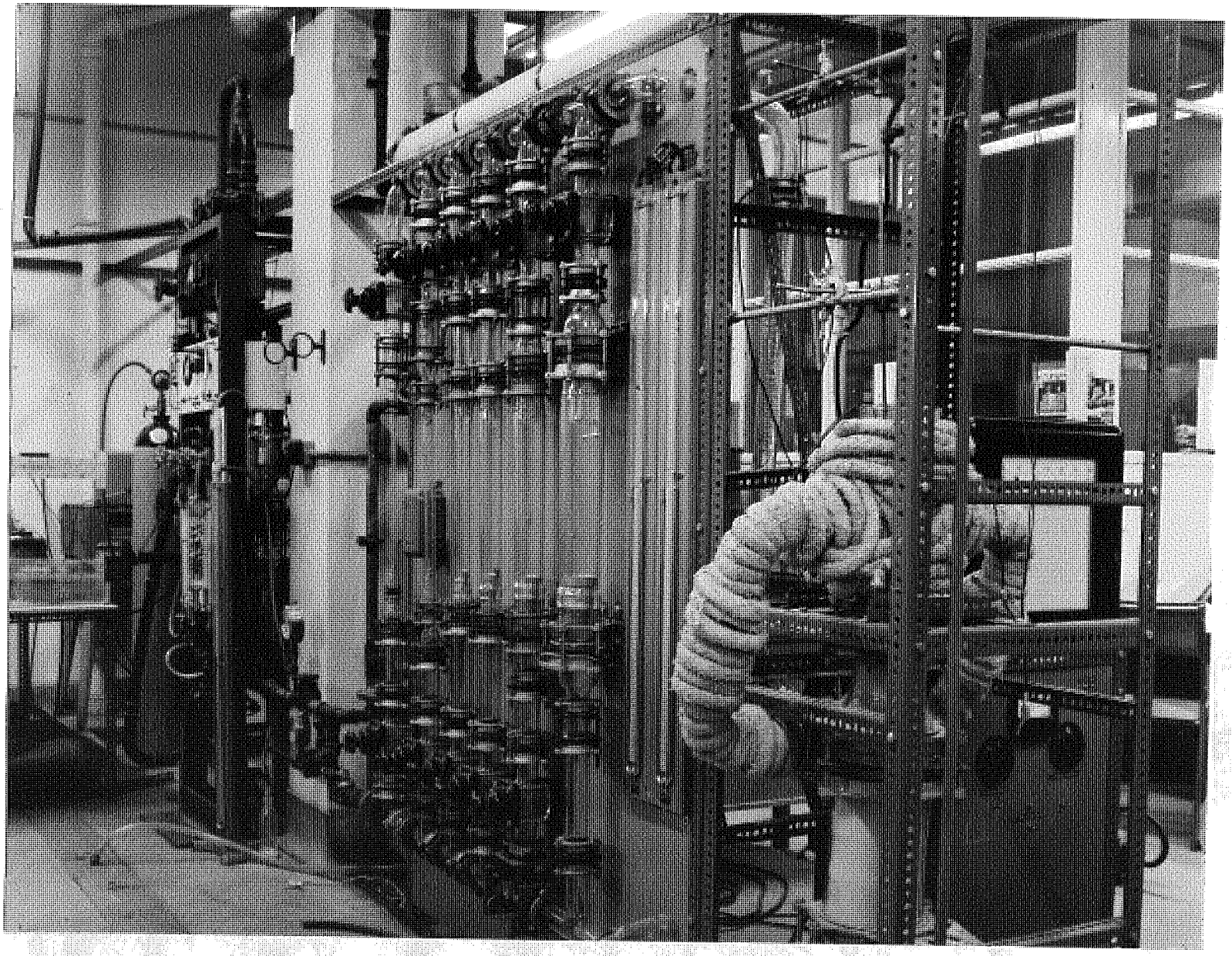

Plate 3 Rotameter Bank

(ii) Moving Bed Heat Transfer (a) Construction of Apparatus

The moving bed apparatus may be seen in Plates 1 and 2, and diagrammatically in Figure 11. This apparatus was designed and built to study the heat transfer of moving beds. It has been seen in Section B that few data are available in this field. Probe scans will not give temperatures that can be identified as gas or solids temperatures, due to radiant and convective heat transfer. This difficulty is similar to that previously discussed in part (i,c) of this section. It is not possible, therefore, to perform moving bed heat transfer analysis in a melting bed.

The moving bed column consisted of either a 3 or 4 inch Q.V.F. section. Hot air was admitted through 2 side arms each of $1\frac{1}{2}$ inch diameter. It was necessary to provide for a continuous downflow of solids and an upflow of gas without any gas escaping down the column. Kuong (78) and Pilpel (79) have reviewed research work on the discharge of fine grains through an orifice. Grains flowing under these conditions are considered not to be in contact with each other. The concept of shear force and head of fluid in fluid flow is not valid in this context. That is, for a given system, the rate of flow of grains through an orifice is independent of the bed height.

A 6 inch Q.V.F. vessel to contain grains of silver sand, was attached below the moving bed section. The moving bed of spheres rested on top of the smallerparticles, to move down the column and into the 6 inch Q.V.F. column as the sand flowed out. Four orifices, two each of $\frac{1}{4}$ inch and 5/16 inch, were provided in a rubber bung for this purpose. By this means, a steady flow of solids in the moving bed was obtained. The solids in the moving bed were observed to be in plug flow. This is in agreement with Denton's experiments (80).

A more consistent flow rate of spheres in the moving bed was obtained on replacing the silver sand by small glass ballotini of about $\frac{1}{4}$ mm. diameter. The flow rate of solids in the moving bed was determined by timing the addition of known weights of spheres. The maximum variation in solids flow rate was 5% at about 300 lb/hr., with virtually no variation at 4,000 lb/hr.

A large bag of thick polythene was tied tightly over the ballotini outlet. This served to catch the flowing ballotini, and to prevent any air from flowing down the column. Runs ceased when all the ballotini had drained into the polythene bag.

Measuring the air temperature at the two hot air inlets to the moving bed column, as shown in Figure 10, was unexpectedly difficult. Hot air passed through a series of 90° bends on each side of the column before entering the bed. Even at Reynolds numbers of about 5,000, air was stratified by the bends. The air temperature at the column air inlet corresponding to the outside of the bends was lowest. Temperature differences of several degrees centigrade were measured across the diameter of the air inlet. The explanation for this phenomenon is that for a length of travel of about 6 feet, from the heater to one air inlet of the column, the hot air supply is stratified, with the maximum velocity at the outside of the curves. More heat transfer between the hot air and the containing pipes, and hence ambient conditions, takes place with the higher velocity air. The air feeds on each side of the column were progressively stripped back till they met at the heater. The temperature change across the pipe diameter was measured and was observed to progressively decrease.

This problem of air inlet temperature distribution was overcome by lagging the air inlet pipes and by the use of two air mixers. One such air mixer is shown on the right hand air inlet in Figure 10. A length of 1 inch i.d. copper tube of about $1\frac{1}{4}$ inches was blanked off at one end with 1/16 inch brass sheet. The open end of the 1 inch tube was soldered to a 1 inch diameter hole in a circular plate of 1/16 inch brass sheet of about $2\frac{1}{2}$ inches diameter. Holes were drilled in the brass plate to correspond to $1\frac{1}{2}$ inch Q.V.F. flange bolt holes. Four holes, each of $\frac{1}{4}$ inch diameter, were drilled at each quadrant, 5/16 inch from the blanked-off end of the 1 inch copper tube. The completed air mixer units were placed between two $1\frac{1}{2}$ inch Q.V.F. gaskets, and bolted between two $1\frac{1}{2}$ inch Q.V.F. buttresses. The air mixers were positioned so that the four holes near the blanked-off end of the copper tube pointed towards the moving bed. Using the air mixers, the two air inlet temperatures were measured to

within $\frac{1}{2}^{\circ}$ C of each other. Temperature scans across each air inlet showed slight temperature changes only.

(b) Operation of the Moving Bed

The 6 inch diameter Q.V.F. section below the moving bed was filled with fine ballotini. The ballotini were freshly sieved to remove agglomerates and extraneous matter. This encouraged a more uniform flow of ballotini out of the rubber bung.

The apparatus was allowed to reach a steady thermal state, with hot air passing through a fixed bed of glass or ceramic spheres placed on top of the fine ballotini. The glass spheres were 6 mm. and 12 mm. diameter ballotini. The ceramic spheres were $\frac{1}{2}$ inch diameter porcelain; that is, alumina ceramic.

The steady thermal state was reached when the gas outlet temperature from the column ceased to rise. The difference in temperature between the gas inlet and outlet corresponds to the heat lost from the column walls. This difference was found experimentally to be less than $\frac{1}{2}^{\circ}$C. in all cases. The minimum temperature drop between gas inlet and outlet during the moving bed experiments was found to be about 20°C. The figures are given in Table 13 , Appendix 3. The heat lost from the column walls relative to the heat transferred from gas to solid is, therefore, $2\frac{1}{2}\%$ at maximum. This figure was considered low enough to be neglected in the evaluation of heat transfer results.

The heat lost from the column walls was low because the column was lagged by two thicknesses of 1 inch asbestos rope wound tightly round the column. McAdams (57) indicates how a heat transfer coefficient may be determined to calculate the heat lost from a vertical cylinder by natural convection and radiation. For an unlagged column, a heat transfer coefficient of 2 Btu/hr ft^2 °F may be calculated as realistic. It will be seen in Section F that a column height of 3 inches was used. If an average temperature difference between the column walls and ambient air is taken as 120°F, the heat lost through the column walls of outside diameter $4\frac{1}{2}$ inches is about 70 Btu/hr. The heat transferred from the gas in the column is $G_g c_g (T_{gi} - T_{go})$. For a minimum gas temperature drop of 20°C i.e. 36°F., in a 4 inch i.d. column during moving bed

experiments, the heat transferred by the gas is $G_g c_g \times \frac{\pi}{4}$.

A specimen value of $G_g c_g$ of 250, representative of an experimental mean, gives the heat transferred by the gas equal to about 200 Btu/hr.

The column lagging is, therefore, very effective. It is suggested in future experiments that before a moving bed experiment begins, the temperature difference between the gas inlet and outlet should be corrected by heat input from an electrical heating coil wound round the column.

A further discussion of the measurement of solids and gas outlet temperatures will be given in Section F.

SECTION F RESULTS

(i) Determination of Glass and Alumina Thermophysical Properties

The required thermophysical properties of the 12 mm. and 6 mm. glass spheres and $\frac{1}{2}$ inch alumina ceramic spheres are the heat capacity and thermal conductivity. Accurate measurement of these qualities is difficult and requires specialist equipment. Specific heats and thermal conductivities were determined after a literature search.

Alumina ceramic

The particular alumina ceramic used was Regalox, made by Royal Worcester Industrial Ceramics Ltd. Regalox was measured to have a specific gravity of 3.45, and contains 88% by weight of aluminium oxide (89). The International Critical Tables (81) classify such an alumina ceramic in the general class of porcelain, and assign an average heat capacity of 0.2 Btu/lb $^{\circ}$F. Wilkes (82) gives an average value of 0.206 Btu/lb $^{\circ}$F between 30°C and 100°C. Searle and Grimshaw (83) give an average value of 0.2 Btu/lb $^{\circ}$F for all aluminas between 3°C and 48°. Goldsmith et al (84) give extensive graphical data of heat capacity and temperature for alumina ceramics. The data of Ginnings and Corruccini (85) for corundum, impure alumina, are representative of that given by Goldsmith et al. These data are given in Table 9, Appendix 4. The five points given in the table were fitted to a quartic equation, to enable computer calculation of average heat capacities for specific runs to be made.

The resulting equation is:

$$C_s \text{ (alumina)} = 0.1730 + 5.18 \times 10^{-4} T - 9.89 \times 10^{-7} T^2 + 3.98 \times 10^{-10} T^3 - 3.79 \times 10^{-12} T^4 \quad \text{.....F 1}$$

Temperatures are measured in degrees centigrade, for convenience, as explained in Section E.

The search in the literature for a representative thermal conductivity of Regalox was more difficult. Powell (86) and Popper (87) give graphical results for the thermal conductivity of various high alumina ceramics with temperature. It is evident that alumina composition, as shown by the ceramic density, has a greater influence on thermal conductivity than heat capacity. High density aluminas have high thermal conductivities. The work of Smoke and Koenig (88) was seen to illustrate this point further. Their results are given in Table 10 and Graph 11 of Appendix 4. Royal Worcester Industrial Ceramics Ltd. (89) give one thermal conductivity value for Regalox of 5.57 Btu/hr. ft. $^{\circ}$F at 195°C. It is evident from Graph 11 that the results of Smoke and Koenig's specimen 8 may be extrapolated with confidence to the single Regalox value. Equation F 2 has been obtained by a linear least mean squares fit of these results:

$$k_s = 7.34 - T_s/111.2 \quad \text{.....F 2}$$

Glass ballotini

Glass ballotini of diameter 6 mm. and above, as supplied by the English Glass Co. Ltd., are made from soda lime glass. A formula for the average heat capacity of the ballotini glass between 20°C and T_s°C is given as (90) :

$$c_{sm}\,(T_s,\ 20^{\circ}C) = \left[\frac{0.00051\ T_s + 0.1749}{0.00146\ T_s + 1}\right] \qquad \text{.....F 3}$$

Equation F 3 is consistent with the general equation for glass heat capacity given by Sharpe and Ginther (91) for heat capacities between 0°C and T_s°C:

$$c_{sm}\,(T_s,\ 0^{\circ}C) = \left[\frac{a\ T_s + c_o}{0.00146\ T_s + 1}\right] \qquad \text{.....F 4}$$

Sharpe and Ginther's equation is applicable in the range 0°C to 1300°C. It is desirable to express equation F 3 in general form, to calculate the average heat capacity from an initial temperature other than 20°C. Using the relationship:

$$c_{sm}\,(T_s,\ T_1) = \frac{1}{T_s - T_1}\int_{T_1}^{T_s} c_s\ dT \qquad \text{.....F 5}$$

and equation F 4, it is readily shown that the constant a is temperature independent.

The constant c in equation F 4 is dependent on the datum temperature chosen and it may be easily shown that the values of c for the given datum temperatures are related by the following equation:

$$c_2 = c_1 \left[\frac{0.00146\ T_1 + 1}{0.00146\ T_2 + 1} \right] + \frac{a(T_2 - T_1)}{(0.00146\ T_2 + 1)} \qquad \text{.....F 6}$$

Also, the mean heat capacity between temperatures T_1 and $T_2\,^{\circ}C$ may be expressed as:

$$c_{2m}(T_2, T_1) = \frac{c_2 T_s - c_1 T_1}{T_2 - T_1} \qquad \text{.....F 7}$$

Using the c and a values of equation F 3, c_1 and c_2 were found in terms of T_1 and T_2 from equation F 6. Substituting these values into equation F 7, the final equation was derived:

$$c_{sm}(T_s, T_1) =$$

$$\frac{\left[\frac{0.1697 + 0.00051\ T_s}{0.00146\ T_s + 1} \right] T_s - \left[\frac{0.1697 + 0.00051\ T_1}{0.00146\ T_1 + 1} \right] T_1}{(T_s - T_1)} \qquad \text{.....F 8}$$

No data for the thermal conductivity of the ballotini were available. The thermal conductivity of glass is an additive property with respect to its chemical constituents (92). The ballotini manufacturers would not reveal the glass composition (93). The 6 mm. and 12 mm. ballotini were chemically analysed (94) to give :

SiO_2	=	71.78%
CaO	=	4.60%
Na_2O	=	13.48%
K_2O	=	4.39%
BaO	=	4.02%
MgO	=	0.20%
Fe_2O_3, Al_2O_3, TiO_2	=	0.39%
SO_3	=	0.48%
SbO_2	=	0.48%
Deficiency	=	0.38%
		100%

Using Ratcliffe's addition formula (92) which is considered accurate to less than 5%, the thermal conductivity of soda glass ballotini was calculated at -100, 0, and 100°C. These results are compared graphically with values given in the literature (97, 98) for glass beads. This comparison may be seen in Graph 12 and Table 11, Appendix 4. A quadratic equation was fitted to the soda glass ballotini results, to give the following equation:

$$k_s = 0.541 + 9.33 \times 10^{-4} T_s - 1.65 \times 10^{-6} T_s^2$$

.....F 9.

The ballotini glass composition was verified by comparing the measured glass density with the theoretical, as calculated using the additive composition formula of Huggins and Sun (99). The calculated and measured values were identical at 2.513 g/cc. The exact comparison is considered fortuitous, but indicates the high accuracy of accepted additive formulae to the calculation of glass physical properties.

The constants a and c referring to equation F 3 were calculated theoretically using the additive composition formulae of Huggins and Sun (99) The given c_{20} value was referred to c_o using equation F 6. This value was 0.1697, to be compared with the theoretical value of 0.1760 calculated from the additive formula. The calculated and given values of a were 0.000508 and 0.00051 respectively, a very close comparison. It is suspected that the English Glass Company's c_{20} value of 0.1749 might be a calculated value, and refer to $0^{\circ}C$. Nevertheless, equation F 8, derived from the English Glass Company's equation F 3, was used for calculation purposes.

(ii) Physical Properties of Air

The thermal conductivity, heat capacity and viscosity of air were required. It was necessary to have these data in the form of temperature functions, which may be integrated with respect to temperature to provide accurate average physical properties of air in the desired range. Five values of temperature data for each physical property were taken (100). These values are given in Table 12, Appendix 4. Each physical property was fitted to a quartic equation, valid in the temperature range 0°C to 116°C:

$$k_g = 0.0140 + 5.798 \times 10^{-5}T - 3.841 \times 10^{-7}T^2 + 4.229 \times 10^{-9}T^3 - 1.683 \times 10^{-11}T^4 \quad \text{.....F 10}$$

$$c_g = 0.2396 + 9.387 \times 10^{-6}T - 7.307 \times 10^{-8}T^2 + 2.494 \times 10^{-9}T^3 - 1.100 \times 10^{-11}T^4 \quad \text{.....F 11}$$

$$\mu_g = 0.0417 + 8.719 \times 10^{-5}T + 1.190 \times 10^{-6}T^2 - 1.607 \times 10^{-8}T^3 + 6.449 \times 10^{-11}T^4 \quad \text{.....F 12}$$

Equation F 12 was used to give an average value of viscosity in preference to the Sutherland equation for viscosity (62) given in Appendix 3, as the Sutherland equation is difficult to use when integrated with respect to temperature.

FIGURE 12. DIAGRAM OF TEMPERATURE CHART RECORDING OF TYPICAL MOVING BED RUN. (Run 87).

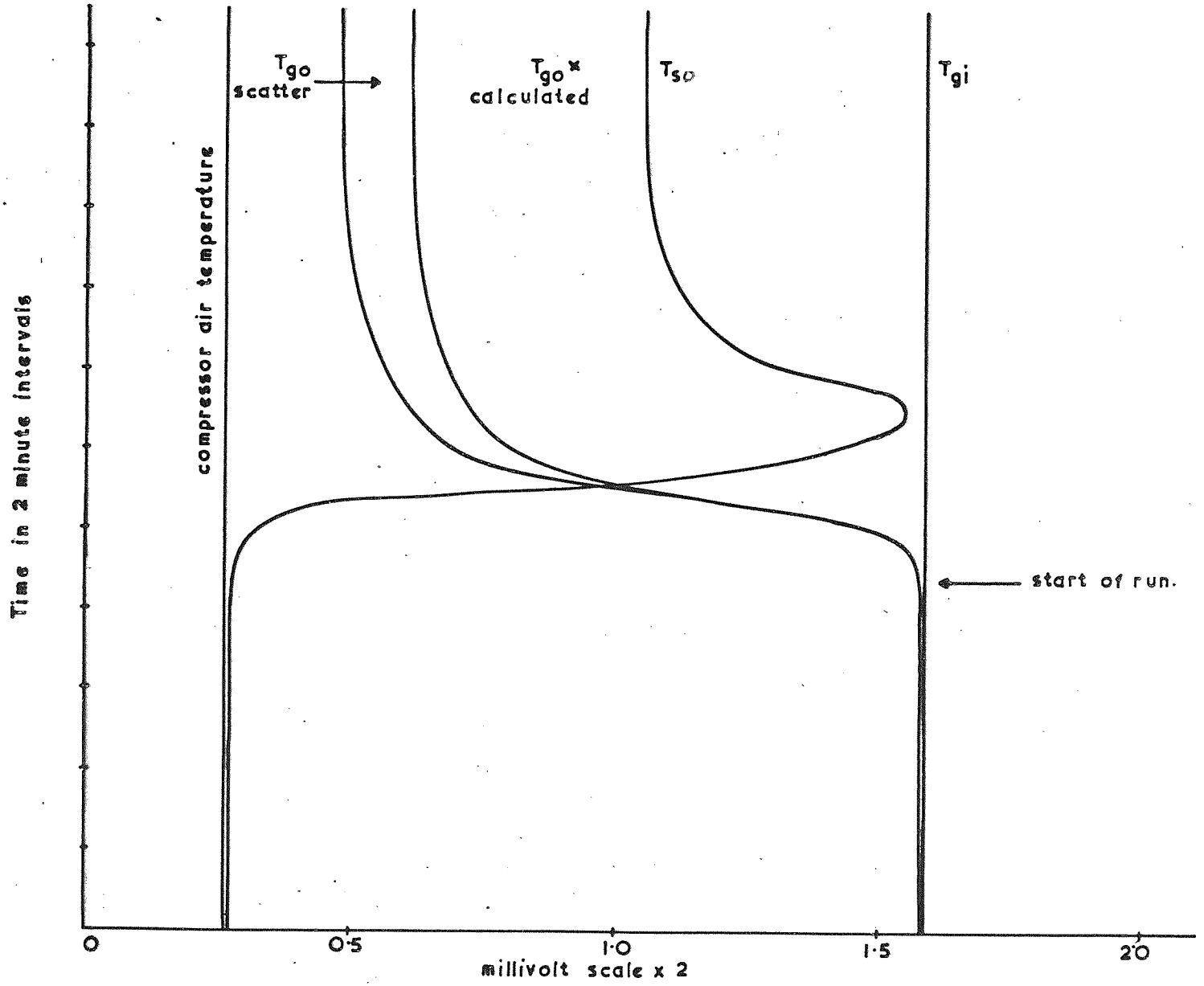

(iii) Moving Bed Heat Transfer Experimental Results

(a) Measurement of Air and Solids Outlet Temperatures

It has been mentioned in Section E that the solids outlet temperature was measured using a thermocouple probe. The probe was positioned about 2 inches below the centre line of the air inlets. The column was well lagged in this position. With no solids in the column, the thermocouple was seen from temperature measurements to be situated out of the hot air stream at the inlet. Before starting a moving bed run, it was observed during the solids warm up period that the thermocouple probe temperature lagged well behind the gas inlet temperature, heat being conducted through the ballotini to the probe. When a run commenced, it was observed that the probe temperature rose up to the gas inlet temperature and remained at that temperature until the initial charge of solid had passed out of the column. The probe temperature then fell to reach a steady equilibrium temperature below the gas inlet temperature. This may be seen in Figure 12, which is taken from a chart recording.

The temperature cycle of the probe during the start up period of a run corresponded to the expected time intervals of the hot bed reaching the probe and passing it. It is considered from this evidence that the probe was measuring a solids temperature. The mechanism of heat transfer to the probe will have been by radiation or conduction from the solids. Voids of air, having a lower thermal capacity on a volumetric basis than the solids, are expected to be at the same temperature as the solids. If a temperature distribution exists in the solids, the probe should record The surface temperature. At the solids temperature measurement point, temperature distribution will have evened out to some extent.

At the column level where the solids temperature is read, heat transfer from gas to solid has not taken place since the solid passed the gas inlet. It is expected that intra-particle temperature distribution will be reduced. Horizontal scans by the probe at the solids temperature measuring height revealed very small differences. Axial temperature scans showed an increase in temperature when the probe was moved to a position immediately below the gas inlet. This may have been caused by either the inlet gas flow pattern or intra-particle temperature distribution. The solids outlet temperature in the recording position is assumed at this stage to be the solids mean outlet temperature. This point will be discussed further in connection with the results recalculated by the analogue computer, assuming intra-particle temperature distribution.

The recorded gas outlet temperature at the top of the column was observed to vary in a radial direction. It was found that temperatures near the column walls were higher than those recorded towards the centre of the bed. This temperature variation is attributed to wall effect. Schwartz and Smith (101) have observed that the maximum air flow occurs at about $1\frac{1}{2}$ particle diameters from the vessel walls. Their air flow rate determinations were made using a hot wire anemometer.

It was concluded that gas bypassing of solid in the column was taking place. To obtain a correct average gas outlet temperature, it would be necessary to evaluate the following expression:

$$\frac{\int_0^{r_v} (G_g c_g T_g)\, r_v\, dr_v}{\int_0^{r_v} (G_g c_g)\, r_v\, dr_v} = T_{gm} \qquad \text{.....F 13}$$

It was not considered feasible to measure the outlet temperature at several radial positions. No account of velocity distribution would be made and the manual addition of solids in even distribution to the moving bed would be complicated by the presence of several thermocouples. Velocity scans of the gas outlet at the top of the column using a pitot tube indicated velocity distribution. It is difficult to determine velocities near solid surfaces (102), and it was considered impractical to attempt an experimental estimation of equation F 13. A suction pyrometer was used to take a more representative sample of gas from the bed. A suction pyrometer thermocouple was wired into the Kent recorder. This arrangement was unsatisfactory, as the suction rate was not sufficiently high to take a representative sample of the outlet air to record the true mean temperature.

It was decided to calculate the gas outlet temperature from the heat balance. Tables 13, Appendix 4, show these results, together with a measured value of gas outlet temperature from the suction pyrometer recording.

(iii)(b) Calculation of Results

Temperature calculations were performed on the PDS 1020 digital computer. This programme is given as Computer Programme (5) Appendix 4. Firstly, the gas mass flow rate Gg was calculated using equations E2 and E3, as explained in Section E. This value, together with the solids mass flow rate G_s and the measured gas and solids outlet temperatures, were the data for a second computer programme, Computer Programme 6 Appendix 4 to calculate a first approximation to the gas outlet temperature, using a constant gas heat capacity of 0.24 Btu/lb°F A further programme, Computer Programme 7 Appendix 4, calculated a more accurate gas outlet temperature using the first approximation and the integrated form of equation F11. These results were those given in Table 13. The solids heat capacity was calculated in both the second and third programmes from the integrated forms of equations F1 or F8 for ceramic or glass spheres.

The third programme then calculated the heat transfer coefficient from equation D6. In order to calculate the Nusselt and Reynolds numbers, the average air thermal conductivity and viscosity were calculated using the integrated forms of equations F10 and F12. The solids average thermal conductivity was calculated from equations F2 or F9 for ceramic or glass spheres in order to calculate the Biot numbers.

All calculations involving temperature varying properties used, therefore, what may be called analytical averages of the property with respect to temperature.

The results of the heat transfer coefficient calculations are shown in Tables 14, Appendix 4. The Reynolds number, Re', is based on the mean hydraulic radius of the flow passages in the moving bed. The bed void fraction was calculated from packed bed observations, using water containing a wetting agent. This method has been used by Denton (80) and is very accurate. Repeated measurements were made, and were found to be very consistent. Values of void fraction are given in Table 15 Appendix 4. In fluid pressure drop measurements through

moving beds Happel (103) used the packed bed void fraction. Happel assumed there was no difference between moving and packed bed void fractions when the bed moved as a solid matrix, with no interparticle separation.

It is pertinent to note that the solid was in plug flow in the moving bed. Results in this respect were in agreement with those of Denton (80) Denton also found deviations from plug flow to occur two column diameters upstream from a narrow constriction.

As a preliminary measure to data interpretation, the heat transfer coefficient was plotted against the gas flow rate to investigate trends of the variables in the results. This is shown in Graph 13, Appendix 4. It is reasonable to expect the heat transfer coefficient to be highly dependent on gas flow rate. This type of data analysis is recommended by Rowe (104) before proceeding to plot dimensionless groups. It is evident from Grayh 13 that there is a wide scatter of results. It was considered necessary to perform an error analysis to determine which results were prone to high errors.

(iii)(c) Error Analysis

The error analysis was based on equation D6, which is rewritten:

$$\ln\left[\frac{\theta_{go} - \theta_{si}}{\theta_{gi} - \theta_{so}}\right] = \frac{h_g}{G_g c_g}\,\frac{6\,(1-e)\,L}{d_p}\left[\frac{1-\beta}{\beta}\right] \qquad \text{F14}$$

The gas outlet temperature was eliminated in equation F14 through the heat balance, as this was the procedure used in the calculation of results. The main sources of error were considered to be in the measurement of θ_{so}, $G_s c_s$, and $G_g c_g$.

By the usual method of error analysis, using differential calculus, the relative error in heat transfer coefficient was determined as a function of the relative error in θ_{so}. This is written:

$$\frac{\Delta h}{h} = \frac{\Delta\theta_{so}}{\theta_{so}}\left\{\frac{\theta_{so}(\beta-1)}{(1-\beta\theta_{so})(1-\theta_{so})}\Big/\ln\left[\frac{1-\theta_{so}}{1-\beta\theta}\right]\right\} \qquad \text{F15}$$

Equation F15 is indeterminate for values of $\beta = 1$, and $\theta_{so} = 0$. Using L'Hôpital's rule, it is readily shown that:

$$\frac{\Delta h}{h} = \frac{\Delta\theta_{so}}{\theta_{so}}\left[\frac{1}{1-\theta_{so}}\right]_{\beta = 1} \qquad \text{F16}$$

and

$$\frac{\Delta h}{h} = \left(\frac{\Delta\theta_{so}}{\theta_{so}}\right)_{\theta_{so} = 0} \qquad \text{F17}$$

The results of this analysis are given in Graph 14 Tables 16, Appendix 4. Graph 14 shows the relative error in the heat transfer coefficient as a function of the relative error in θ_{so}. It is evident that errors in the heat transfer coefficient due to errors in the measurement of θ_{so} are serious when the solids outlet temperature is high and increase with increase in β. This indicates the desirability of short column lengths in experiments, to minimise errors.

From equation F14, the equation relating the relative error in h to the relative error in $G_s c_s$, as a function of θ_{so}, is written:

$$\frac{\Delta h}{h} = \frac{\Delta G_s c_s}{G_s c_s}\left\{\frac{1}{1-\beta} + \frac{\beta\theta_{so}}{1-\beta\theta_{so}} \Big/ \ln\left[\frac{1-\theta_{so}}{1-\beta\theta_{so}}\right]\right\} \qquad \text{F18}$$

As in the previous case, equation F18 is indeterminate for values of $\beta = 1$, and $\theta_{so} = 0$. Hence:

$$\frac{\Delta h}{h} = \frac{\Delta G_s c_s}{G_s c_s}\left[\frac{2-\theta_{so}}{2(1-\theta_{so})}\right]_{\beta = 1} \qquad \text{F19}$$

and

$$\frac{\Delta h}{h} = \left[\frac{\Delta G_s c_s}{G_s c_s}\right]_{\theta_{so} = 0} \qquad \text{F20}$$

A similar analysis in terms of $G_g c_g$ gave the relation:

$$\frac{\Delta h}{h} \Big/ \frac{\Delta G_s c_s}{G_s c_s} = 1 - \frac{\Delta h}{h} \Big/ \frac{\Delta G_g c_g}{G_g c_g} \qquad \text{F21}$$

The results of these two analyses are given in Graphs 15 and 16, Tables 16, Appendix 4. It is evident that errors are serious at high values of θ_{so} and β.

An arbitrary gradient of the error curve of less than 20 was chosen as the criterion for selecting valid experimental results. A point on Graph 14 at $\beta = 1.5$, having a gradient of 20, is shown by a cross. It is of interest to note that for a beta value of unity, curves on Graphs 14, 15 and 16 are identical in shape. For beta values less than unity, curves on Graph 14 are steeper, but for values greater than unity, curves on Graph 14 are less steep than those on Graphs 15 and 16.

Table 17, Appendix 4, shows the errors $\frac{\Delta h}{h} \Big/ \frac{\Delta \theta_{so}}{\theta_{so}}$, $\frac{\Delta h}{h} \Big/ \frac{\Delta G_s c_s}{G_s c_s}$, and their rate of change of error with respect to θ_{so}. Graph 17, Appendix 4 shows the h against G_g graph for the selected results having probable low errors. Graph 17 indicates that increasing solids flow rate tends to reduce the heat transfer coefficient. This relationship is not a simple one, and demonstrates the need for further analysis assuming the presence of intraparticle temperature distribution.

The error analysis is strictly applicable to cases of cocurrent and countercurrent flow with only axial temperature distribution. It is considered that the error analysis can be applied with some success to the present results where, as it is shown in Table 18, Appendix 4, the Biot number is less than unity.

FIGURE 13. MODIFIED ANALOGUE COMPUTER CIRCUIT DIAGRAM FOR THE ITER .ATIVE SOLUTION OF MOVING BED HEAT TRANSFER.

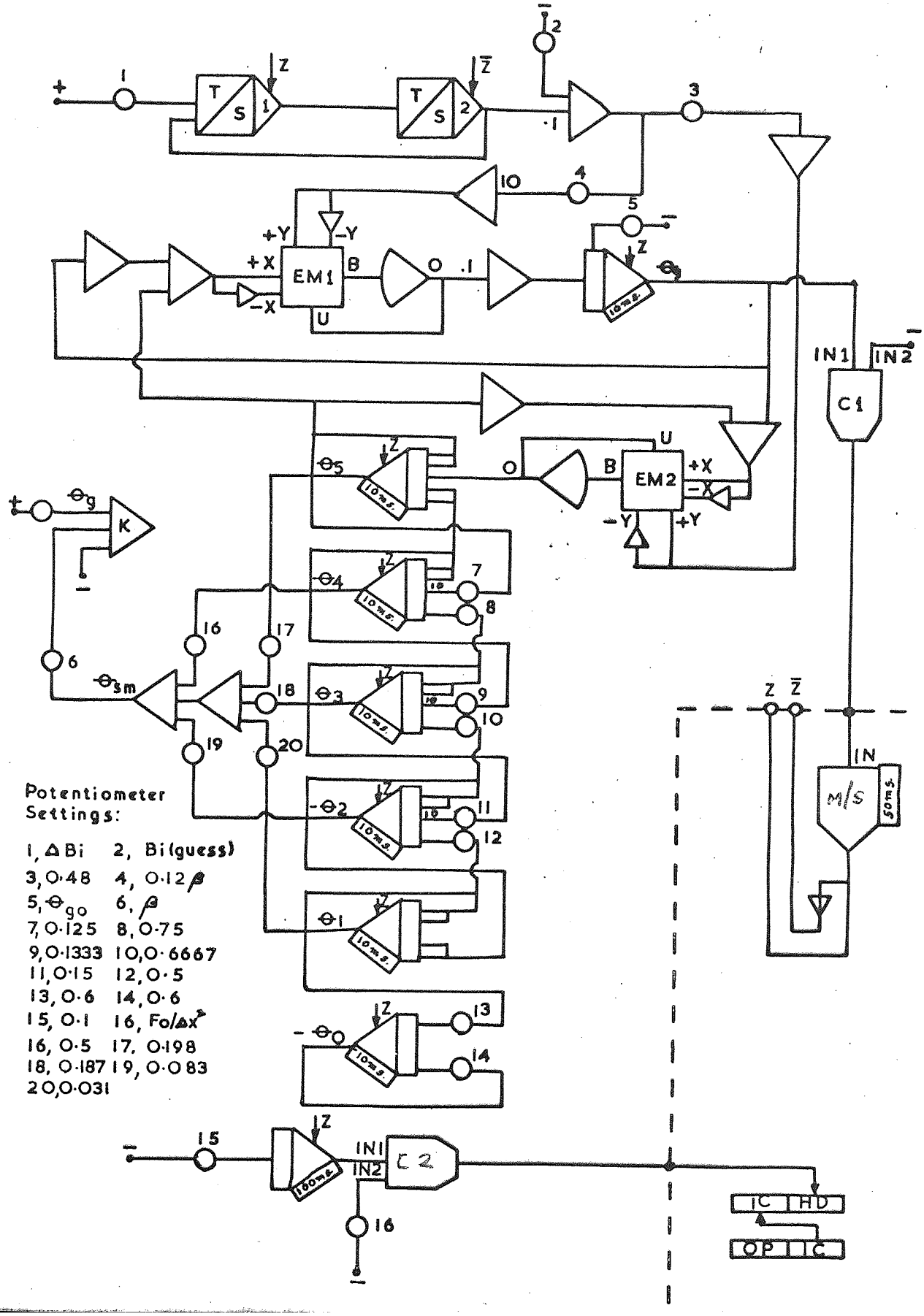

Potentiometer Settings:

1, ΔBi	2, Bi(guess)
3, 0·48	4, 0·12 β
5, θ_{go}	6, β
7, 0·125	8, 0·75
9, 0·1333	10, 0·6667
11, 0·15	12, 0·5
13, 0·6	14, 0·6
15, 0·1	16, $Fo/\Delta x^2$
16, 0·5	17, 0·198
18, 0·187	19, 0·083
20, 0·031	

(iv) Moving Bed Heat Transfer with Intraparticle Temperature Distribution

An outline of the analogue computer analysis of moving bed heat transfer results was proposed in Section D, Part (v). Considerable labour was taken out of the analysis using a hybrid TR48 computer. This machine is basically a medium sized analogue computer, with 48 high gain amplifiers. The hybrid TR48 has a separate logic section for logic and mode control.

It will be appreciated that the analysis in the first instance where the measured solids outlet temperature is argued to be θ_{sm}, is a two point boundary value problem. That is, the computation must be stopped when the gas temperature reaches unity at the bottom of the column. The time of computation must compare with $Fo'/\Delta x^2$ for the Biot number to be realistic. The basic equations being solved are D24 and D25. These equations were given in Section D(iii)b, where a statement of the criteria to be met was made.

The computation may be stopped using an electronic comparator, C1 in Figure 13, to monitor the gas temperature. The computation is held at this point, and the time of computation may be read from the output of a separate integrator for this purpose.

The Biot number enters the computation through two potentiometers, shown as C and D in Figure 7A. Using two track store amplifiers, shown as TS1 and TS2 in Figure 13 , controlled by a logic signal from a monostable M/S in Figure 13, controlled by the comparator monitoring the gas outlet temperature, it is possible to increment the Biot number. Potentiometers C and D are then replaceable by two electronic multipliers, EM1 and EM2 in Figure 13. It is possible, therefore, to start the computation with a high value of the Biot number, giving a time of computation too short for the problem. The Biot number may then be incremented in a negative direction. A comparator may be used, shown as C2 in Figure 13, to monitor the computation time so that the calculation, which has now become repetitive, may be stopped when the Biot number has reached a value that gives the correct length of computation.

A further advantage of the hybrid TR48 computer is that the calculation may be speeded up considerably. An integrator time constant of 10 ms. enables a computation to be made in 2 seconds rather than 200.

In the second instance, the measured solids outlet temperature was assumed to be the surface temperature. The computation was repeated, therefore, using trial and error values of the gas outlet temperature as the initial condition on potentiometer 5, Figure 13. The analysis remains a two point boundary problem, with the added condition that the computed surface temperature θ_{ss} must match the measured solids outlet temperature, previously used as θ_{sm}. The computation is concluded when the Biot number gives a gas temperature of unity, the computation time requirement is fulfilled, and the solids surface temperature matche the measured solids temperature. It is necessary that the heat balance, given by equation D27, should still be satisfied.

Amplifier K, shown in Figure 13, indicates the heat balance. If the computer model of the moving bed is fulfilling the heat balance there is no output from amplifier K. At Biot numbers less than about 0.2, the heat balance was found to be sensitive to the last figure in the setting of potentiometer 9. Whilst the computer circuit shown in Figure 13 was found satisfactory for the analysis of results, further investigation of the circuit behaviour would be advantageous.

The results of this analysis applied to the results selected by error analysis are shown in Table 18, Appendix 4. Graph 18, Appendix 4 shows a plot of Nusselt number from the heat transfer coefficient, found from analogue computer analysis, against modified Reynolds number. The heat transfer coefficient used assumes that the measured solids temperature is the mean solids temperature. It will be seen from Table 18 that the two values of Biot number calculated, assuming the measured solids temperature was the mean and the surface temperature, generally lie above and below the Biot number calculated assuming no temperature distribution in the particles. This point is discussed further in Section G with regard to the measurement of solids outlet temperature.

Section G. Discussion of Results

(i) Measurement of Solids Temperature

It has been seen in Section F that, when the measured solids outlet temperature is taken to be the mean solids outlet temperature, analogue computer analysis of results tends to raise the Biot number above that calculated by logarithmic mean temperature difference. For the reasons expressed in Section D, part (v), this is to be expected.

As the gas outlet temperature was calculated from the heat balance, the hybrid TR48 computer was used to re-evaluate selected data, assuming that the measured solids temperature was the solids surface temperature. This was possible using an iterative technique to decrease the Biot number with manual variation of the gas outlet temperature. It will be recalled from Section F, part (iv), that this procedure was required to maintain the computation time at a value consistent with that predicted by the physical properties of the moving bed through the modified Fourier number Fo_1. It was possible, therefore, to calculate in this manner very accurate heat transfer coefficients for the moving bed whilst still fulfilling the heat balance. This analysis was carried out on the results selected after application of the error analysis. The results of these computations are given in Table 18, Appendix 4.

The solids temperature measuring probe was sited about 2 inches below the gas inlet. This means that for 2 inches of travel before the probe, the spherical solids have been out of contact with the gas stream. The bed length was 3 inches in the heat transfer section, so that modified Fourier numbers for the bed travel before the solids temperature recording were about $^2/_3$ of those in the heat transfer section. This value allows an appreciable time for intraparticle temperature distribution to even out. The modified Fourier number Fo_1 is equivalent to the Fourier number $k_s t/c_s \rho_s Ro^2$, where t has been replaced by $\ell(1 - e)\rho_s/G_s$. It will be appreciated that in this post-heat transfer section, further heat exchange will be

limited to that between stagnant gas and solids. The Biot number in this region will be, therefore, virtually negligible. Gurney and Lurie charts (57), for very low Biot numbers and Fourier numbers greater than 0.2, indicate very little intraparticle temperature distribution.

It is considered that the thermocouple probe was measuring a temperature close to the mean solids outlet temperature. The results given in Tables 18, Appendix 4, assuming the measured solids temperature to be the surface temperature, have not been presented in graphical form.

(ii) Presentation of Moving Bed Results in terms of Nusselt and Reynolds Numbers

Graphs 19 and 20, Appendix 4, show the uncorrected and corrected plots of Nusselt against Reynolds number. The term correction refers to results analysed using the hybrid TR48 computer. Graph 20 shows most of the points given on Graph 19. Points that are missing on Graph 20 are due in the main to difficulties caused by the computer circuit becoming unstable at low Biot numbers. Results for runs 19 to 22 and 24 for 12 mm. ballotini in the 3 inch column proved impossible to analyse on the hybrid TR48 computer. It may be significant that these results show high rates of change of the error with solids outlet temperature.

The correlations of Yoshida (48) for packed bed heat transfer, given by equations C15 and C16, have been re-expressed to give:

$$Nu = 2.035\ Re'^{0.49}\ (1 - e) \text{ for } Re' < 300 \qquad G1$$

and

$$Nu = 1.19\ Re'^{0.59}\ (1 - e) \text{ for } Re' > 300 \qquad G2$$

This re-expression assumed the Prandtl number of air to be constant at 0.72. Equations G1 and G2 have been drawn onto Graphs 19 and 20 to compare the present heat transfer with heat transfer in the corresponding packed beds.

It is apparent that the bulk of the moving bed heat transfer results lie well below the packed bed correlations given on Graphs 19 and 20. It was considered that the corrected results might compare with packed bed correlations. That is, the gas film heat transfer coefficient might be the same for packed and moving bed heat transfer. The reason for the difference probably concerns wall effect. Gamson et al.(20) and Wilke and Hougen's (47) equations, given previously as C12 and C14, agree closely with Yoshida's equations. Gamson et al.,

and Wilke and Hougen used particles of varying sizes, but all experiments were conducted at very high d_v/d_p ratios.

Happel (103) has found from experiments that the pressure drop in moving beds was slightly higher than in packed beds. Happel had high d_v/d_p ratios in his experiments. On the basis of an analogy between momentum and heat transfer, this suggests that wall effects were present to a significant extent in the results under review.

It may be seen from the packed bed correlations, given by equations G1 and G2 and shown on Graphs 19 and 20, that beds having higher void fractions may be expected to have a lower Nusselt number for a given Reynold number. This is realistic, as low voidage beds have a higher fluid velocity and hence a higher heat transfer coefficient. This trend is not clearly shown in Graphs 19 and 20 for different solids in either the 3 or 4 inch columns. (Values of the voidages are given in Table 15, Appendix 4). The trend of reduced heat transfer with higher void fraction is more evident for the 3 inch than the 4 inch column. This indicates that the effect is not simply increased void fraction reducing gas velocity, and hence heat transfer. The results show a definite increase in wall effect from the 4 inch to the 3 inch column when separately comparing 6 mm. and 12 mm. ballotini. It is of interest to note that all the results for 12 mm. ballotini are invalidated by the error analysis. These heat transfer results have higher Nusselt numbers, as shown on Graph 19 for uncorrected results, than might be expected when the difference due to wall effect for 6 mm. ballotini between 4 inch and 3 inch columns is noted.

In considering the results shown in Graph 20, after analogue computer analysis, groupings can be attempted in terms of β values. Each group contains anomalies and whilst it is evident that high β values tend to reduce the heat transfer coefficient, even for corrected results, no clear pattern can be discerned.

Graph 18, for the corrected Nusselt number against Reynolds number, was plotted for results selected from error analysis. Graph 21 shows the same points as Graph 18, that is, the results selected after the error analysis, but without analogue computer analysis. Comparison of Graphs 18 and 21 shows that analogue computer analysis of the selected results tends to change the points at high Reynolds number, to indicate that a straight line could be drawn through the points. It is considered that the correlating line through the points on Graph 18 should not take account of the results for 6 mm. ballotini in the 3 inch column, as these results are lower than a simple voidage correction term would suggest.

An equation is proposed, therefore, to describe the gas film heat transfer coefficient in terms of the gas velocity. The limits of the equation will be similar to those under which the experimental results were obtained. That is, bed to particle diameter greater than 8:1. The gas flow rate is constrained between the range 268 to 3,471 lb/hr. ft^2, and the solids flow rate between 518 and 4,516 lb/hr. ft^2.

$$Nu = 0.002568\ Re'^{1.290} \qquad G3$$

The correlation constants were determined by a least mean squares fit of the selected data shown on Graph 18.

It will be noticed from a comparison of the heat transfer data in Graphs 19 and 20 and Tables 14 and 18, Appendix 4, that there is very little intraparticle temperature distribution in the $\frac{1}{2}$ inch ceramic spheres. The reason for this is the low Biot number and high modified Fourier number for these results, because of the high thermal conductivity of alumina ceramics. It is suggested that equation G 3 could be used to predict moving bed gas film heat transfer coefficients in a 4 inch column for spherical particles of diameter between 6 mm. and 12 mm., and of thermal conductivity between that of the ballotini and alumina ceramic.

Equation G 3 predicts only the gas film heat transfer coefficient. From this value, a Biot number can be calculated. The modified Fourier number can be calculated from the physical measurements of the bed and solids thermal conductivity. To determine the temperatures of the gas and solids outlets, it is necessary to use an analogue computer to take account of the intraparticle temperature distribution.

(iii) Moving Bed Results in terms of h_g and G_g/d_p

Löf and Hawley (19) and Ross (1) are apparently the only researchers to use the h_g against G_g/d_p form of correlation. It will be recalled from sections A and C that Löf and Hawley, and Ross did not calculate the specific surface for heat transfer, a, but chose to plot $h_g a$. Graph 22 shows all the uncorrected moving bed results plotted as h_g against G_g/d_p. Ross's equation, given by A 3, has been seen to take the form of equation B 4.

It is seen from Graph 22 that Ross's correlation, when used in the form of equation B 4, separates the results widely. For each sphere and column diameter, the constant $\frac{0.025\ d_p}{Ax\ (1-e)}$ from equation B 4 has been evaluated for the moving bed results, and the corresponding correlation lines drawn on Graph 22. These lines drawn from equation B 4 do not correlate the experimental results. There is some correspondence between the 12 mm. ballotini and $\frac{1}{2}$ inch ceramic spheres in the 4 inch column but no correlation may be made. Ross's form of equation is seen in Graph 22 to predict higher heat transfer coefficients for 6 mm. and 12 mm. ballotini in 3 inch than in 4 inch columns. This is incorrect, as may be seen both from the experimental results on Graph 22 and Graphs 19 and 20. Equation B 4 is considered to take insufficient account of particle diameter. The difference between the form of Ross's equation B 4, and Yoshida's equations expressed as C 17 and C 18, is the appearance of the term (1-e) in the denominator of Ross's equation and the numerator of Yoshida's equation.

The form of h_g correlation in terms of G_g/d_p, as suggested by Löf and Hawley, and Ross, is not found to be of any advantage in correlating the moving bed results.

(iv) Comparison of Theoretical Moving Bed Heat Transfer Data With and Without Intraparticle Temperature Distribution

Some work has been carried out to investigate the difference between the analogue computer analysis and results calculated from equation D 6. For a Biot number of 0.05 and 0.1, β values of 0.5, 1, 2, and 2.5 were chosen.

The TR 10 analogue computer was used in the following manner. An initial condition, that is, gas outlet temperature, was chosen, and the computation begun. The computation was stopped when the gas temperature reached a value of unity. This is the value corresponding to the bottom of the column. The time of computation was recorded to give the modified Fourier number. The mean solids outlet temperature was noted, and the following expression was calculated:

$$f(T) = \frac{T_{go} - T_{si}}{T_{gi} - T_{sm}} = \frac{\theta_{go} - 0}{1 - \theta_{sm}} \qquad \ldots\ldots\ldots G\ 4$$

For each value of Biot number and β, a table of f (T) against Fo_1 was drawn up to try using different initial conditions, that is, gas outlet temperatures.

For values of f(T) calculated by the analogue computer, values of Fo_1 were calculated from equation D 6 for the same Biot number and β value. These results are given in Table 19 and Graphs 23 and 24, Appendix 4.

Graphs 23 and 24 show that intraparticle temperature distribution is present in theoretical models of moving beds even at low Biot numbers. Intraparticle temperature distribution is more significant at the Biot number of 0.1 rather than 0.05

Some criterion by which the significance of the separation of the curve pairs on Graphs 23 and 24 is desirable. It is suggested for design purposes that equation D 6 be used to calculate a value of f(T) for a value of the Biot number, β, and Fo_1. From graphs, which might be prepared similar to Graphs 23 and 24, the separation in f(T) could be observed between the two methods of calculation for the same Biot number. If the separation is greater than an acceptable value, it would then be necessary to resort to an analogue computer to calculate the correct Biot number and f(T).

(v) Suggestions for Future Work

The need has been stressed in part (ii) of this section for more reliable moving bed experimental data. Several recommendations can be made in the design of moving bed experimental apparatus.

It is desirable that the gas outlet temperature may be measured correctly. This is difficult because the intermittent nature of the addition of solids has a marked effect on the gas outlet temperature at any instant. Regular and even addition of solids could be made through side arms at the top of the bed. Such side arms could be made quite airtight with a sliding shutter to control solids addition. Outlet gas could then be expelled to the atmosphere through a small orifice. A thermocouple placed in this orifice would be able to record the temperature of the mixed gas outlet. This recording would give the true mean gas outlet temperature.

For measuring the solids outlet temperature, a thermocouple, made from fine gauge wire, would be better positioned from below the gas inlet than from above as in the present work. This arrangement would eliminate any gas bypassing around the thermocouple probe. Thermocouple probes are of a design unnecessarily robust for this purpose, and tend to have a temperature response time of minutes rather than seconds.

With the suggested gas and solids outlet temperature recording, it is considered that much of the scatter evident in the present results could be eliminated. It is desirable to study moving beds of larger column diameter to reduce wall effects. It would not be desirable to perform all experiments without wall effects as this would make the problem unrealistic for many applications.

The model of the moving bed, as applied to the analogue computer solution, could readily be extended to include an axial diffusion term to account for wall effect. This is the technique suggested by Bischoff and Levenspiel (105) when no large scale bypassing of fluid is taking place. This analysis could be developed for use with the hybrid TR48 computer.

It has been shown in this section that graphs similar to Graphs 23 and 24 might prove useful to estimate the importance of intraparticle temperature distribution. It is suggested that further computation to extend Graphs 23 and 24 would help the design of moving bed heat transfer apparatus.

CONCLUSIONS

An apparatus has been constructed and used to study moving bed heat transfer. A thermocouple probe, placed out of the gas inlet stream, was used to record the solids outlet temperature. It was considered more probable that this temperature was the mean temperature of the solids outlet than the surface temperature of the solids. The solids outlet temperature was used to calculate the gas outlet temperature through the heat balance.

The heat transfer coefficient results obtained in this manner were subjected to an error analysis, to eliminate those results having probable high errors with respect to errors in solids outlet temperature measurements. The selected results were analysed further, assuming intraparticle temperature distribution. This analysis was carried out using a hybrid TR48 computer. The results analysed in this manner showed a relation between the Nusselt number, based on the gas film heat transfer coefficient, and Reynolds number, and the following equation was proposed:

$$Nu = 0.002568\ Re'^{1.290}$$

It was proposed that this equation should be used to calculate a gas film heat transfer coefficient for a given gas flow rate for a moving bed. This equation is applicable for d_v/d_p ratios of 8:1, for gas flow rates between 268 and 3,471 lb/hr ft^2 and solids flow rates between 518 and 4,516 lb/hr ft^2. It was appreciated that increasing solids flow rates tended to reduce gas film heat transfer coefficients, due to increased intraparticle temperature distribution. No definite relationship between the gas film heat transfer coefficient and the solids flow rate was evident. It is considered that the proposed equation is independent of solids flow rate under the conditions specified for its use.

Moving bed heat transfer research could be continued experimentally and theoretically. An improved experimental arrangement is proposed, and suggestions are made for futher computer analysis of moving bed mathematical models.

Appendix 1

(Referring to Section B)

GRAPH 1. PLOT OF BOWERS AND REINTJES (18) AND NORTON'S (14) DATA.

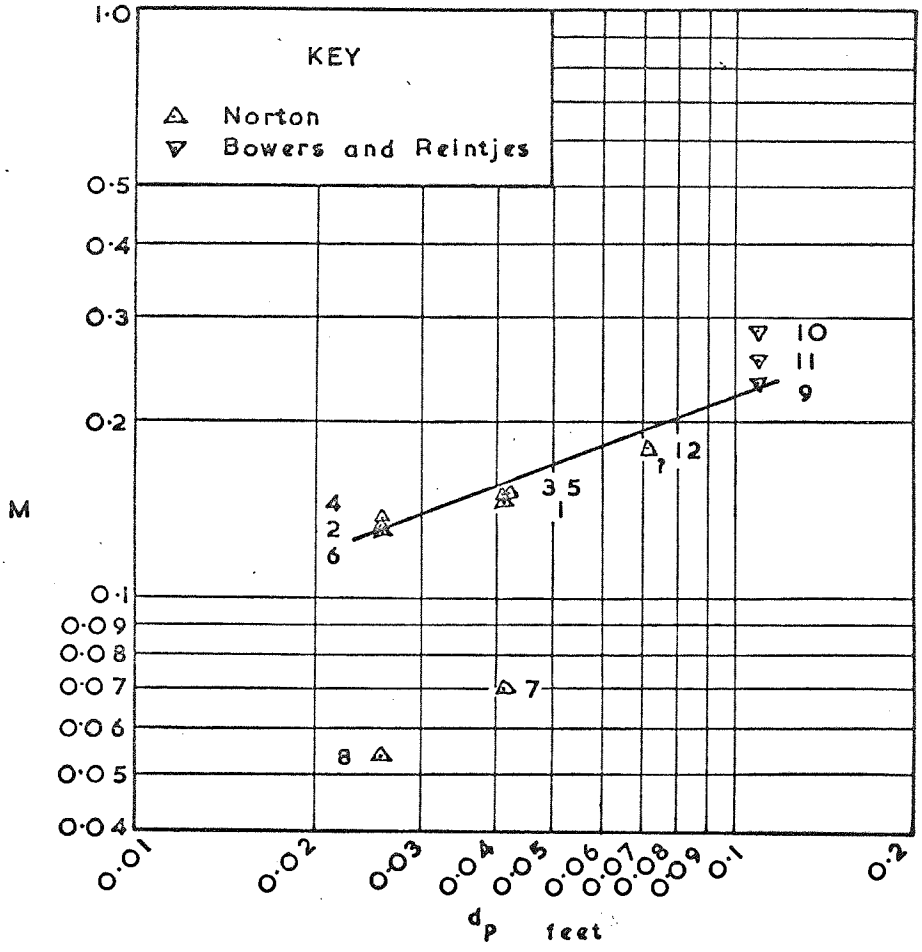

GRAPH 2 PLOT OF HEAT TRANSFER COEFFICIENT AGAINST GAS MASS FLOW RATE FOR THE RESULTS OF BOWERS AND REINTJES (18) AND NORTON (14). Key as for graph 1.

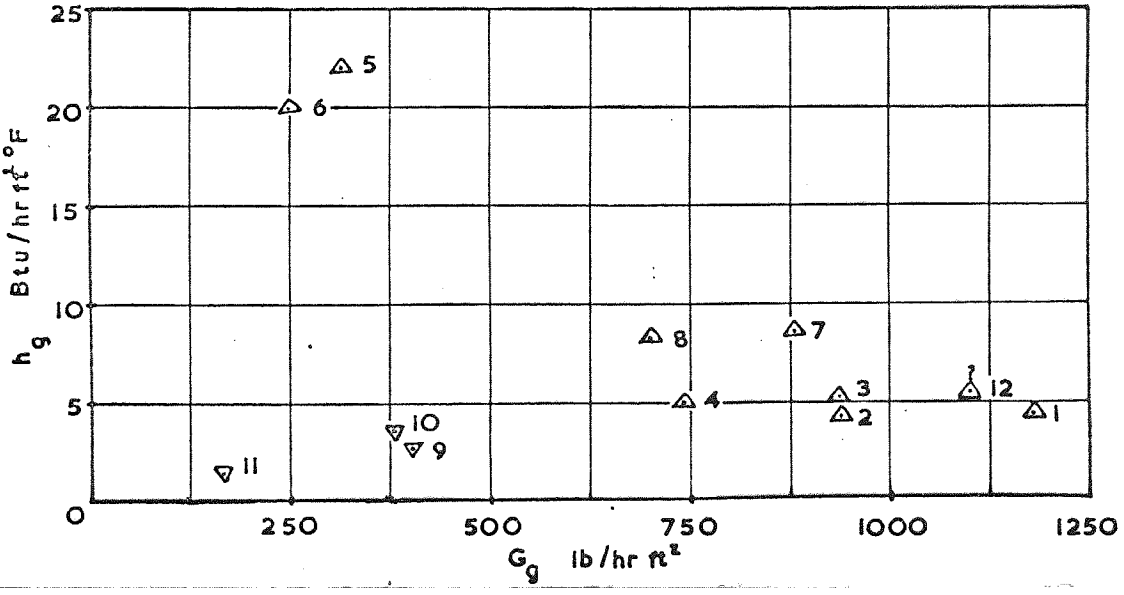

GRAPH 3. BOWERS AND REINTJES'S INTERPRETATION OF LÖF AND HAWLEY'S RESULTS (19) TABLES 2 TO 5.

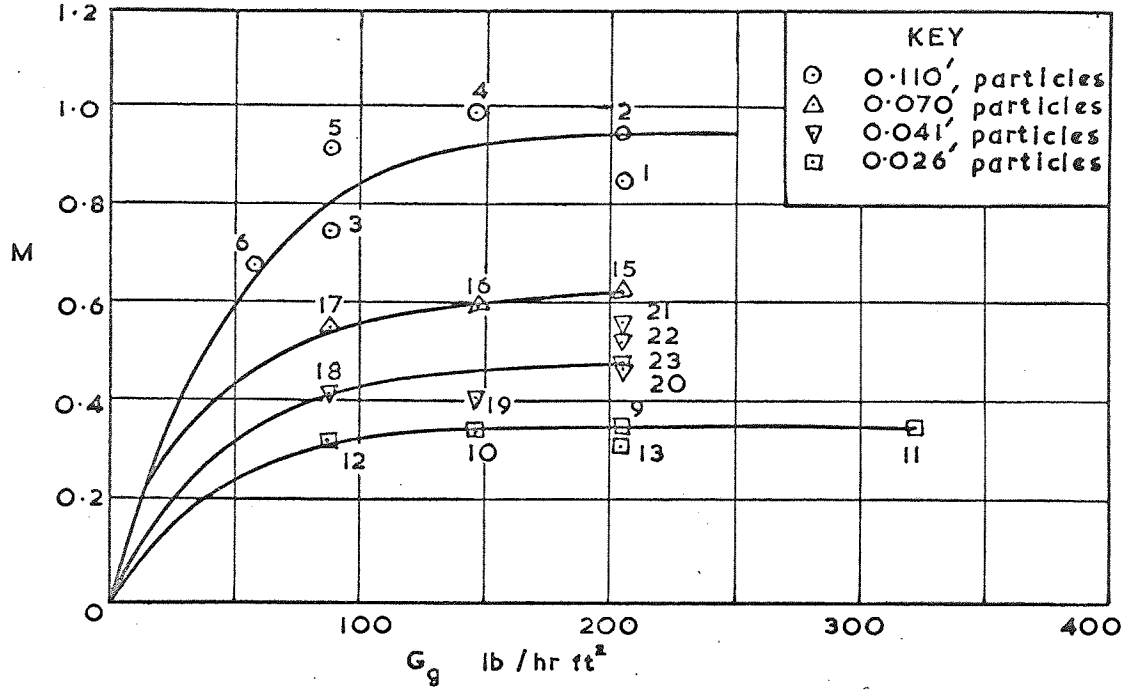

GRAPH 4 BOWERS AND REINTJES'S PLOT OF LÖF AND HAWLEY'S DATA (19) TABLES 2 TO 5.

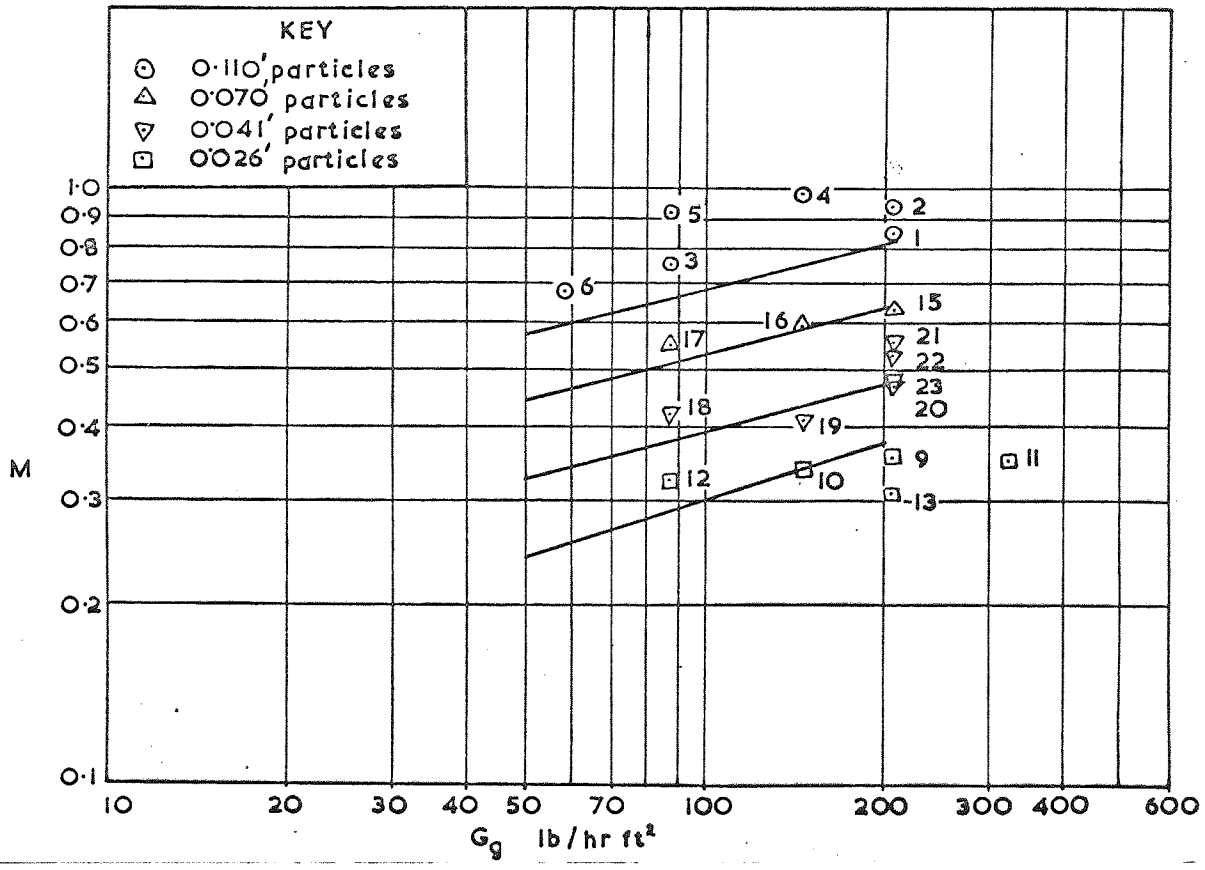

Table 1 Results of Bowers and Reintjes (18) and Norton (14)

Results	Fluid	Solid	G_g	h_g	M	d_p	References
1	Air	Pebbles	1180	4.5	0.145*	0.0416	14
2	Air	"	938	4.3	0.131*	0.0260	"
3	Steam	"	933	5.3	0.148*	0.0416	"
4	Steam	"	748	5.0	0.133*	0.0260	"
5	Hydrogen	"	312	22.0	0.148*	0.0416	"
6	Hydrogen	"	248	20.0	0.129*	0.0260	"
7	Methane	"	880	8.7	0.0695	0.0416	"
8	Methane	"	698	8.2	0.0536	0.0260	"
9	CO_2, N_2 Steam	Coal Briquettes	404*	2.8*	0.230*	0.110	18
10	"	"	379*	3.6*	0.280*	0.110*	"
11	"	"	166*	1.5*	0.250*	0.110*	"
12	Steam	Pebbles	1100*	5.6*	0.178*	0.072	"

* Values calculated by Bowers and Reintjes (18)

Table 2 Lof and Hawley's Results (19) for the heating of a fixed bed of gravel by air

Void fraction = 0.434, particle diameter = 0.1095 ft,
Specific surface a = 31.0 ft^{-1}, a^* = 32.0 ft^{-1}.

Results	G_g	T_{gi} °F	$h_g a$	h_g^*	h_g	M^*	$T_g^*(av)$ °F
1	204.5	200	146	4.55	4.71	0.85	150
2	204.5	160	162	5.05	5.22	0.94	125
3	87.6	150	76	2.37	2.45	0.75	125
4	145.8	200	139	4.35	4.48	0.99	150
5	87.6	200	97	3.03	3.13	0.92	150
6	58.2	200	56	1.75	1.81	0.68	150
+ 7	204.5	250	194	6.05	6.26		
+ 8	204.5	250	194	6.05	6.26	1.09	187

*Values calculated by Bowers and Reintjes (18)

+ Erroneous points, omitted by Lof and Hawley from their final equation (B14), and not shown on graphs 2 and 3

Table 3 Löf and Hawley's results (19) for the heating of a fixed bed of gravel by air

Void fraction = 0.454, particle diameter = 0.0262 ft,
Specific surface a = 125.5 ft^{-1}, a^{*} = 128.0 ft^{-1}

Results	G_g	T_{gi} °F	$h_g a$	h_g^{*}	h_g	M*	$T_{g(av)}$ °F
9	204.5	200	437	3.42	3.46	0.355	150
10	145.8	200	346	2.70	2.76	0.340	150
11	322	200	561	4.39	4.46	0.350	150
12	87.6	200	242	1.89	1.93	0.325	150
13	204.5	250	404	3.15	3.24	0.320	187
+ 14	204.5	150	534	4.16	4.24	0.450	125

Table 4 Löf and Hawley's results (19) for the heating of a fixed bed of gravel by air

Void fraction = 0.436, particle diameter = 0.0697 ft
Specific surface a = 48.7 ft^{-1}, a^{*} = 51.2 ft^{-1}

Results	G_g	T_{gi} °F	$h_g a$	h_g^{*}	h_g	M*	$T^{*}_{g(av)}$ °F
15	204.5	200	210	4.10	4.31	0.630	150
16	145.8	200	162	3.17	3.33	0.595	150
17	87.6	200	111	2.17	2.24	0.550	150

* Values calculated by Bowers and Reintjes (18)

\+ Erroneous point, omitted by Löf and Hawley from their final equation (B14), and not shown on graphs 2 and 3

Table 5 "Lof and Hawley's results (19) for the heating of a fixed bed of gravel by air

Void fraction = 0.426, particle diameter = 0.0411 ft,
Specific surface a = 84.2 ft^{-1}, a* ≃ 85.0 ft^{-1}

Results	G_g	T_{gi} °F	$h_g a$	h_g^*	h_g	M	$T^*_{g(av)}$ °F
18	87.6	200	174	2.05	2.10	0.420*	150
19	145.8	200	231	2.72	2.74	0.410*	150
20	204.5	200	291	3.81 (3.43?)	3.46	0.470*	150
21	204.5	200	340	-	4.04	0.558	-
22	204.5	200	324	-	3.85	0.527	-
23	204.5	200	291	-	3.46	0.477	-

* Values calculated by Bowers and Reintjes (18)

Table 6 Data of Kilpatrick et al. (15,16,17), recalculated by Bowers and Reintjes (18)

Fluid	Solid	G_g	h_g	M	d_p
Flue Gas	Pebbles	630	2.6	0.09	0.031
"	"	630	2.4	0.078	"
"	"	620	2.5	0.085	"
"	"	600	1.2	0.043	"

APPENDIX 2

(Refers to Section D.)

Computer Programme 1

Calculation of eigenvalue of tan a_n = a_n /(1 - Bi)
Newton's Method.

1	INP	19	C4
2	C1-	20	L5-
3	D1-	21	M2-
4	C6-	22	S4-
5	S1-	23	D7-
6	C1-	24	C7
7	INP	25	/A/
8	C2-	26	S8
9	COSINE	27	IF - JMP 31
10	C4-	28	L2-
11	M4-	29	S7-
12	M1-	30	JMP 8
13	C5-	31	L2-
14	S6-	32	S7
15	C7-	33	C/R
16	L2-	34	TYPE
17	SINE	35	JMP 7
18	M4-	36	RETAIN

Step 1 inputs the Biot number. Step 7 inputs an approximate eigenvalue. Eigenvalues are accurately estimated from plots of tan a_n against a_n, and $a_n/(1 - Bi)$ against a_n.

A test value Δ is stored in scratchpad location 8, and is used in the programme to test between successive values of the eigenvalue found from the programme's successive application of Newton's Method. This is shown as step 26; and the conditional jump, step 27. The programme then returns to step 7 to determine another eigenvalue.

Specimen results are shown below

Bi	a_1	a_2	a_3	a_4	a_5
0.1	0.5424	4.5157	7.7382	10.9133	14.0734
0.2	0.7593	4.5379	7.7511	10.9225	14.0804
0.3	0.9208	4.5601	7.7641	10.9316	14.0874
0.4	1.0528	4.5822	7.7770	10.9408	14.0946
0.5	1.1656	4.6043	7.7899	10.9499	14.1018
0.6	1.2644	4.6262	7.8028	10.9592	14.1088
0.7	1.3525	4.6480	7.8156	10.9683	14.1160
0.8	1.4320	4.6696	7.8284	10.9774	14.1230
0.9	1.5044	4.6911	7.8413	10.9865	14.1301
1.0	1.5703	4.7120	7.8537	.0.9954	14.1372

Table 6

SOLUTION OF EQUATION D 22

COMPUTER PROGRAMME 2

```
RET  1+
1.   INP
2.   C 3-
3.   D 3-
4.   C 5-
5.   S 5-
6.   C 6-
7.   C 7-
8.   INP
9.   C 8-
10.  INP
11.  C 1-
12.  M 1-
13.  M 3-
14.  C 2-
15.  L 6-
16.  S 2-
17.  EXP
18.  C 2-
19.  L 8-
20.  M 1-
21.  C 8-
22.  SINE
23   D 8-
24.  C 8-
25.  L 1-
26.  SINE
27.  C 4
28.  L 1-
29.  COSINE
30.  C 9-
31.  M 1-
32.  C 10-
33.  L 9-
34.  M 4-
35.  C 11-
36.  L 1-
37.  S 11-
38.  C 11-
39.  L 4-
40.  S 10-
41.  D 11-
42.  C 11-
43.  A 11-
44.  M 8-
45.  M 2-
46.  A 7-
47.  C 7-
48.  L 5-
49.  S 7-
50.  C/R
51.  TYPE
52.  JMP 10-
53.  RETAIN
```

Steps 1 and 8 correspond to inputs of τ and x. Successive eigenvalues a are input at step 10 until the answer θ_s converges to a constant value.

When x = 0, equation D 22 becomes indeterminate. By L'Hopital's rule, equation D 22 becomes:

$$\theta_s = 1 - 2 \sum_{n=1}^{n=\infty} \left[\frac{\text{Sin } a_n - a_n \text{ Cos } a_n}{a_n - \text{sin } a_n \text{ Cos } a_n} \right] e^{-a_n^2 \tau}$$

For the sphere centre, the following programme is used.

COMPUTER PROGRAMME 3

RET 2+

1.	INP	23.	M 1-
2.	C 3-	24.	C 10-
3.	D 3-	25.	L 9-
4.	C 5-	26.	M 4-
5.	S 5-	27.	C 11-
6.	C 6-	28.	L 1-
7.	C 7-	29.	S 11-
8.	INP	30.	C 11-
9.	C 1-	31.	L 4-
10.	M 1-	32.	S 10-
11.	M 3-	33.	D 11-
12.	C 2-	34.	C 11-
13.	L 6-	35.	A 11-
14.	S 2-	36.	M 2-
15.	EXP	37.	A 7-
16.	C 2-	38.	C 7-
17.	L 1-	39.	L 5-
18.	SINE	40.	S 7-
19.	C 4-	41.	C/R
20.	L 1-	42.	TYPE
21.	COSINE	43.	JMP 8
22.	C 9-	44.	RETAIN

Step 1 is for input of τ. Step 8 is for successive eigenvalues, a.

GRAPH 5.

Unsteady State Heat Transfer to a Sphere, Convection Boundary Conditions.

Biot Number = 1·000, x = 1·000

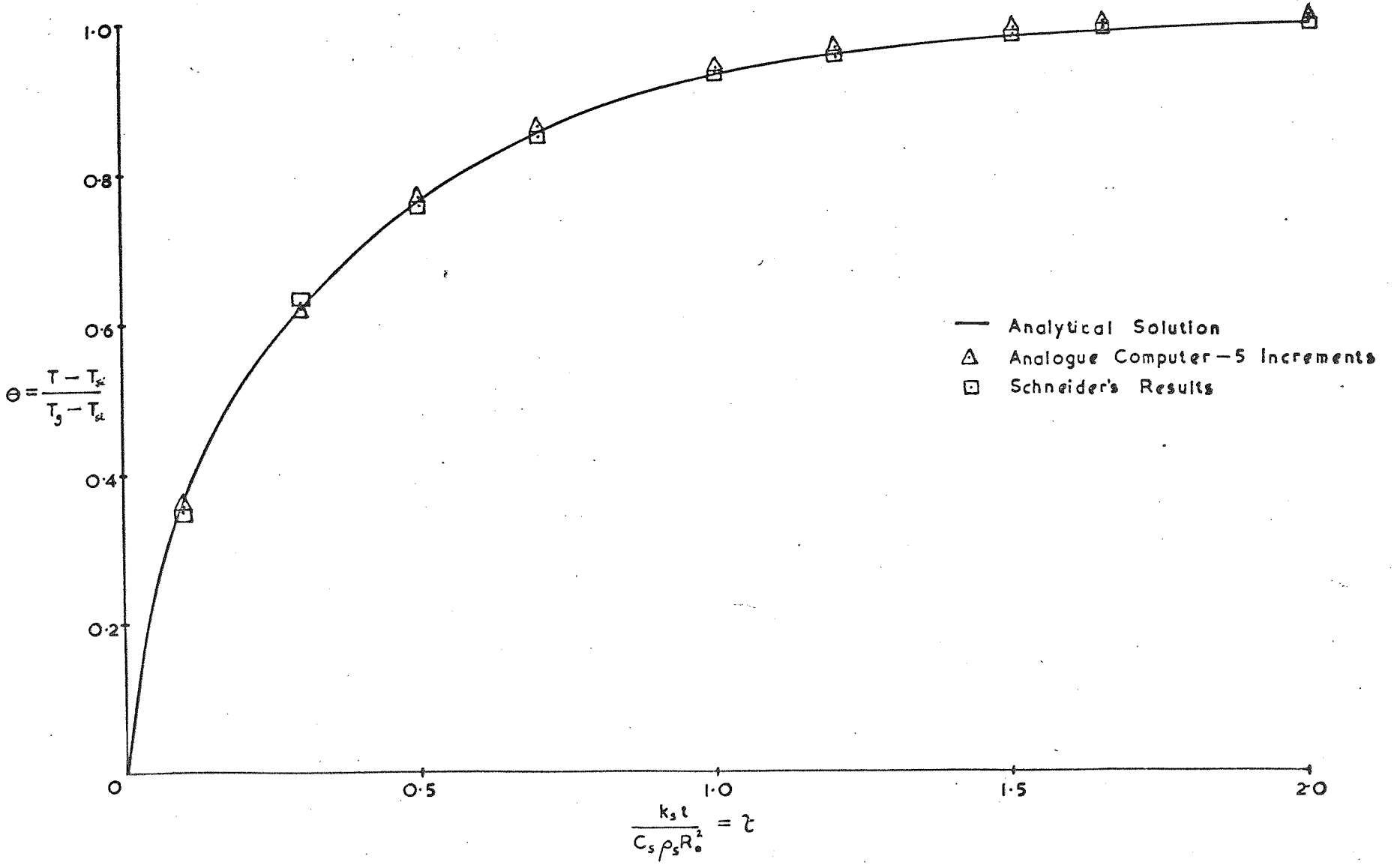

GRAPH 6.

Unsteady State Heat Transfer to a Sphere, Convection Boundary Conditions.

Biot Number = 1·000, x = 0·800

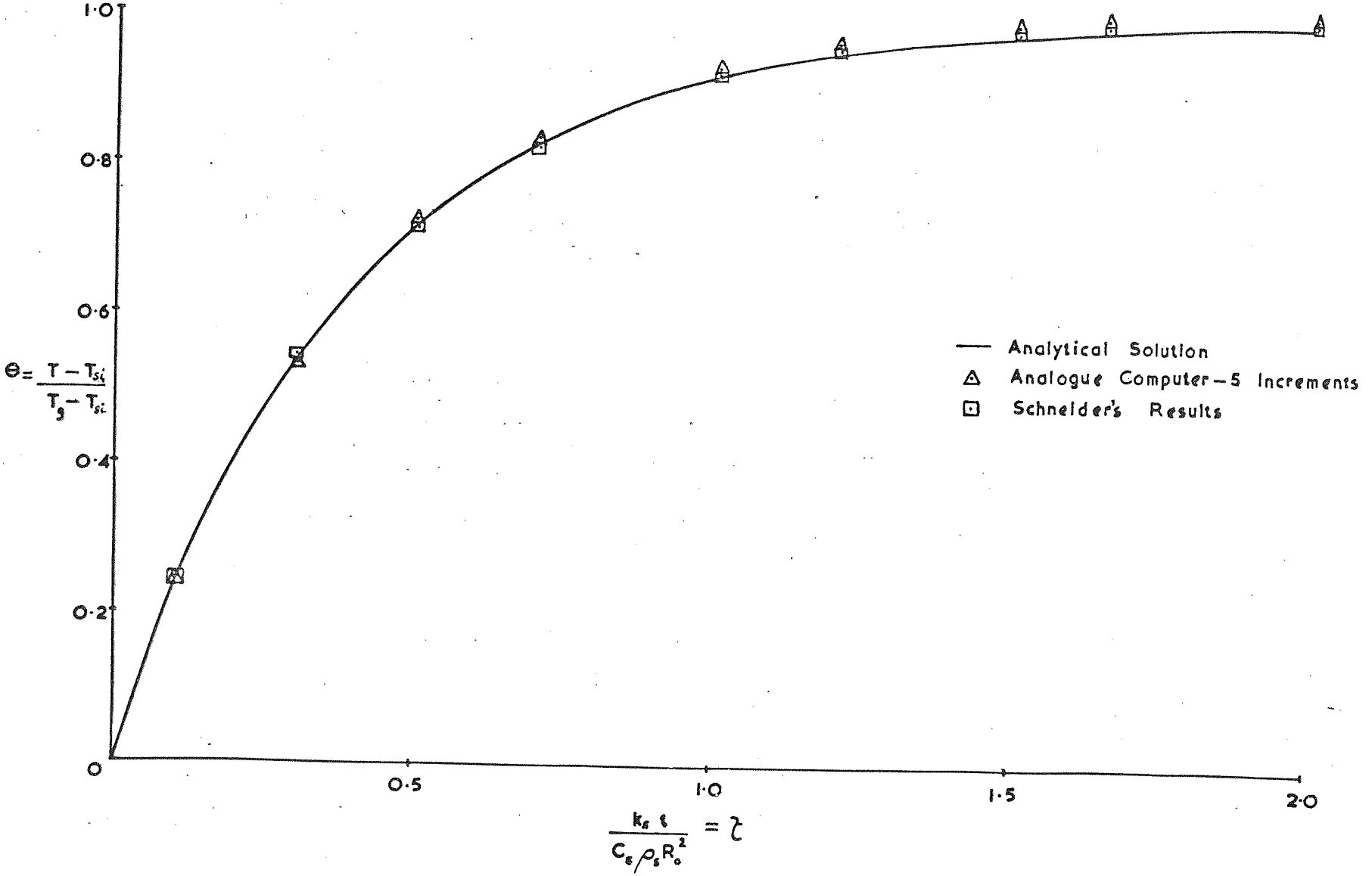

GRAPH 7.

Unsteady State Heat Transfer to a Sphere, Convection Boundary Conditions.

Biot Number = 1·000 , x = 0·400

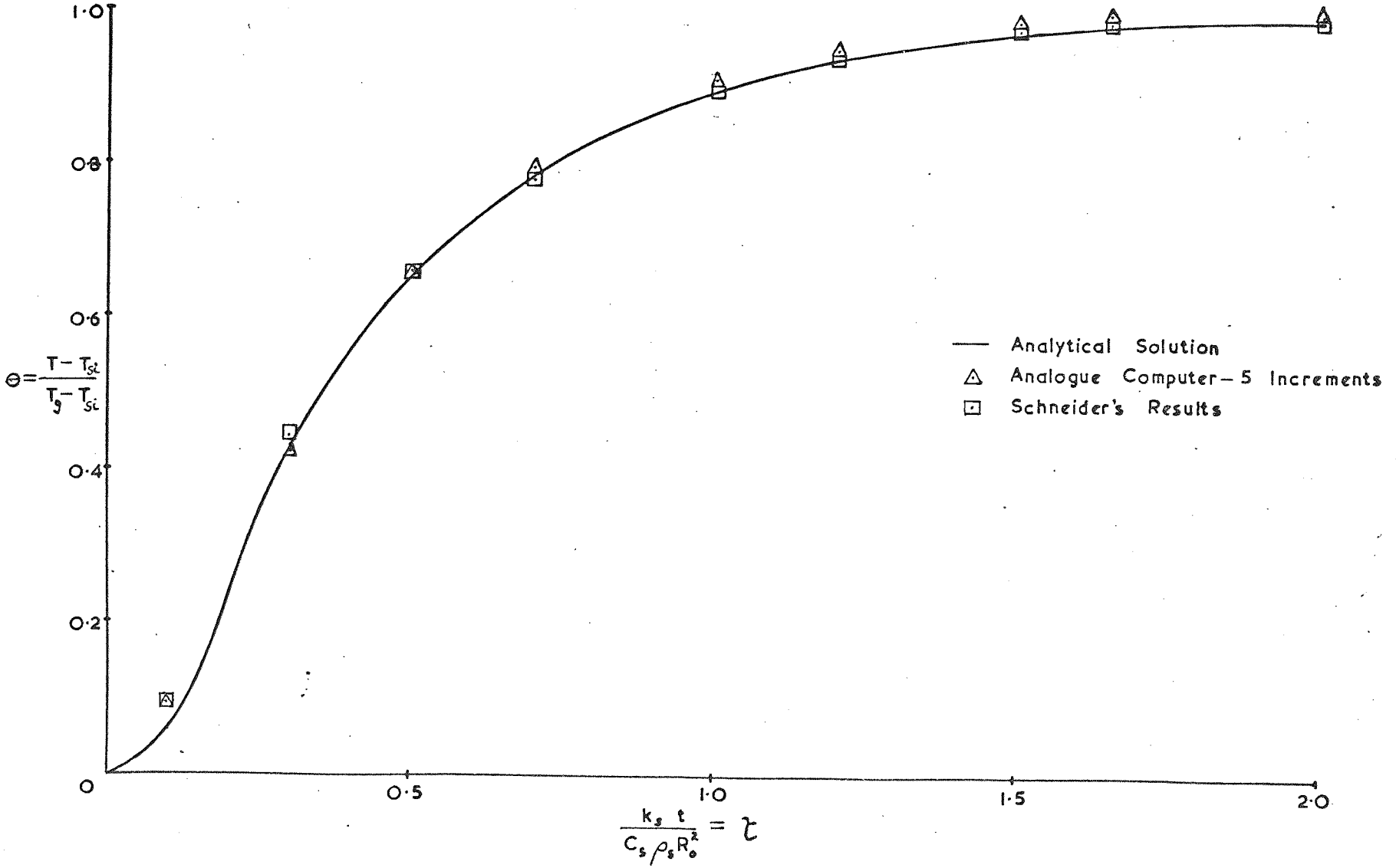

GRAPH 8.

Unsteady State Heat Transfer to a Sphere, Convection Boundary Conditions.

Biot Number = 1·000 , x = 0·000

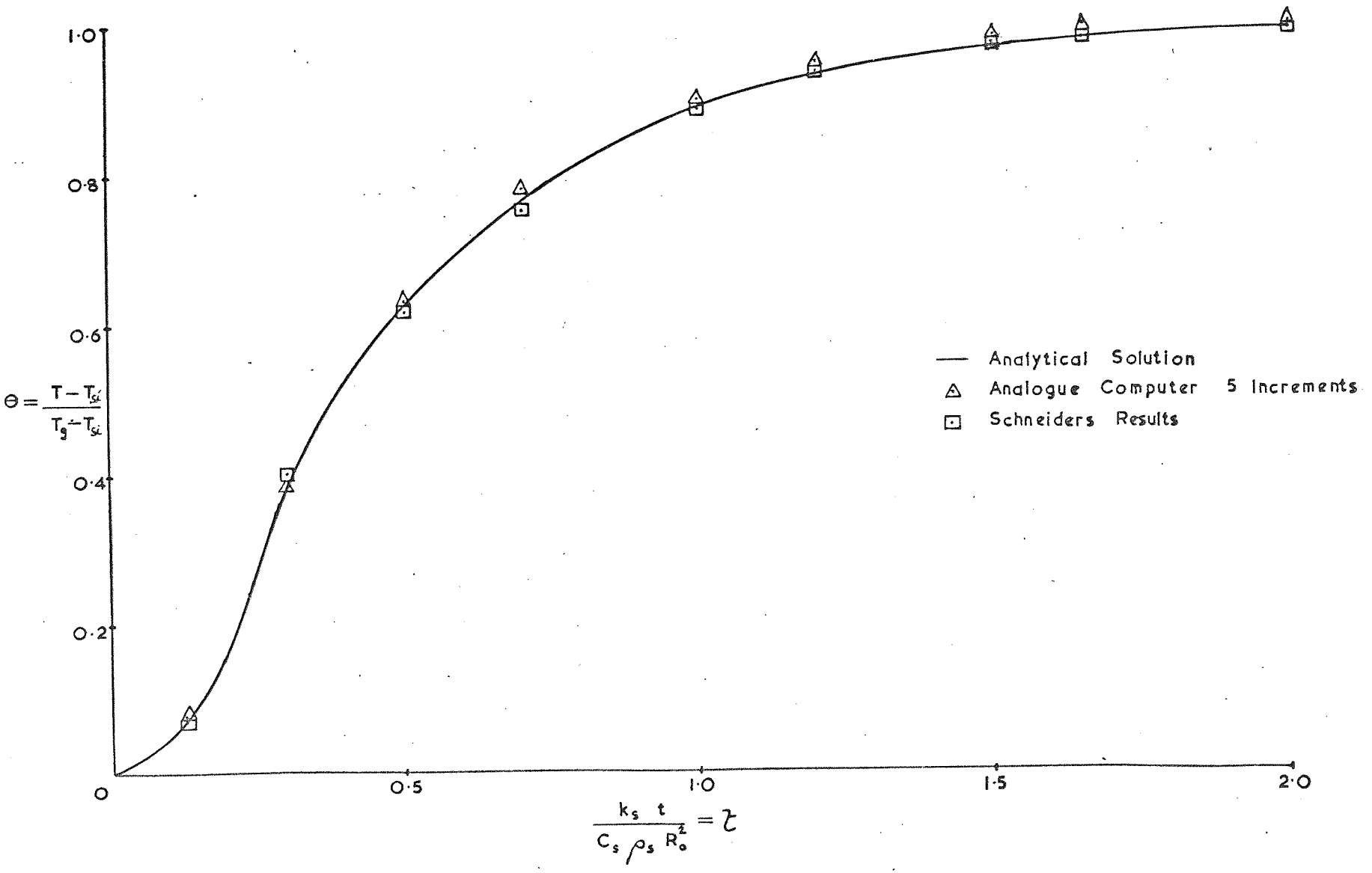

Table 7

Unsteady State Heat Transfer to a Sphere. (Biot No. = 1.000)

	τ	0.1	0.3	0.5	0.7	1.0	1.2	1.5	1.65	2.0	2.5
	Schneider(55)	0.355	0.620	0.760	0.850	0.935	0.960	0.982	0.990	0.998	-
x = 1	Analogue	0.360	0.612	0.766	0.863	0.940	0.969	0.993	1.000	1.000	-
	Analytical	0.3681	0.6131	0.7637	0.8557	0.9311	0.9579	0.9799	0.9861	0.9942	-
									1.69		
	Schneider(55)	0.242	0.542	0.715	0.820	0.920	0.955	0.980	0.990	0.998	1.000
x = 0.8	Analogue	0.242	0.538	0.724	0.836	0.928	0.962	0.990	1.000	1.000	1.000
	Analytical	0.2412	0.5400	0.7192	0.8285	0.9181	0.9500	0.9761	0.9851	0.9930	0.9980
									1.69		
	Schneider(55)	0.098	0.445	0.655	0.780	0.898	0.940	0.972	0.985	0.992	1.000
x = 0.4	Analogue	0.097	0.429	0.658	0.798	0.912	0.954	0.988	1.000	1.000	1.000
	Analytical	0.0590	0.4315	0.6529	0.7880	0.8988	0.9382	0.9705	0.9815	0.9914	0.9975
									1.70		
	Schneider(55)	0.050	0.410	0.620	0.755	0.890	0.938	0.970	0.980	0.990	0.998
x = 0.0	Analogue	0.057	0.389	0.633	0.783	0.904	0.949	0.986	1.000	1.000	1.000
	Analytical	0.0506	0.3930	0.6290	0.7734	0.8919	0.9340	0.9685	0.9808	0.9908	0.9973

Table of Temperature Comparisons

GRAPH 9.
LOVELL & KARNOFSKY'S
CALCINATION OF LIME PROBLEM.

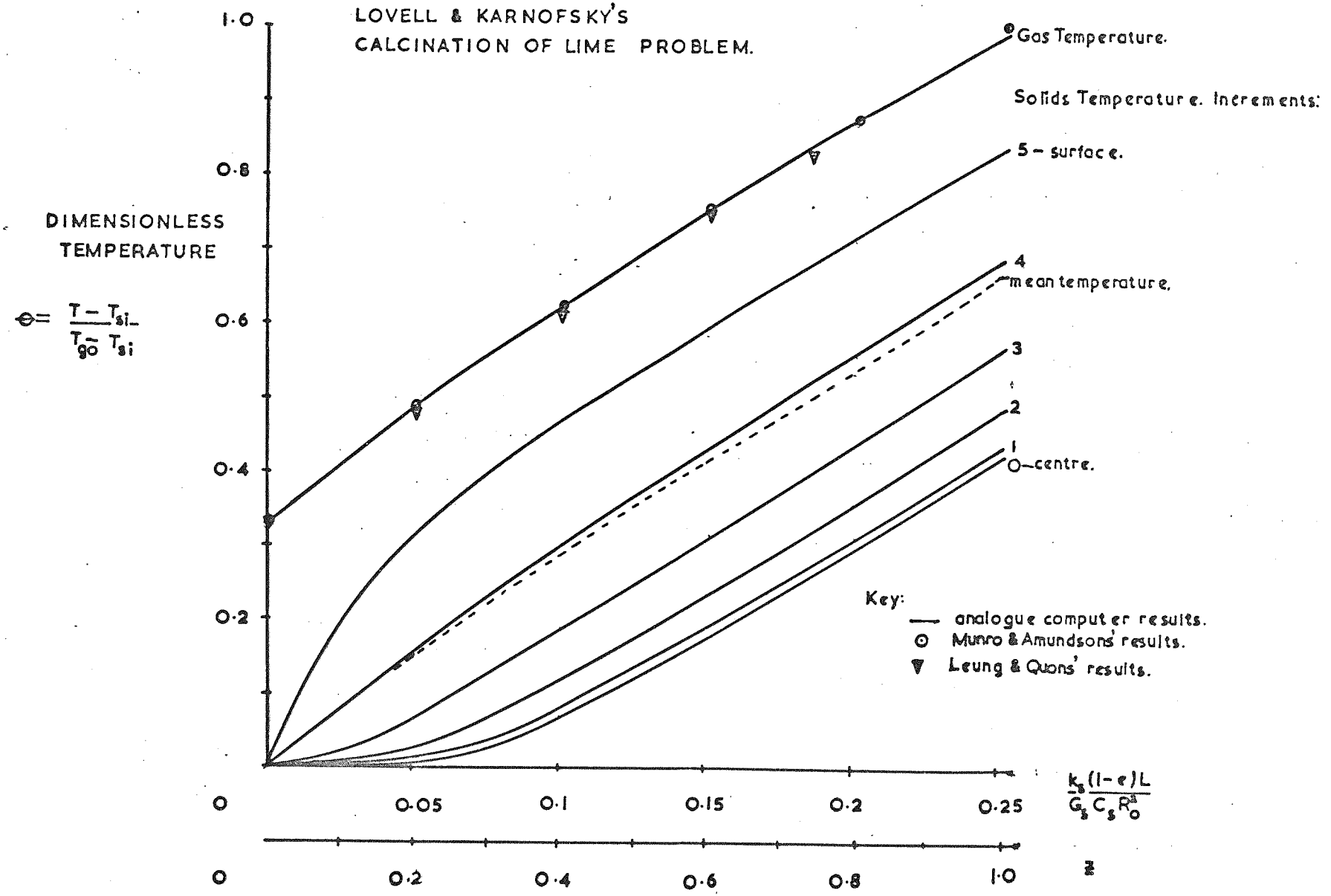

Table 8 - Comparison of Solutions to Lovell and Karnofsky's Problem (56)

(A) - Results of Munro and Amundson (49) and Leung and Quon (50).

$\frac{k_s(1-e)1}{G_s c_s R_o^2}$	Z	Munro and Amundson θ *	Leung and Quon θ digital	θ analogue +
0.253	1.000	1.000		
0.202	0.800	0.874		
0.185	0.733		0.830	0.833
0.152	0.600	0.747		
0.150	0.593		0.743	0.740
0.101	0.400	0.620		
0.100	0.395		0.616	0.617
0.0506	0.200	0.488		
0.050	0.198		0.486	0.490
0	0	0.333	0.333	0.333

* Recalculated during present research.

(B) - Result of Present Computation on a PACE TRIO Analogue Computer

z	1.000	0.800	0.600	0.400	0.200	0.000
θ	0.998	0.870	0.747	0.620	0.488	0.333
θ_5	0.835	0.710	0.581	0.451	0.313	0
θ_4	0.683	0.558	0.430	0.300	0.158	0
θ_3	0.566	0.440	0.316	0.190	0.069	0
θ_2	0.482	0.359	0.236	0.120	0.026	0
θ_1	0.432	0.310	0.190	0.080	0.010	0
θ_o+	0.419	0.294	0.173	0.070	0.006	0
θ_m	0.667	0.536	0.413	0.287	0.155	0

+ Not plotted on Graph 9 for the sake of clarity.

APPENDIX 3

(Referring to Section E)

Computer Programme 4 Calculation of Gas Flow Rates from Rotameter Measurements

RETAIN 1+

1. INP
2. C1-
3. INP
4. C2-
5. INP
6. C10-
7. INP
8. C11-
9. INP
10. C7-
11. INP
12. A6-
13. C8-
14. L3-
15. M7-
16. D5-
17. M6-
18. D8-
19. C9-
20. L2-
21. S9-
22. C17-
23. L8-
24. M6-
25. LOG
26. M12-
27. EXP
28. C15-
29. L8-
30. A13-
31. C16-
32. L6-
33. A13-
34. D16-
35. M15-
36. M14
37. D9-
38. C4-
39. L2-
40. M9-
41. D1-
42. D17-
43. SQRT
44. C20-
45. M10-
46. M4-
47. LOG
48. D19-
49. A18-
50. C/R
51. TYPE
52. L11-
53. D20-
54. TYPE
55. C21-
56. INP
57. TYPE
58. M21-
59. M7-
60. D5-
61. M6-
62. D8-
63. M22-
64. D24-
65. M23-
66. M18-
67. D26-
68. D26-
69. D25-
70. TYPE
71. JMP 9
72. RETAIN

Constants are required in the following Scratchpad locations before the programme is commenced

Scratchpad Location	3	5	6	12	13	14	18
Constant	1.293×10^{-3}	76.0	273.1	1.5	114.0	1.709×10^{-4}	4

Inputs at steps 1,3,5, and 7 are the Rotameter and float constants W, σ, K_1, and K_2. Upstream conditions for each result are input at steps 9 and 11 as pressure, cm. H_g, and temperature, ^{o}C. The computer calculates and prints out values of I and F_T. A value of f, taken from the appropriate rotameter chart of I against scale reading, is entered at step 56. The value of G_g is then calculated and printed out. The programme returns to step 9 for a further result.

The programme uses the Sutherland equation (62) to calculate air viscosity as a function of temperature:

$$\mu_g = 1.709 \times 10^{-4} \left[\frac{T_c + 114}{T_c + 387.1}\right] \left[\frac{T + 273.1}{T}\right]^{1.5}$$

GRAPH 10. CALIBRATION OF ROTAMETERS USING VENTURI METERS.

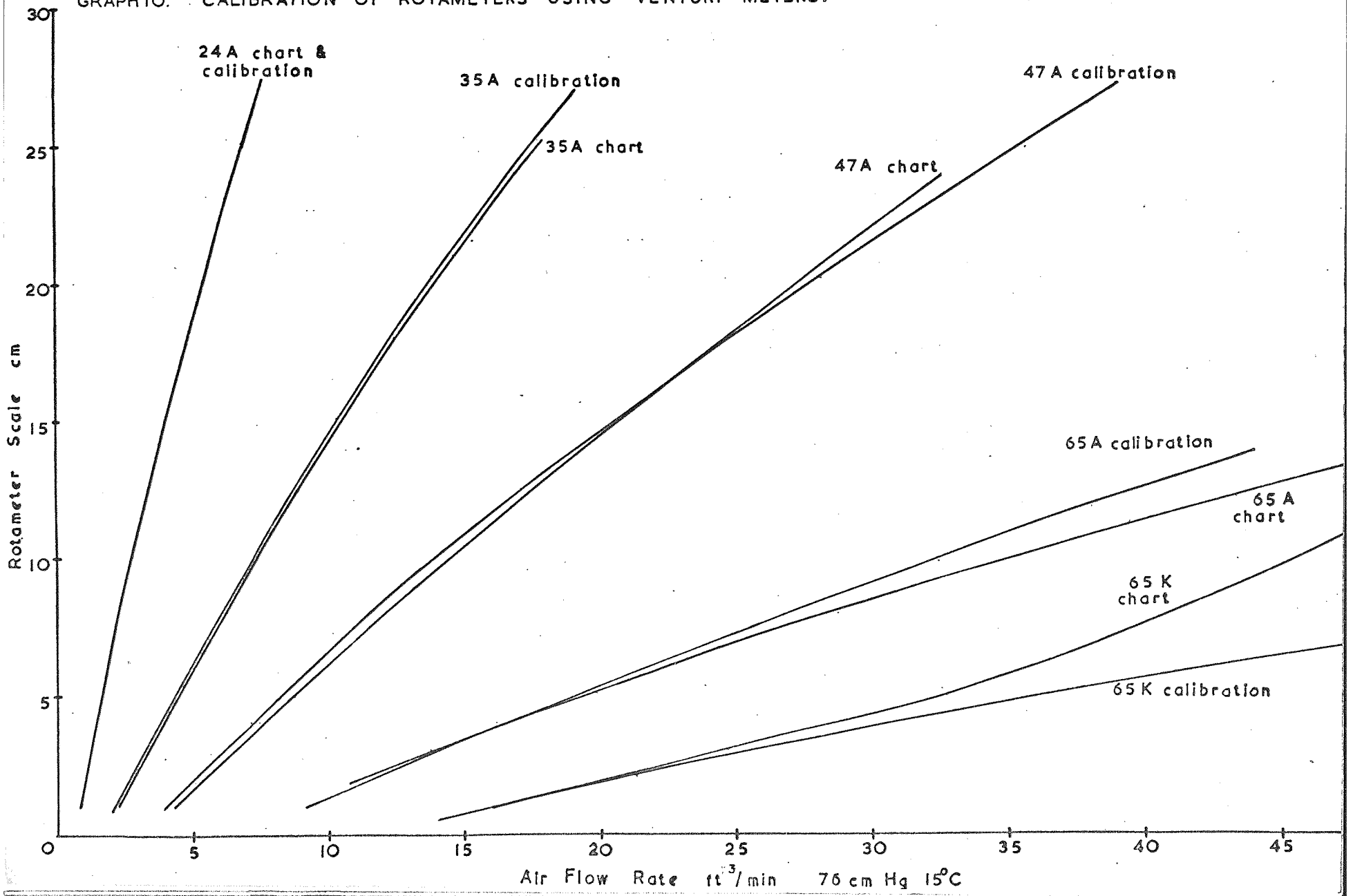

Table 8 Comparison of Rotameter Charts with Venturi Calibration
Q = ft^3/min at 76 cm H_g, 15°C

Rotameter 24A

Scale (cm)	2	5	10	15	19.5	25
Q (chart)	1.06	1.71	2.83	4.06	5.30	6.89
Scale (cm)	1	4.95	10.1	15	20	27.4
Q (Venturi)	0.76	1.63	2.78	3.99	5.35	7.55

Rotameter 35A

Scale (cm)	1	8	11	18	21	25.3
Q (chart)	2.30	6.18	7.95	12.36	14.60	17.65
Scale (cm)	0.85	5.1	10.2	15.05	20.25	26.9
Q (Venturi)	2.11	4.41	7.38	10.28	13.83	19.03

Rotameter 47A

Scale (cm)	1	5	9	14	19.5	24
Q (chart)	4.41	8.83	13.25	19.40	26.50	32.65
Scale (cm)	0.9	4.05	10.08	15.27	20.29	27.3
Q (Venturi)	4.01	7.22	14.14	20.87	28.15	39.03

Rotameter 65A

Scale (cm)	1	4.5	8	10	12	14
Q (Chart)	9.18	17.65	26.83	32.50	38.15	44.00
Scale (cm)	1.8	5.1	8	10.1	12.3	13.9
Q (Venturi)	10.8	19.85	28.75	35.4	43.4	49.5

Rotameter 65K

Scale (cm)	0.5	3	5	8	11	
Q (Venturi)	14.12	24.70	32.80	40.60	47.80	
Scale (cm)	0.95	2.1	4.1	5.1	5.95	7.25
Q (Chart)	16.07	21.35	31.18	36.47	41.24	49.44

GRAPH II.

THERMAL CONDUCTIVITY AGAINST TEMPERATURE FOR VARIOUS HIGH ALUMINA CERAMICS.

Results of Smoke and Koenig. Refer to Table 10.

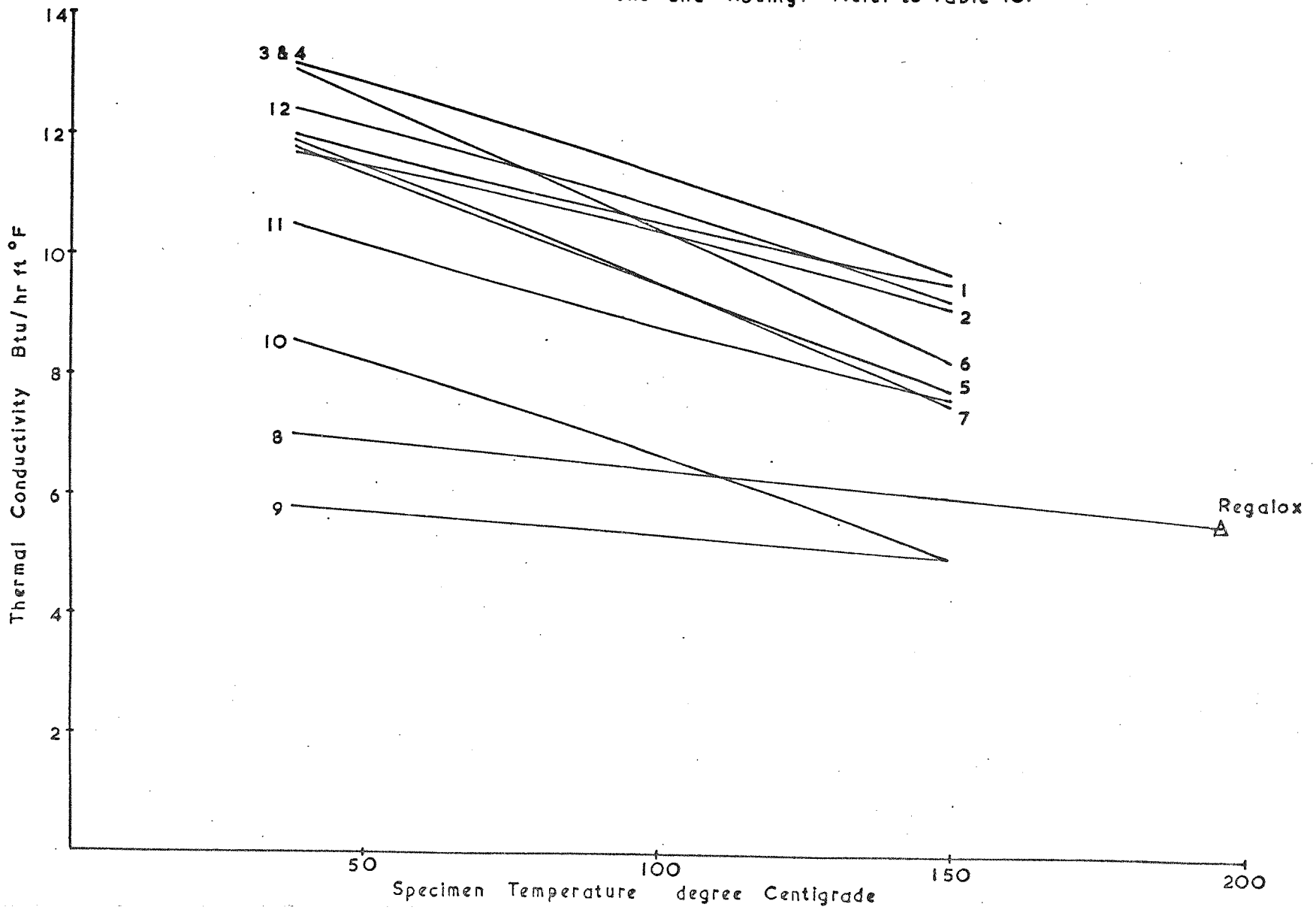

TABLE 9

RESULTS OF GINNINGS AND CORRUCCINI (85) FOR THE HEAT CAPACITY OF IMPURE ALUMINA IN THE TEMPERATURE RANGE 20 to 120°C.

c_s Btu/lb°F	0.183	0.192	0.201	0.216	0.224
T°C	20	40	60	100	120

TABLE 10

RESULTS OF SMOKE AND KOENIG (88) FOR THE THERMAL CONDUCTIVITY OF VARIOUS HIGH ALUMINA CERAMICS. (SEE GRAPH 11)

SPECIMEN	ALUMINA COMPOSITION	SPECIFIC GRAVITY	THERMAL CONDUCTIVITY, k_s Btu/hr ft °F		
			37.8°C	93.3°C	149°C
1	98%	3.70	12.0	10.7	9.6
2	95%	3.73	11.7	10.6	9.2
3	95%	3.67	13.2	11.6	9.8
4	95%	3.63	13.2	11.6	9.8
5	95%	3.54	11.8	10.0	7.8
6	94.5%	3.68	13.1	10.7	8.3
7	92.5%	3.59	11.9	9.8	7.6
8	89%	3.40	7.0	6.5	6.0
9	85%	3.31	5.8	5.4	5.0
10	85%	3.36	8.6	6.9	5.0
11	high	-	10.5	9.0	7.7
12	high	3.57	12.4	11.0	9.3
REGALOX	88%	2.45	5.57 at 195°C		

GRAPH 12.
THERMAL CONDUCTIVITY OF SODA GLASS BALLOTINI. Refer to Table II.

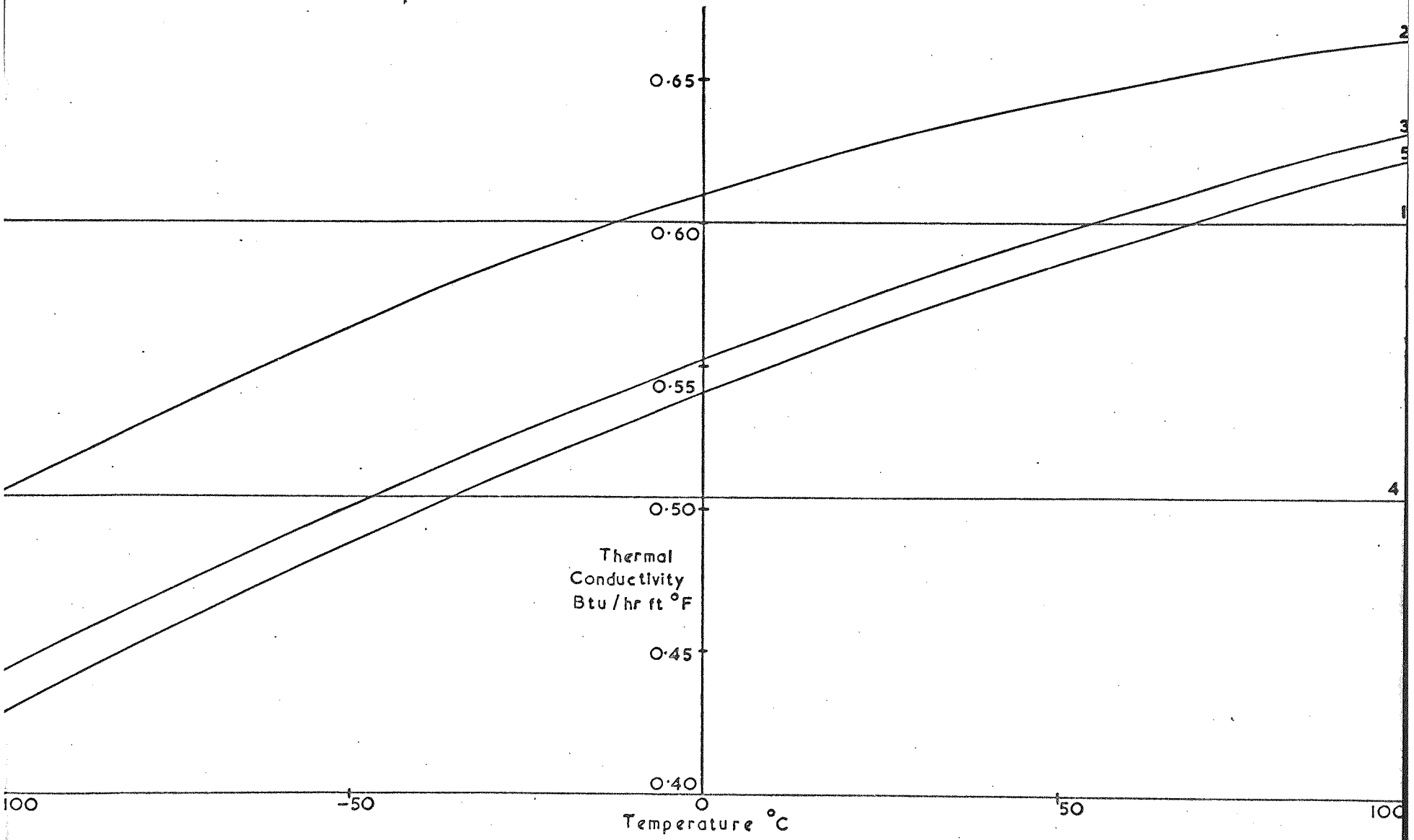

TABLE 11

THERMAL CONDUCTIVITY RESULTS FOR VARIOUS BALLOTINI

(SEE GRAPH 12)

KEY	k_s	T°C	REFERENCE
1	0.6		95
2	0.505	-100	97
	0.610	0	97
	0.665	100	97
3	0.442	-100	98
	0.553	0	98
	0.634	100	98
4	0.504		96
5	0.426	-100	PRESENT
	0.541	0	RESULTS
	0.623	100	"

TABLE 12

PHYSICAL PROPERTIES OF AIR

	0°C	32.4°C	60.2°C	88.0°C	115.8°C
k_g (Btu/hrft °F)	0.0140	0.0156	0.0168	0.0180	0.0191
C_g (Btu/lb°F)	0.2396	0.2399	0.2403	0.2409	0.2316
μ_g (lb/hrft)	0.0417	0.0453	0.0486	0.0515	0.0544

Computer Programmes 5, 6, and 7

are to be found in the folder at the back of the thesis

TABLE 13

OUTLET AIR TEMPERATURE RESULTS

(a) 12 m.m Ballotini in 3" Column

				Measured	Calculated		
RUN	T_{si}	T_{so}	T_{gi}	T_{go}	T_{go}	β	ΔT_g
19	19.76	51.24	77.84	26.84	25.03	1.678	52.81
20	17.08	65.39	73.20	62.22	27.48	0.990	45.72
21	16.84	40.26	74.91	23.67	17.71	2.443	57.20
22	20.74	98.82	108.58	34.16	35.41	0.935	73.17
24	20.01	109.8	126.39	43.92	44.28	0.917	82.11

(b) 6 m.m Ballotini in 3" Column

				Measured	Calculated		
RUN	T_{si}	T_{so}	T_{gi}	T_{go}	T_{go}	β	ΔT_g
25	20.01	87.84	123.22	23.42	38.22	1.253	85.00
26	21.47	43.92	111.26	24.4	62.71	2.169	48.55
28	19.64	53.92	98.82	24.4	56.32	1.239	42.50
30	11.22	48.80	75.15	14.64	29.12	1.226	46.03
31	10.74	63.93	78.08	17.57	31.16	0.885	46.92
32	10.25	74.18	91.74	19.52	46.11	0.714	45.63
33	10.25	71.25	91.74	24.89	48.35	0.709	43.39
34	19.52	56.12	129.32	48.80	67.82	1.675	61.50

Missing page(s) from the bound copy

PAGE 126

(d) $\frac{1}{8}$" Ceramic Spheres in 4" Column

Measured | Calculated

RUN	T_{si}	T_{so}	T_{gi}	T_{go}	T_{go}	β	ΔT_{go}
36	20.01	93.14	104.92	48.32	53.11	0.699	51.81
38	20.25	68.32	105.90	32.2	45.01	1.271	60.89
40	23.42	95.65	109.80	51.00	62.21	0.658	47.59
42	19.03	87.35	96.38	45.38	61.81	0.505	34.57
44	19.52	89.30	93.21	48.80	59.23	0.488	33.98
45	19.03	83.45	87.60	50.02	60.46	0.421	27.14
47	18.54	87.84	90.28	56.32	59.61	0.442	30.67
56	20.50	81.25	83.20	51.24	57.55	0.422	25.70
58	20.74	82.47	85.16	48.80	60.01	0.407	25.15
60	20.50	69.54	72.71	49.04	54.78	0.366	17.93
61	21.47	87.84	91.50	55.29	68.72	0.343	22.78
64	20.50	67.34	98.33	30.50	49.93	1.033	48.40
67	20.74	79.54	89.79	43.92	55.22	0.588	34.57
68	20.98	94.18	109.31	45.14	59.82	0.676	49.49
70	20.98	56.12	113.22	27.82	57.50	1.585	55.72
74	19.76	31.72	84.42	21.96	58.19	2.193	26.23
75	14.40	58.56	81.98	30.50	41.24	0.926	40.78
77	21.96	53.68	86.86	33.18	48.55	1.208	38.31
81	19.03	40.50	89.30	31.72	57.48	1.482	31.82
87	12.44	51.73	77.59	28.21	44.47	0.847	33.12

(e) 12 m.m Ballotini in 4" Column

RUN	T_{si}	T_{so}	T_{gi}	T_{go} Measured	T_{go} Calculated	β	ΔT_g
46	19.03	85.89	87.60	60.15	66.89	0.310	20.71
51	21.96	87.84	99.06	57.97	68.47	0.464	30.59
54	21.47	83.94	88.08	55.63	60.44	0.442	27.64
55	20.49	84.67	86.62	65.64	67.90	0.292	18.72
57	20.74	81.50	84.18	61.63	64.89	0.318	19.29
59	20.49	70.76	72.59	56.53	59.09	0.269	12.50
62	20.49	90.28	98.33	39.53	53.88	0.637	44.45
63	20.50	78.08	98.33	43.92	53.33	0.781	45.00
65	20.50	84.42	89.30	49.78	60.59	0.449	28.71
73	19.76	41.48	84.92	23.42	49.20	1.645	35.72
76	13.42	65.88	81.98	39.04	55.71	0.671	26.27
78	21.96	60.76	88.57	41.48	56.62	0.827	31.95
79	18.54	80.28	82.00	62.70	63.28	0.303	18.72
80	19.52	66.86	80.32	47.63	51.49	0.603	28.83
82	20.50	43.68	82.47	44.24	50.57	1.376	31.90
83	20.74	72.96	82.47	50.65	56.68	0.494	25.79
84	20.25	65.88	81.98	45.38	53.57	0.623	28.41
85	20.01	65.88	81.50	41.48	51.18	0.662	30.32
86	14.14	65.39	81.0.	39.38	44.98	0.704	36.03
88	22.94	68.81	85.89	49.75	57.61	0.616	28.28
89	21.96	71.74	87.84	47.34	57.03	0.619	30.81
90	22.94	88.92	70.28	63.44	71.15	0.290	19.13
91	17.08	79.54	80.76	60.76	61.22	0.313	19.54
92	20.25	83.94	85.16	65.39	64.15	0.330	21.01

Appendix 4

(Referring to Sections F and G)

GRAPH 13.
PLOT OF MOVING BED HEAT TRANSFER RESULTS — HEAT TRANSFER COEFFICIENT AGAINST GAS FLOW RATE.

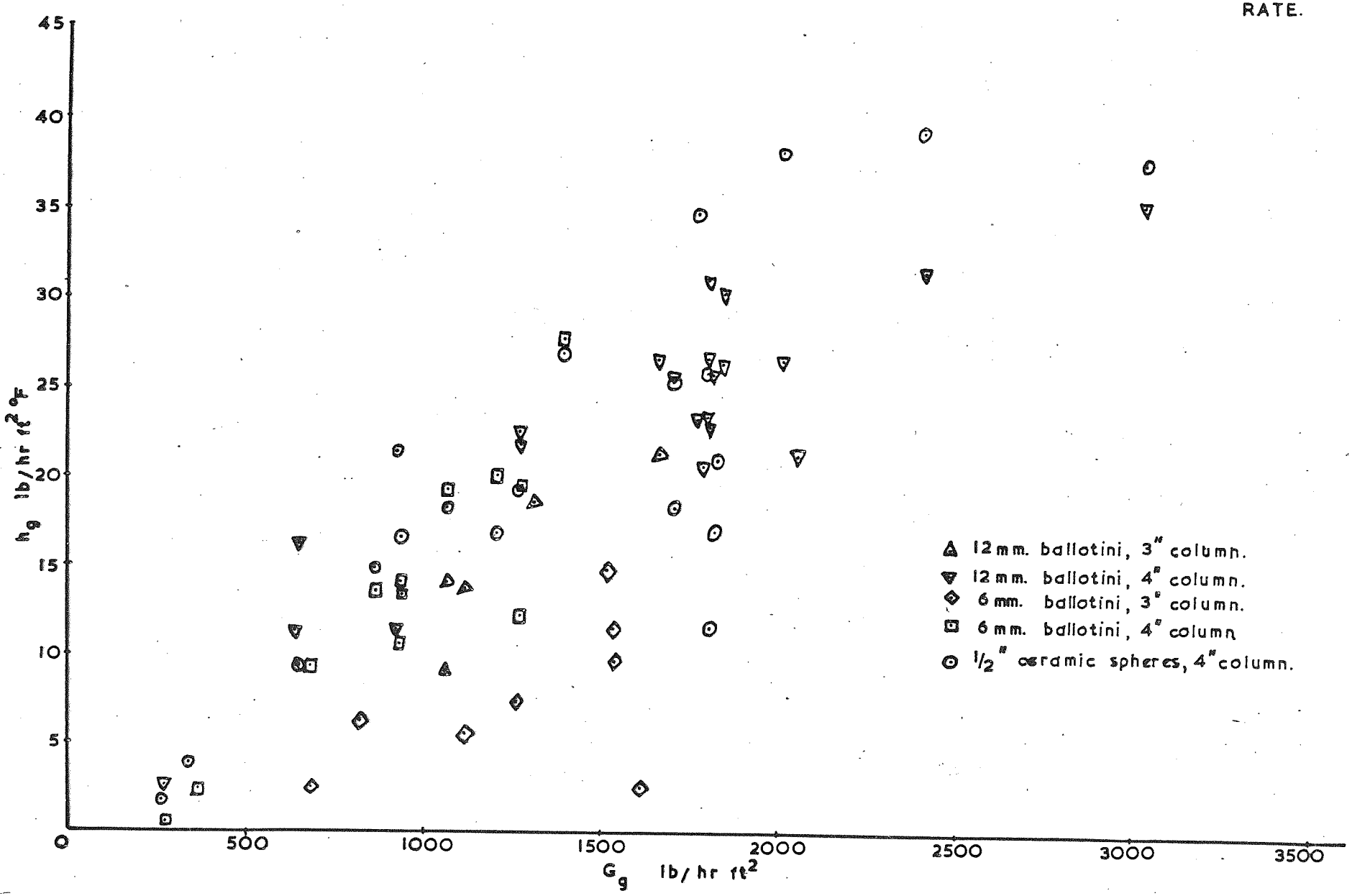

TABLE 14

HEAT TRANSFER COEFFICIENT RESULTS

(a) 12 m.m. Ballotini in 3" Column

RUN	G_g	G_s	Re′	h_g	Nu
19	1065.50	2297.66	1486.01	9.036	20.829
20	1102.85	1382.66	1544.64	13.778	31.928
21	1061.97	3389.16	1499.57	14.011	32.762
22	1650.74	1889.73	2205.34	21.245	46.400
24	1292.03	1431.08	1684.45	18.589	39.380

(b) 6 m.m Ballotini in 3" Column

RUN	G_g	G_s	Re′	h_g	Nu
25	1251.00	1939.49	824.78	7.286	8.380
26	1609.58	4516.51	1050.31	2.602	2.953
28	681.07	1084.07	451.50	2.518	2.919
30	815.17	1301.02	568.88	6.061	7.492
31	1518.91	1716.22	1053.75	14.720	18.068
32	1533.41	1388.04	1032.67	9.648	11.419
33	1533.41	1388.04	1030.47	11.478	13.550
34	1103.75	2380.65	706.37	5.566	6.168

(c) 6 mm. Ballotini in 4" Column

RUN	G_g	G_s	Ré	h_g	Nu
35	927.69	827.57	584.48	14.058	16.275
37	937.30	1408.09	595.49	13.362	15.672
39	1058.70	856.37	660.33	19.241	22.045
41	1193.42	736.63	750.30	20.004	23.176
43	1379.79	859.40	972.60	27.710	32.362
49	671.52	592.64	425.29	9.215	10.776
52	922.87	698.74	579.91	10.509	12.165
53	1260.63	941.25	804.96	11.571	13.685
66	1265.83	953.38	807.22	19.518	23.041
69	853.84	708.59	530.61	13.519	15.412
71	353.63	518.37	219.06	2.367	2.687
72	268.30	636.59	168.90	0.440	0.511

(d) $\frac{1}{2}$" Ceramic Spheres in 4" Column

RUN	G_g	G_s	Re'	h_g	Nu
36	927.69	809.38	1026.97	21.293	40.658
38	937.30	1508.12	1044.89	16.494	31.769
40	1058.70	865.46	1157.74	18.330	34.435
42	1193.42	756.33	1319.86	16.890	32.229
44	1379.79	839.70	1533.71	26.960	51.799
45	1696.17	897.29	1892.32	25.223	48.715
47	1753.62	971.56	1953.42	34.894	67.244
56	1994.86	1057.96	2240.58	38.106	74.257
58	2395.73	1224.69	2679.68	39.205	75.984
60	3081.50	1427.79	3505.37	37.508	74.309
61	3608.10	1547.53	3981.77	42.856	81.564
64	640.63	841.21	715.33	9.114	17.605
67	1260.63	932.16	1410.80	19.372	37.557
68	853.84	718.44	936.06	14.934	28.149
70	353.63	719.96	387.25	3.803	7.158
74	268.30	773.01	300.82	1.382	2.688
75	1787.64	2121.98	2044.46	25.746	51.288
77	1838.33	2849.52	2076.57	20.993	41.135
81	1796.63	3470.95	2007.11	11.688	22.609
87	1696.98	1855.22	1942.29	17.283	34.478

(e) 12 mm. Ballotini in 4" Column

RUN	G_g	G_s	Re'	h_g	Nu
46	1696.17	651.75	2132.02	25.549	55.203
51	922.87	528.98	1147.06	11.464	24.380
54	1260.63	691.16	1592.95	22.588	49.147
55	1994.86	721.47	2507.41	26.406	57.055
57	2398.73	945.70	3025.95	31.449	68.401
59	3115.03	1051.90	4000.10	35.100	78.026
62	650.00	502.45	806.08	16.085	34.820
63	640.00	624.47	806 70	11.143	24.146
65	1265.83	704.80	1595.56	21.883	47.532
73	268.30	574.45	343.96	2.680	5.941
76	1787.64	1527.83	2302.95	26.696	59.534
78	2046.36	2139.41	2494.63	21.158	46.235
79	1800.81	680.55	2282.49	25.759	56.290
80	1794.30	1367.16	2304.65	24.305	54.017
82	1802.17	3217.07	2312.38	16.896	37.496
83	1768.30	1095.09	2254.24	23.086	50.822
84	1837.46	1446.74	2350.83	22.194	49.080
85	1762.98	1473.26	2261.95	23.898	53.035
86	1642.78	1471.74	2122.37	26.622	59.577
88	1784.57	1381.56	2265.79	20.434	44.741
89	1791.24	1390.65	2271.42	22.805	49.844
90	1822.44	651.75	2276.96	26.278	56.307
91	1834.56	717.68	2332.38	30.164	66.182
92	1786.98	731.33	2256.50	31.732	68.990

Table 15

Void Fractions and Particle Diameters

COLUMN	PARTICLE TYPE	PARTICLE DIAMETER	VOIDAGE
3"	6 mm. ballotini	0.0204'	0.385
3"	12 mm. ballotini	0.0379'	0.426
4"	6 mm. ballotini	0.0204'	0.352
4"	12 mm. ballotini	0.0379'	0.396
4"	½" ceramic	0.0336'	0.393

GRAPH 14.
RATIO OF THE RELATIVE ERRORS IN THE HEAT TRANSFER COEFFICIENT TO THE SOLIDS OUTLET TEMPERATURE.

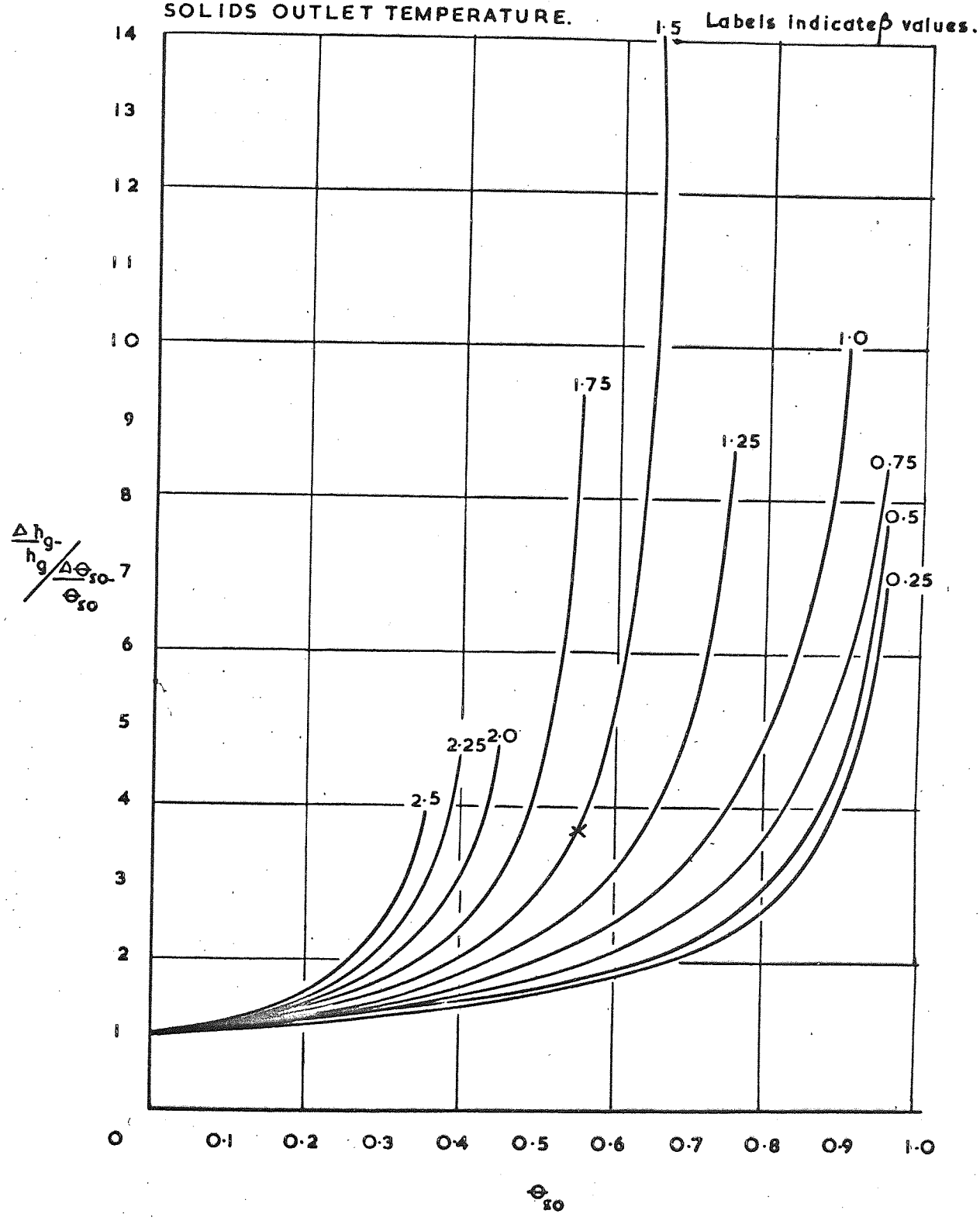

GRAPH 15. RATIO OF THE RELATIVE ERROR IN THE HEAT TRANSFER COEFFICIENT TO THE RELATIVE ERROR IN $G_s c_s$.
Labels indicate β values.

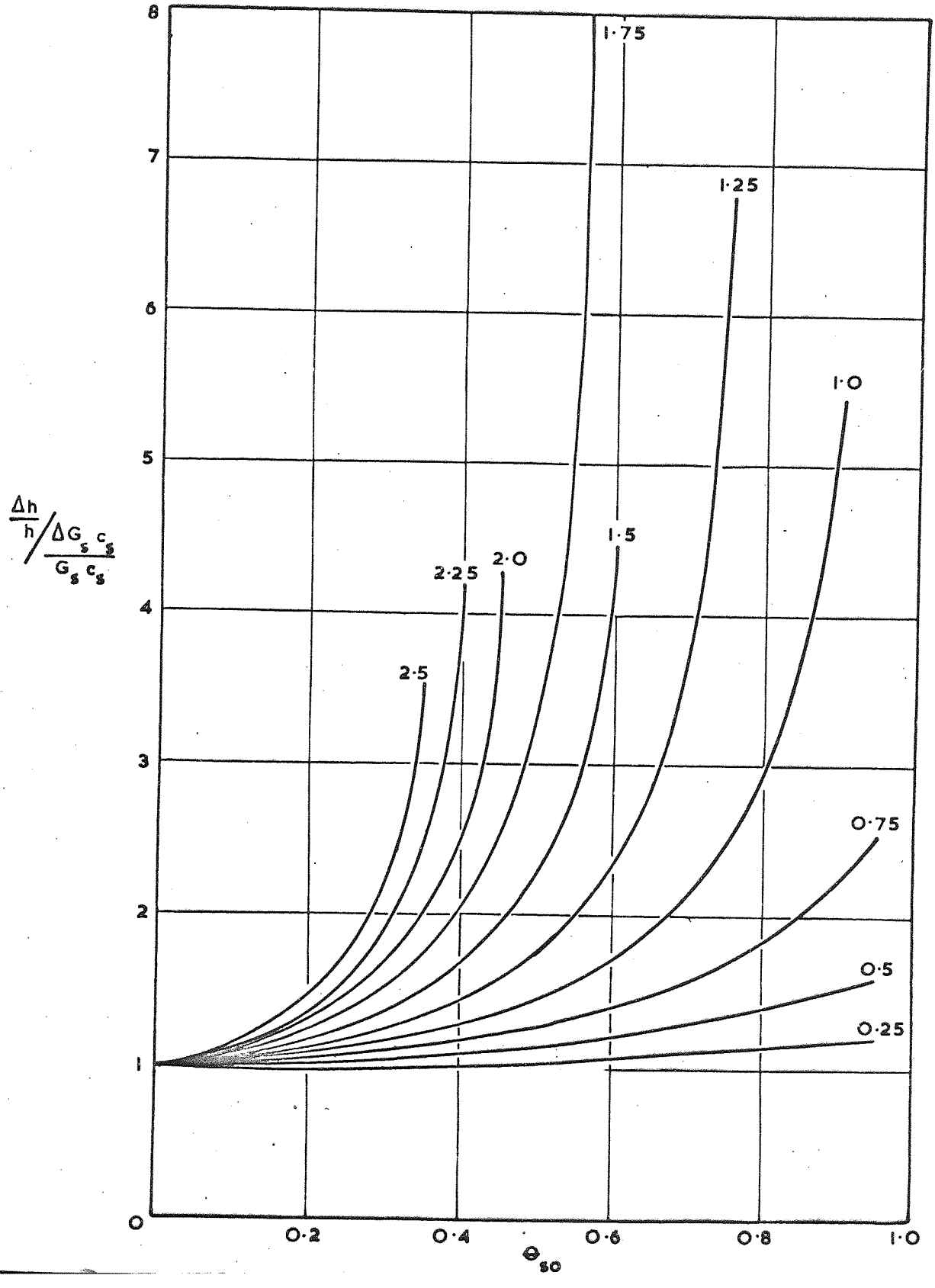

GRAPH 16. RATIO OF THE RELATIVE ERROR IN HEAT TRANSFER COEFFICIENT TO THE RELATIVE ERROR IN $G_g c_g$.
Labels indicate β values.

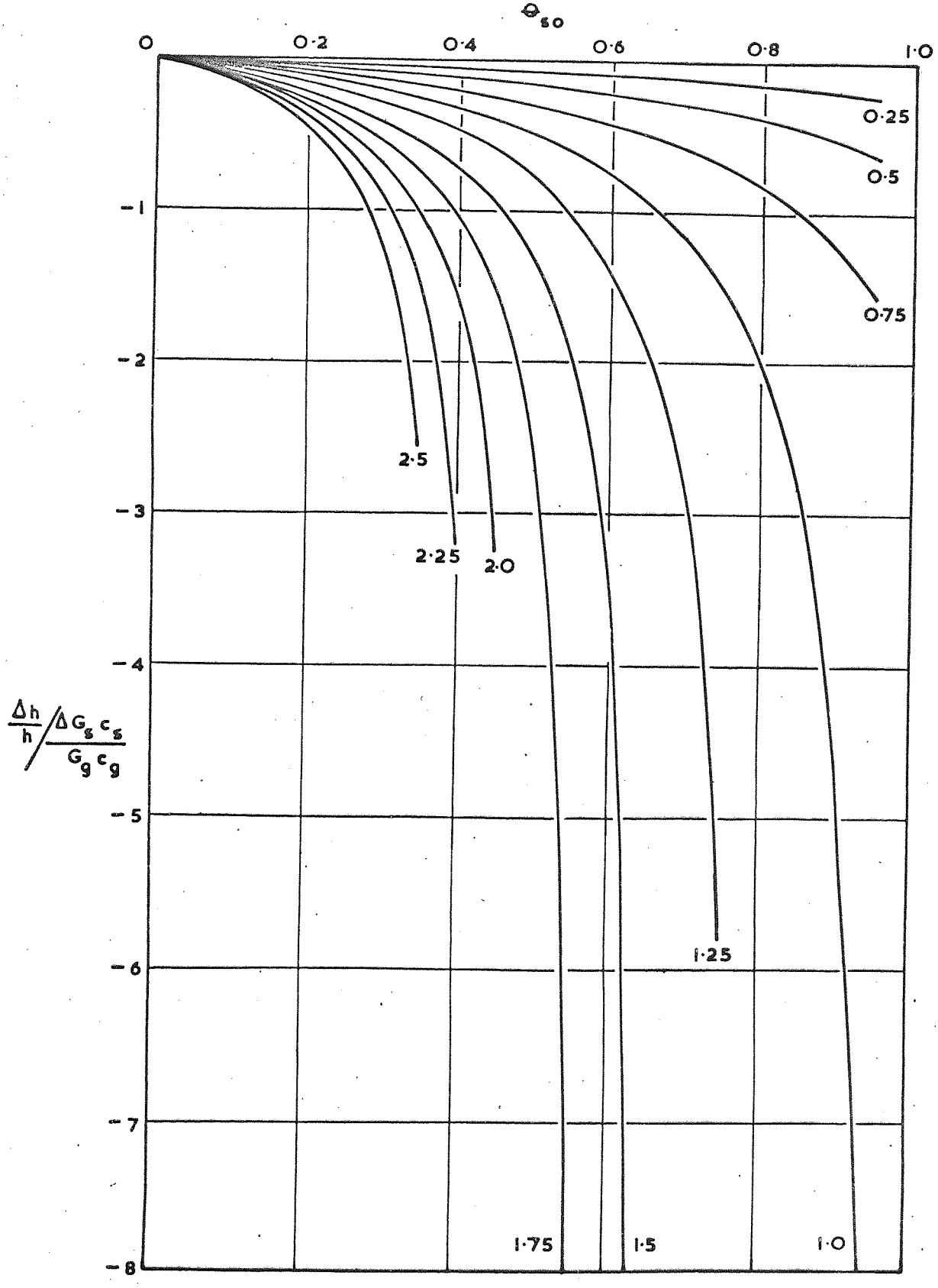

Table 16

Countercurrent Heat Exchange Error Calculation

(Columns A, B, . . . refer to Graphs 14 to 16)

	A	B	C
$\beta = 0.25$ θ_{so}	$\frac{\Delta h}{h} / \frac{\Delta\theta_{so}}{\theta_{so}}$	$\frac{\Delta h}{h} / \frac{\Delta G_B C_s}{G_s C_s}$	$\frac{\Delta h}{h} / \frac{\Delta G_B C_B}{G_B C_B}$
0	1.000	1.000	0
0.1	1.068	1.013	-0.013
0.2	1.148	1.027	-0.027
0.3	1.247	1.042	-0.042
0.4	1.379	1.059	-0.059
0.5	1.532	1.078	-0.078
0.6	1.756	1.099	-0.099
0.7	2.097	1.124	-0.124
0.8	2.705	1.153	-0.153
0.9	4.253	1.192	-0.192

	A	B	C
$\beta = 0.5$ θ_{so}	$\frac{\Delta h}{h} / \frac{\Delta\theta_{so}}{\theta_{so}}$	$\frac{\Delta h}{h} / \frac{\Delta G_s C_s}{G_s C_s}$	$\frac{\Delta h}{h} / \frac{\Delta G_B C_B}{G_B C_B}$
0	1.000	1.000	0
0.1	1.082	1.027	-0.027
0.2	1.179	1.057	-0.057
0.3	1.298	1.091	-0.091
0.4	1.448	1.131	-0.131
0.5	1.644	1.178	-0.178
0.6	1.915	1.234	-0.234
0.7	2.321	1.304	-0.304
0.8	3.034	1.393	-0.393
0.9	4.799	1.520	-0.520

	A	B	C
$\beta = 0.75$ θ_{so}	$\frac{\Delta h}{h} \Big/ \frac{\Delta \theta_{so}}{\theta_{so}}$	$\frac{\Delta h}{h} \Big/ \frac{\Delta G_s C_s}{G_s C_s}$	$\frac{\Delta h}{h} \Big/ \frac{\Delta G_g C_g}{G_g C_g}$
0	1.000	1.000	0
0.1	1.096	1.041	-0.041
0.2	1.213	1.089	-0.089
0.3	1.358	1.148	-0.148
0.4	1.545	1.220	-0.220
0.5	1.793	1.311	-0.311
0.6	2.141	1.431	-0.431
0.7	2.672	1.595	-0.595
0.8	3.60	1.836	-0.836
0.9	5.874	2.238	-1.238

	A	B	C
$\beta = 1$ θ_{so}	$\frac{\Delta h}{h} \Big/ \frac{\Delta \theta_{so}}{\theta_{so}}$	$\frac{\Delta h}{h} \Big/ \frac{\Delta G_s C_s}{G_s C_s}$	$\frac{\Delta h}{h} \Big/ \frac{\Delta G_g C_g}{G_g C_g}$
0	1.00	1.00	0
0.1	1.111	1.056	-0.056
02	1.250	1.125	-0.125
0.3	1.429	1.214	-0.214
0.4	1.667	1.333	-0.333
0.5	2.000	1.500	-0.500
0.6	2.500	1.750	-0.750
0.7	3.333	2.167	-1.167
0.8	5.000	3.000	-2.000
0.9	10.000	5.500	-4.500

$\beta = 1.25$ θ_{so}	A $\frac{\Delta h}{h} \Big/ \frac{\Delta\theta_{so}}{\theta_{so}}$	B $\frac{\Delta h}{h} \Big/ \frac{\Delta G_s C_s}{G_s C_s}$	C $\frac{\Delta h}{h} \Big/ \frac{\Delta G_g C_g}{G_g C_g}$
0	1.000	1.000	0
0.05	1.060	1.033	-0.033
0.15	1.203	1.115	-0.115
0.25	1.393	1.224	-0.224
0.35	1.655	1.380	-0.380
0.45	2.043	1.618	-0.618
0.55	2.681	2.033	-1.033
0.65	3.967	2.943	-1.943
0.75	8.656	6.820	-5.820

$\beta = 1.5$ θ_{so}	A $\frac{\Delta h}{h} \Big/ \frac{\Delta\theta_{so}}{\theta_{so}}$	B $\frac{\Delta h}{h} \Big/ \frac{\Delta G_s C_s}{G_s C_s}$	C $\frac{\Delta h}{h} \Big/ \frac{\Delta G_g C_g}{G_g C_g}$
0	1.000	1.000	0
0.05	1.067	1.040	-0.040
0.15	1.233	1.143	-0.143
0.25	1.463	1.291	-0.291
0.35	1.807	1.524	-0.524
0.45	2.393	1.948	-0.948
0.55	3.697	2.992	-1.992
0.65	14.074	12.778	-11.778

	A	B	C
$\beta = 1.75$ θ_{so}	$\frac{\Delta h}{h} \Big/ \frac{\Delta \theta_{so}}{\theta_{so}}$	$\frac{\Delta h}{h} \Big/ \frac{\Delta G_s C_s}{G_s C_s}$	$\frac{\Delta h}{h} \Big/ \frac{\Delta G_g C_g}{G_g C_g}$
0	1.000	1.000	0
0.05	1.0741	1.048	-0.048
0.15	1.264	1.174	-0.174
0.25	1.545	1.370	-0.370
0.35	2.015	1.722	-0.722
0.45	3.037	2.5644	-1.564
0.55	9.037	8.996	-7.996

	A	B	C
$\beta = 2.00$ θ_{so}	$\frac{\Delta h}{h} \Big/ \frac{\Delta \theta_{so}}{\theta_{so}}$	$\frac{\Delta h}{h} \Big/ \frac{\Delta G_s C_s}{G_s C_s}$	$\frac{\Delta h}{h} \Big/ \frac{\Delta G_g C_g}{G_g C_g}$
0	1.000	1.000	0
0.05	1.082	1.055	-0.055
0.10	1.179	1.123	-0.123
0.15	1.298	1.207	-0.207
0.20	1.448	1.317	-0.317
0.25	1.644	1.466	0.466
0.30	1.9.5	1.680	-0.680
0.35	2.321	2.018	-1.018
0.40	3.034	2.641	-1.641
0.45	4.800	4.279	-3.279

	A	B	C
$\beta = 2.25$ θ_{so}	$\frac{\Delta h}{h} \Big/ \frac{\Delta\theta_{so}}{\theta_{so}}$	$\frac{\Delta h}{h} \Big/ \frac{\Delta G_s c_s}{G_s c_s}$	$\frac{\Delta h}{h} \Big/ \frac{\Delta G_g c_g}{G_g c_g}$
0	1.000	1.000	0
0.05	1.089	1.063	-0.063
0.10	1.198	1.142	-0.142
0.15	1.336	1.244	-0.244
0.20	1.516	1.384	-0.384
0.25	1.767	1.585	-0.585
0.30	2.148	1.907	-0.907
0.35	2.83[illegible]	2.515	-1.515
0.40	4.651	4.223	-3.223

	A	B	C
$\beta = 2.5$ θ_{so}	$\frac{\Delta h}{h} \Big/ \frac{\Delta\theta_{so}}{\theta_{so}}$	$\frac{\Delta h}{h} \Big/ \frac{\Delta G_s c_s}{G_s c_s}$	$\frac{\Delta h}{h} \Big/ \frac{\Delta G_g c_g}{G_g c_g}$
0	1.000	1.000	0
0.05	1.097	1.070	-0.070
0.10	1.219	1.162	-0.162
0.15	1.377	1.285	-0.285
0.20	1.596	1.461	-0.461
0.25	1.924	1.738	-0.738
0.30	2.497	2.247	-1.247
0.35	3.919	3.579	-2.579

Table 17. Error Function of the Experimental Results

$$\frac{\Delta h}{h}\Big/\frac{\Delta\theta_{so}}{\theta_{so}} = E(\theta_{so}) \qquad \frac{\Delta h}{h}\Big/\frac{\Delta G_s c_s}{G_s c_s} = E(G_s c_s)$$

RUN	$E(\theta_{so})$	$d[E(\theta_{so})]/d\theta_{so}$	$E(G_s c_s)$	$d[E(G_s c_s)]/d\theta_{so}$	Selection
19	5.39	65.83	4.65	61.46	x
20	6.89	47.32	3.85	22.20	x
21	18.73	2201.07	17.22	2193.78	x
22	7.39	54.86	3.66	19.34	x
24	5.33	28.18	2.80	10.01	x
25	4.14	21.70	3.08	16.32	x
26	1.72	5.45	1.54	4.39	√
28	1.95	4.37	1.56	2.70	√
30	2.96	10.28	2.20	6.91	√
31	3.98	15.49	2.22	5.43	√
32	3.32	10.98	1.71	2.37	√
33	2.96	8.52	1.63	2.02	√
34	1.86	5.06	1.59	3.76	√
35	5.20	31.11	2.06	4.29	x
36	4.46	22.12	1.89	3.27	x
37	3.68	15.85	2.66	10.98	√
38	2.83	9.64	2.15	6.64	√
39	7.52	83.37	2.07	4.76	x
40	3.85	16.03	1.71	2.35	√
41	15.55	611.81	1.71	4.08	x
42	4.35	24.83	1.51	1.49	x
43	24.87	1887.66	1.77	5.93	x
44	7.33	95.65	1.58	2.13	x
45	6.46	73.75	1.44	1.46	x
46	11.62	345.25	1.32	1.356	x
47	9.80	206.50	1.53	2.20	x
49	4.81	26.15	1.98	3.76	x
51	3.67	16.58	1.40	1.09	√
52	4.86	29.66	1.74	2.55	x
53	4.07	19.31	1.63	1.9[illegible]	√

Table 17 continued

RUN	$E(\theta_{so})$	$d[E(\theta_{so})]/d(\theta_{so})$	$E(G_s c_s)$	$d[E(G_s c_s)]/d(\theta_{so})$	Selection
54	6.41	70.93	1.48	1.59	x
55	10.19	253.04	1.29	1.12	x
56	10.27	236.17	1.50	2.09	x
57	7.94	134.26	1.31	1.06	x
58	8.32	141.01	1.45	1.67	x
59	8.90	183.92	1.25	0.898	x
60	6.28	71.65	1.36	1.11	x
61	6.89	92.47	1.33	1.08	x
62	5.16	33.62	1.82	2.95	x
63	3.05	8.93	1.74	2.60	✓
64	2.58	6.76	1.81	3.55	✓
65	5.88	56.58	1.48	1.52	x
66	7.06	75.68	1.89	3.64	x
67	3.90	17.59	1.60	1.84	✓
68	3.73	15.17	1.74	2.45	✓
69	5.99	46.39	2.02	4.15	x
70	2.04	5.90	1.71	4.37	✓
71	2.24	5.52	1.71	3.30	✓
72	1.26	2.27	1.17	1.56	✓
73	1.82	4.77	1.56	3.50	✓
74	1.44	3.64	1.32	2.80	✓
75	2.70	7.04	1.78	3.06	✓
76	1.98	3.53	1.34	1.02	✓
77	2.19	5.41	1.69	3.35	✓
78	2.15	4.31	1.48	1.64	✓
79	10.89	295.77	1.31	1.25	x
80	3.01	9.24	1.51	1.46	✓
81	1.63	3.41	1.40	2.29	✓
82	1.82	4.06	1.51	2.67	✓
83	3.59	15.35	1.44	1.19	✓
84	2.72	7.23	1.48	1.38	✓
85	2.84	7.88	1.54	1.64	✓
86	3.11	9.50	1.65	2.10	✓

Table 17 concluded

RUN	$E(\theta_{so})$	$d[E(\theta_{so})]/d(\theta_{so})$	$E(G_s c_s)$	$d[E(G_s c_s)]/d(\theta_{so})$	Selection
87	2.27	4.84	1.54	1.88	✓
88	2.64	6.74	1.45	1.30	✓
89	2.84	8.00	1.50	1.44	✓
90	12.78	440.26	1.30	1.32	x
91	14.12	552.91	1.33	1.60	x
92	14.43	577.17	1.36	1.76	x

GRAPH 17 PLOT OF SELECTED MOVING BED HEAT TRANSFER RESULTS — HEAT TRANSFER COEFFICIENT AGAINST GAS FLOW RATE.

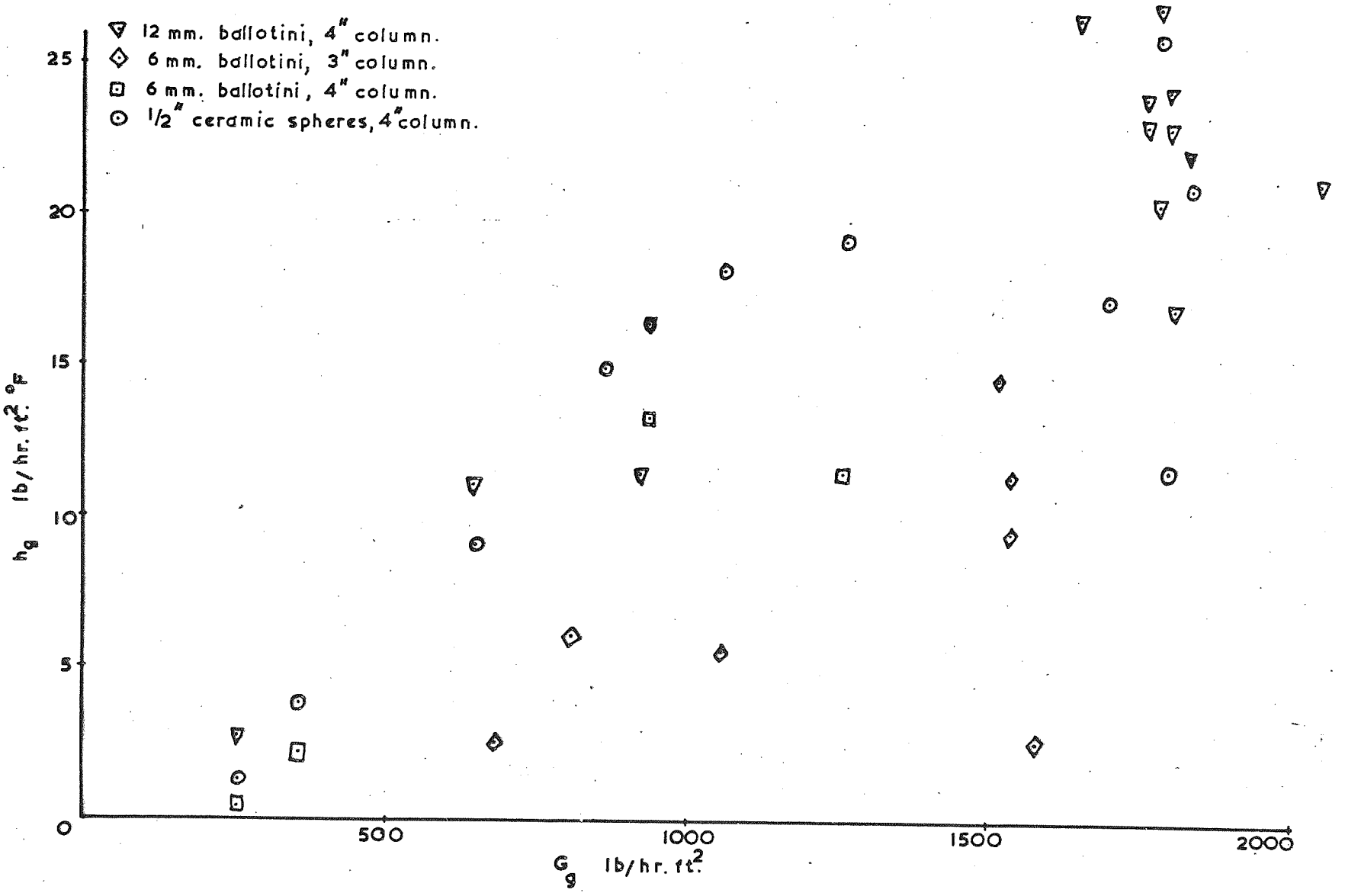

GRAPH 18. PLOT OF Nu CORRECTED AGAINST R_e' FOR SELECTED MOVING BED RESULTS.

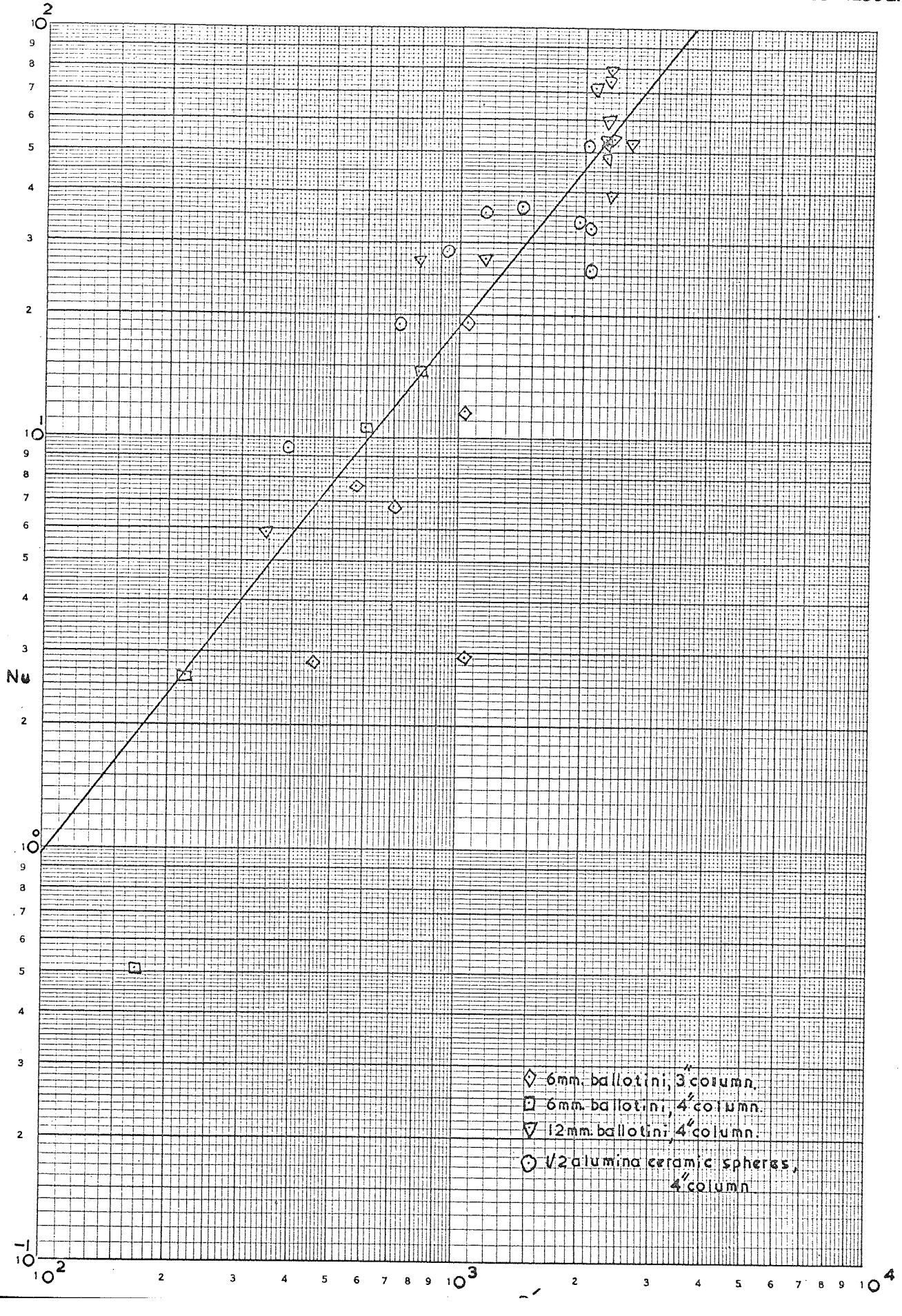

GRAPH 19. PLOT OF Nu (UNCORRECTED) AGAINST Re' FOR ALL MOVING BED RESULTS.

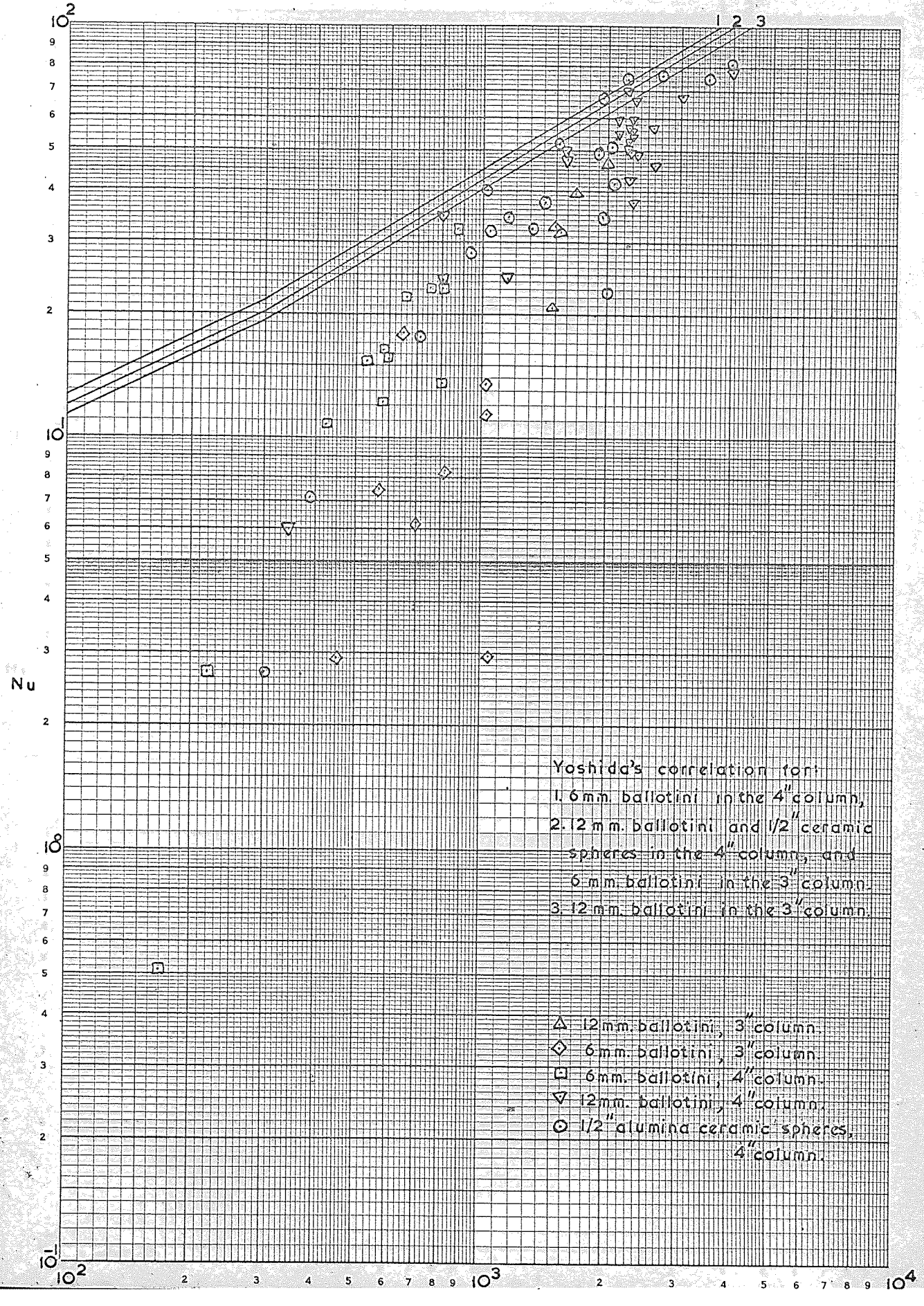

GRAPH 20. PLOT OF Nu AGAINST Re' FOR CORRECTED MOVING BED RESULTS.

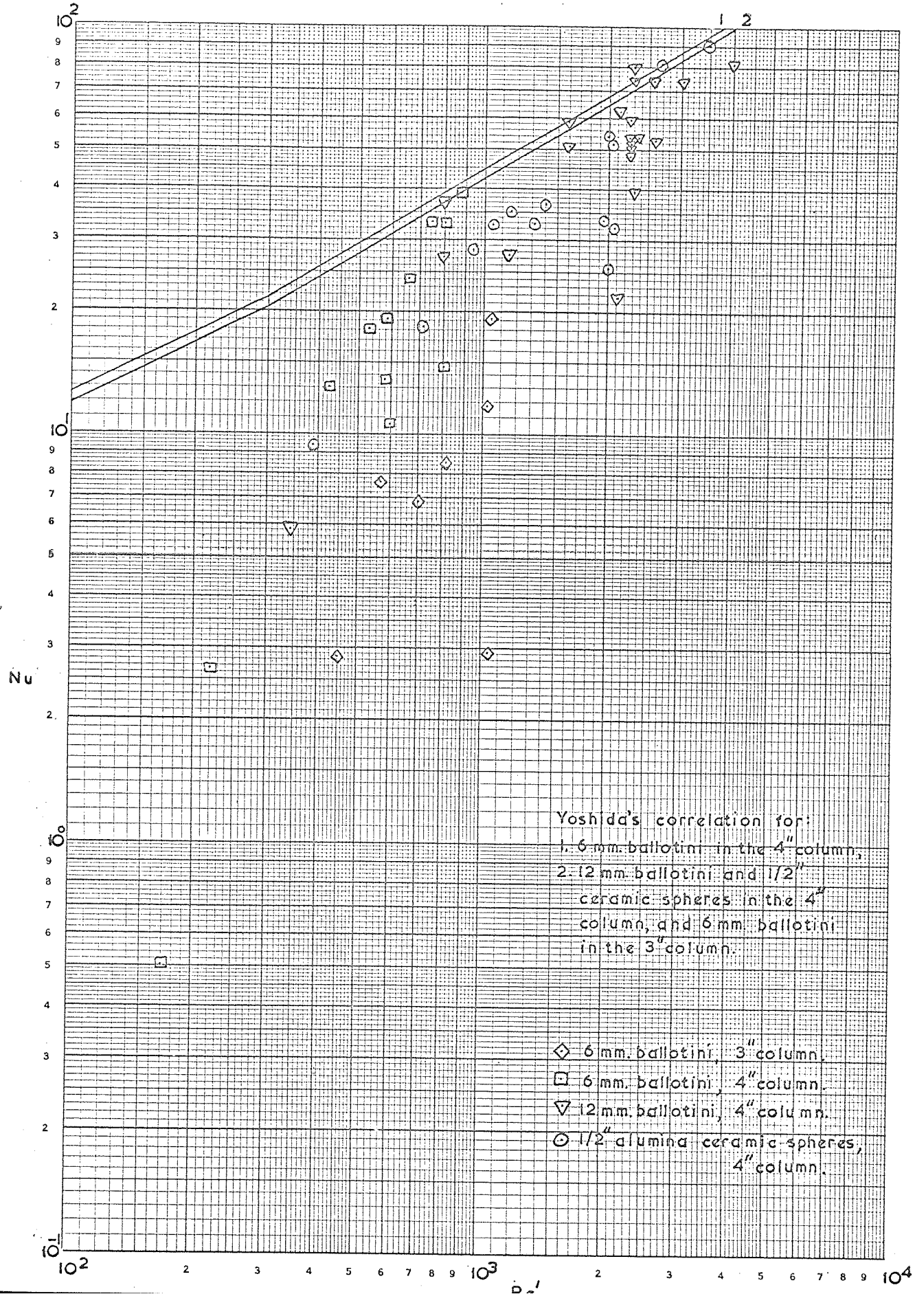

GRAPH 21. PLOT OF Nu (UNCORRECTED) AGAINST Re' FOR SELECTED MOVING BED RESULTS.

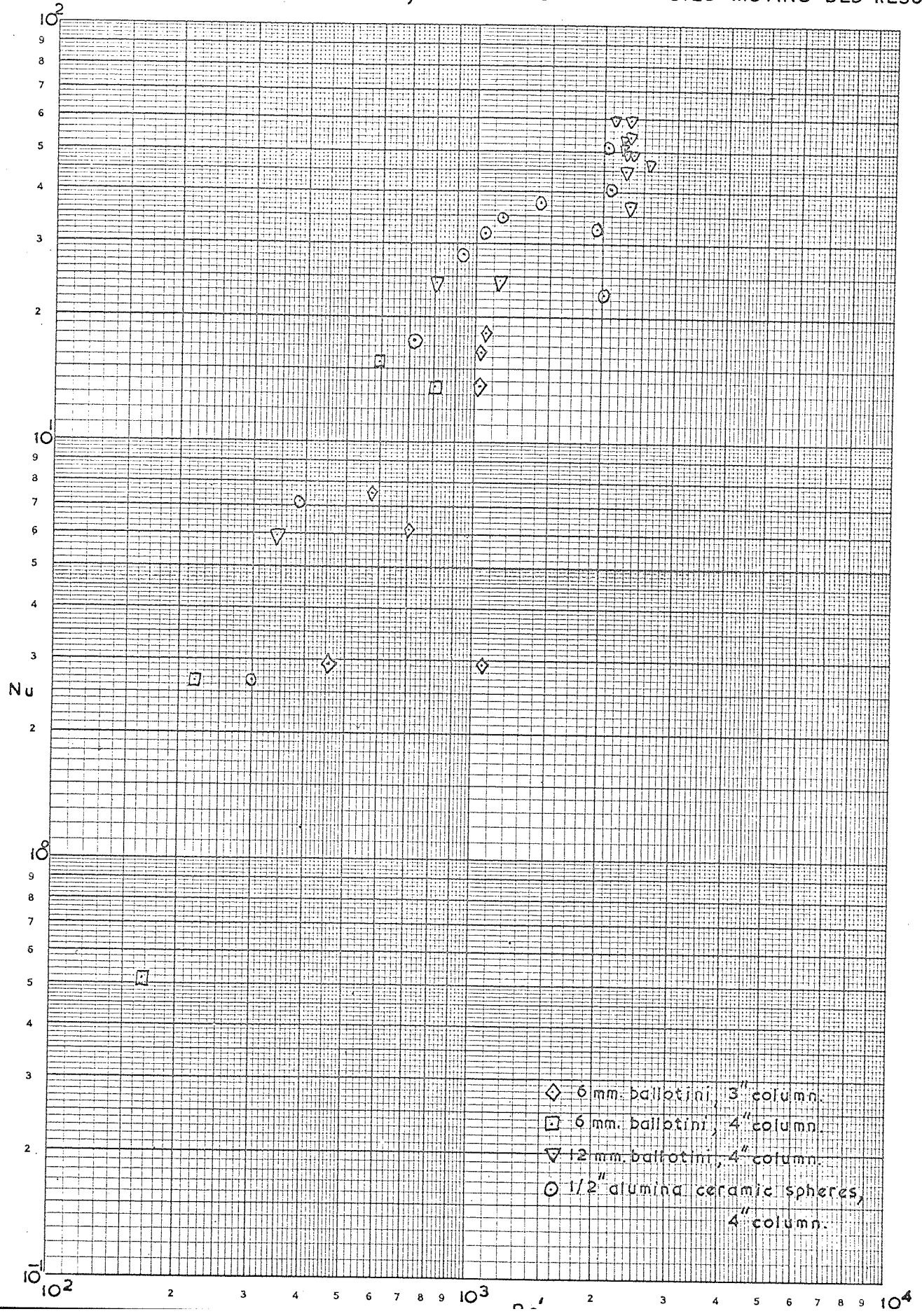

GRAPH 22. PLOT OF h_g (UNCORRECTED) AGAINST G_g/d_p FOR ALL MOVING BED RESULTS.

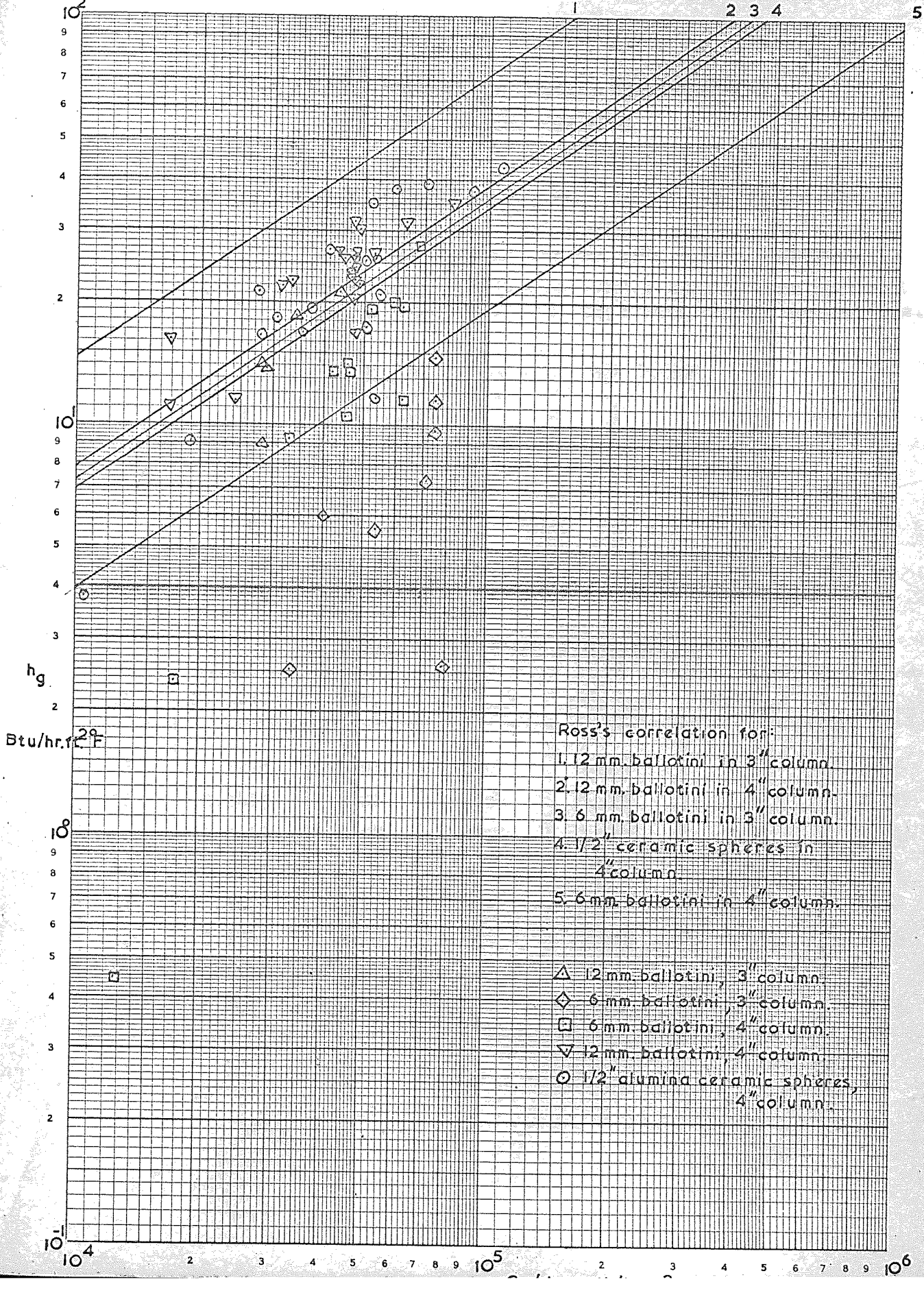

Table 18 Biot Numbers and Nusselt Numbers from Analogue Computer Analysis

$Bi(l.m.)$ = Biot number from log.mean temperature difference.

$Nu(\theta_{sm}), Bi(\theta_{sm})$ = Biot number and Nusselt number assuming the measured solids temperature was the mean solids temperature.

$Nu(\theta_{ss}), Bi(\theta_{ss})$ = Biot number and Nusselt number assuming the measured solids temperature was the solids surface temperature.

(A) 12 mm. Ballotini in 3 inch Column

RUN	Bi(l.m.)	Fo_1
19	0.299	2.66
20	0.452	4.39
21	0.469	1.81
22	0.683	3.16
24	0.313	2.50

(B) 6 mm. Ballotini in 3 inch Column

RUN	Bi(l.m.)	Fo_1	$Bi(\theta_{sm})$	$Bi(\theta_{ss})$	$Nu(\theta_{sm})$	$Nu(\theta_{ss})$
25	0.1276	6.91	0.129	0.114	8.55	7.56
26	0.0465	3.02	0.0460	0.044	2.92	2.79
28	0.0448	6.28	0.0439	0.0434	2.85	2.82
30	0.1091	5.27	0.1112	0.102	7.66	7.02
31	0.262	3.97	0.276	0.265	19.10	18.40
32	0.1761	4.88	0.181	0.173	11.70	11.20
33	0.2031	1.12	-	-	-	-
34	0.099	2.06	0.110	0.100	6.85	7.53

(C) 12 mm. Ballotini in 4 inch Column

RUN	Bi(l.m.)	Fo_l	$Bi(\theta_{sm})$	$Bi(\theta_{ss})$	$Nu(\theta_{sm})$	$Nu(\theta_{ss})$
46	0.828	1.94	0.846	-	62.1	-
51	0.371	2.39	0.416	0.391	27.41	25.75
54	0.7326	1.83	0.870	-	58.40	-
55	0.856	1.75	1.110	-	74.00	-
57	1.023	1.34	1.104	-	73.81	-
59	1.148	1.21	1.200	-	81.60	-
62	0.519	2.51	0.552	-	37.05	-
63	0.363	2.03	0.394	0.364	27.20	25.10
65	0.709	1.80	0.670	-	50.41	-
73	0.0895	2.25	0.0892	0.0860	5.921	5.71
76	0.830	0.838	1.042	0.883	74.70	6.33
78	0.696	0.598	0.793	0.637	52.71	42.40
79	0.838	1.871	0.793	-	50.62	-
80	0.797	0.934	1.170	0.900	79.50	61.11
82	0.563	0.401	0.602	0.446	39.10	29.00
83	0.754	1.16	0.796	0.706	53.69	47.60
84	0.728	0.882	0.796	0.692	53.70	46.70
85	0.784	0.866	0.882	0.754	59.71	51.00
86	0.828	0.870	0.996	0.828	71.61	59.60
88	0.668	0.922	0.718	0.622	48.12	41.70
89	0.745	0.915	0.773	0.769	51.58	51.30
90	0.848	1.941	-	-	-	-
91	0.983	1.771	-	-	-	-
92	1.029	1.731	-	-	-	-

(D) 6 mm. Ballotini in 4 inch Column

RUN	Bi(l.m.)	Fo_1	$Bi(\theta_{sm})$	$Bi(\theta_{ss})$	$Nu(\theta_{sm})$	$Nu(\theta_{ss})$
35	0.243	5.67	0.288	-	19.25	-
37	0.234	5.05	0.159	0.153	10.62	10.22
39	0.331	5.45	0.360	-	24.00	-
41	0.346	6.37	0.496	-	33.15	-
43	0.485	5.47	0.586	-	39.05	-
49	0.160	7.94	0.194	-	13.05	-
52	0.182	6.72	0.204	-	13.61	-
53	0.202	5.02	0.216	0.214	14.61	14.50
66	0.334	4.86	0.435	-	30.01	-
69	0.232	6.59	0.274	-	18.18	-
71	0.0416	9.15	0.0410	0.0408	2.67	2.66
72	0.008	7.60	0.0078	-	0.499	-

(E) $\frac{1}{2}$ inch Ceramic Spheres in 4 inch Column

RUN	Bi(l.m.)	Fo_1	$Bi(\theta_{sm})$	$Bi(\theta_{ss})$	$Nu(\theta_{sm})$	$Nu(\theta_{ss})$
36	0.0524	23.46	-	-	-	-
38	0.0399	13.06	0.0411	0.0401	32.60	31.80
40	0.0453	21.78	0.0463	0.0425	35.21	32.35
42	0.0414	25.38	0.0423	0.0412	32.89	31.30
44	0.0661	22.78	-	-	-	-
45	0.0616	21.51	0.0682	0.0636	54.01	50.40
47	0.0854	19.76	-	-	-	-
56	0.0930	18.26	-	-	-	-
58	0.0958	15.74	0.104	0.100	81.62	78.50
60	0.0909	13.77	0.101	-	80.89	-
61	0.1051	12.35	-	-	-	-
64	0.0220	23.45	0.0235	0.0210	18.43	16.48
67	0.0472	20.77	0.0462	0.0460	36.68	36.55
68	0.0368	26.38	0.0371	0.0365	28.30	27.85
70	0.00914	27.64	0.0121	0.0115	9.41	8.94
74	0.00327	27.00	-	-	-	-
75	0.0617	9.51	0.0621	0.0618	51.63	51.30
77	0.0538	7.05	0.0422	0.0420	32.22	32.05
81	0.0278	5.94	0.0312	0.0262	25.55	21.45
87	0.0412	11.03	0.0401	0.0389	33.60	32.70

Table 19

Theoretical Results for Moving Bed Heat Transfer

$$f(T) = \frac{T_{go} - T_{si}}{T_{gi} - T_{sm}}$$

T_{sm} = mean solids outlet temperature

Bi = 0.05 β = 0.5

f(T)	Fo_1(analogue)	Fo_1(l.m.)
1.026	0.356	0.342
1.056	0.744	0.727
1.126	1.592	1.582
1.220	2.640	2.651
1.347	3.936	3.972
1.520	5.550	5.582
1.804	7.724	7.867
2.270	10.744	10.930
3.333	15.660	16.052

Bi = 0.05 β = 1.0

Fo_1(analogue)	f(T)(analogue)	f(T)(l.m.)
0.364	1.001	1.0
0.764	1.001	1.0
1.704	1.003	1.0
2.916	1.004	1.0
4.532	1.005	1.0
6.812	1.006	1.0
10.268	1.008	1.0
16.564	1.091	1.0

Bi = 0.05 β = 1.5

f(T)	Fo_1(analogue)	Fo_1(l.m.)
0.984	0.244	0.208
0.965	0.492	0.481
0.925	1.092	1.041
0.879	1.820	1.734
0.822	2.732	2.615
0.755	3.912	3.742
0.675	5.532	5.250
0.573	7.872	7.437
0.432	11.700	11.191
0.265	19.824	17.697

Bi = 0.05 β = 2.0

f(T)	Fo_1(analogue)	Fo_1(l.m.)
0.947	0.364	0.360
0.890	0.808	0.778
0.824	1.320	1.287
0.753	1.960	1.893
0.670	2.764	2.668
0.576	3.824	3.674
0.466	5.272	5.093
0.338	7.536	7.224
0.183	11.864	11.304

Bi = 0.05 β = 2.5

f(T)	Fo_1(analogue)	Fo_1(l.m.)
0.938	0.296	0.287
0.871	0.642	0.616
0.799	1.040	0.947
0.716	1.524	1.485
0.627	2.128	2.078
0.528	2.910	2.841
0.418	3.956	3.873
0.296	5.542	5.406
0.158	8.484	8.195

Bi = 0.1 β = 0.5

f(T)	Fo_1(analogue)	Fo_1(l.m.)
1.057	0.376	0.370
1.129	0.816	0.809
1.345	1.980	1.981
1.777	3.848	3.832
3.175	7.664	7.701

Bi = 0.1 β = 1.0

Fo_1(analogue)	f(T)(analogue)	f(T)(l.m.)
0.184	1.000	1.0
0.384	1.001	1.0
0.860	1.003	1.0
1.476	1.004	1.0
2.296	1.010	1.0
3.452	1.016	1.0
5.202	1.028	1.0
8.176	1.053	1.0
14.584	1.200	1.0

Bi = 0.1 β = 1.5

f(T)	Fo_1(analogue)	Fo_1(l.m.)
0.982	0.124	0.118
0.965	0.256	0.240
0.923	0.554	0.536
0.876	0.920	0.882
0.820	1.376	1.326
0.753	1.972	1.891
0.671	2.776	2.659
0.568	3.944	3.769
0.445	6.108	5.392
0.259	9.736	9.004

Bi = 0.1 β = 2.0

f(T)	Fo_1(analogue)	Fo_1(l.m.)
0.974	0.0920	0.0866
0.947	0.188	0.180
0.890	0.408	0.389
0.824	0.669	0.643
0.753	0.992	0.946
0.669	1.388	1.338
0.575	1.916	1.846
0.467	2.660	2.541
0.340	3.790	3.600
0.187	5.932	5.590
0.0996	8.368	7.689

Bi = 0.1 β = 2.5

f(T)	Fo_1(analogue)	Fo_1(l.m.)
0.970	0.0720	0.0668
0.938	0.146	0.143
0.871	0.324	0.308
0.796	0.524	0.506
0.715	0.768	0.745
0.627	1.072	1.039
0.528	1.468	1.418
0.419	1.996	1.933
0.297	2.800	2.700
0.158	4.260	4.094
0.0822	5.828	5.551

GRAPH 23.

TEMPERATURE FUNCTIONS FOR MOVING BEDS. Biot No=0·05.

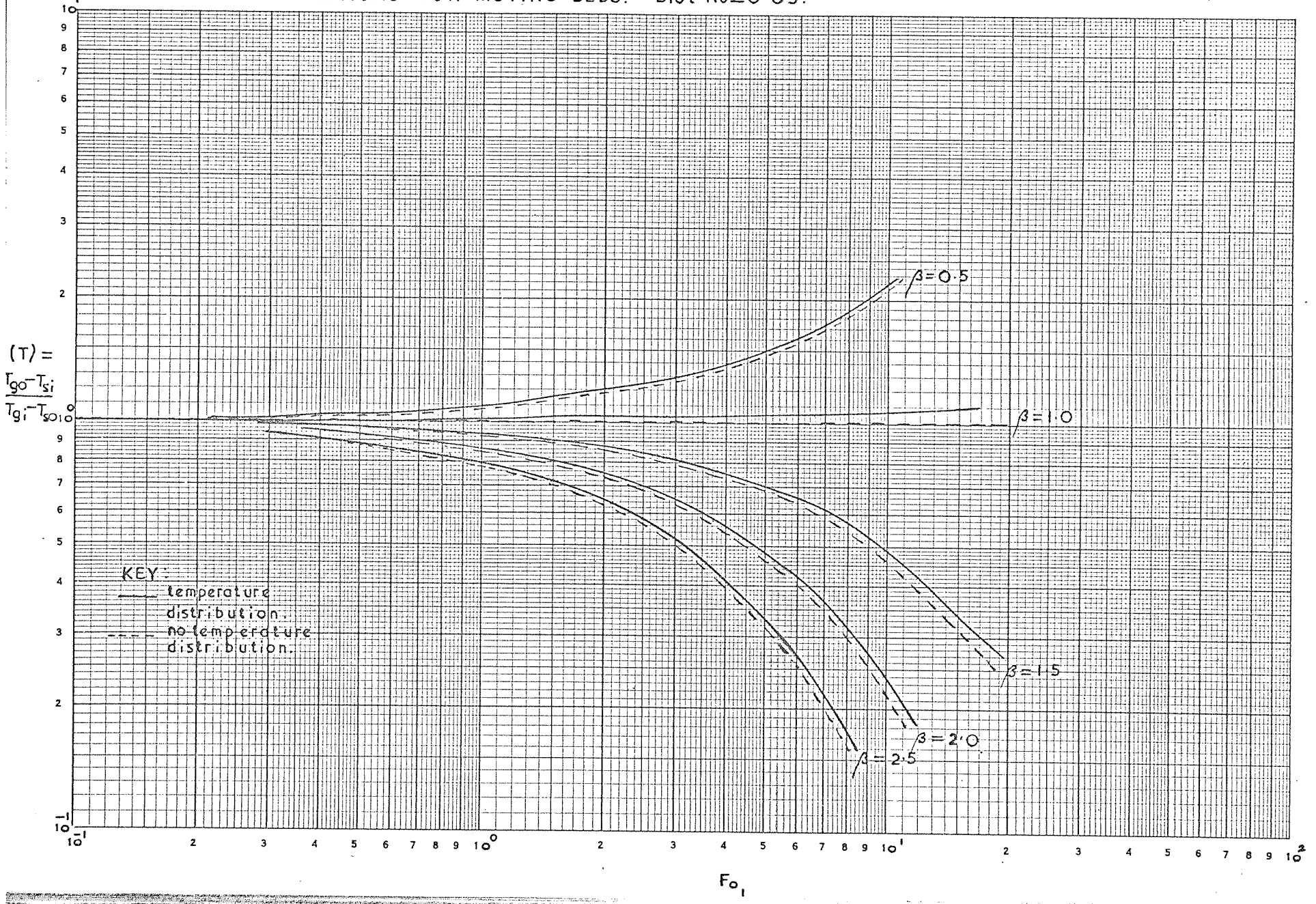

GRAPH 24.

TEMPERATURE FUNCTIONS FOR A MOVING BED. Biot No = 0·1.

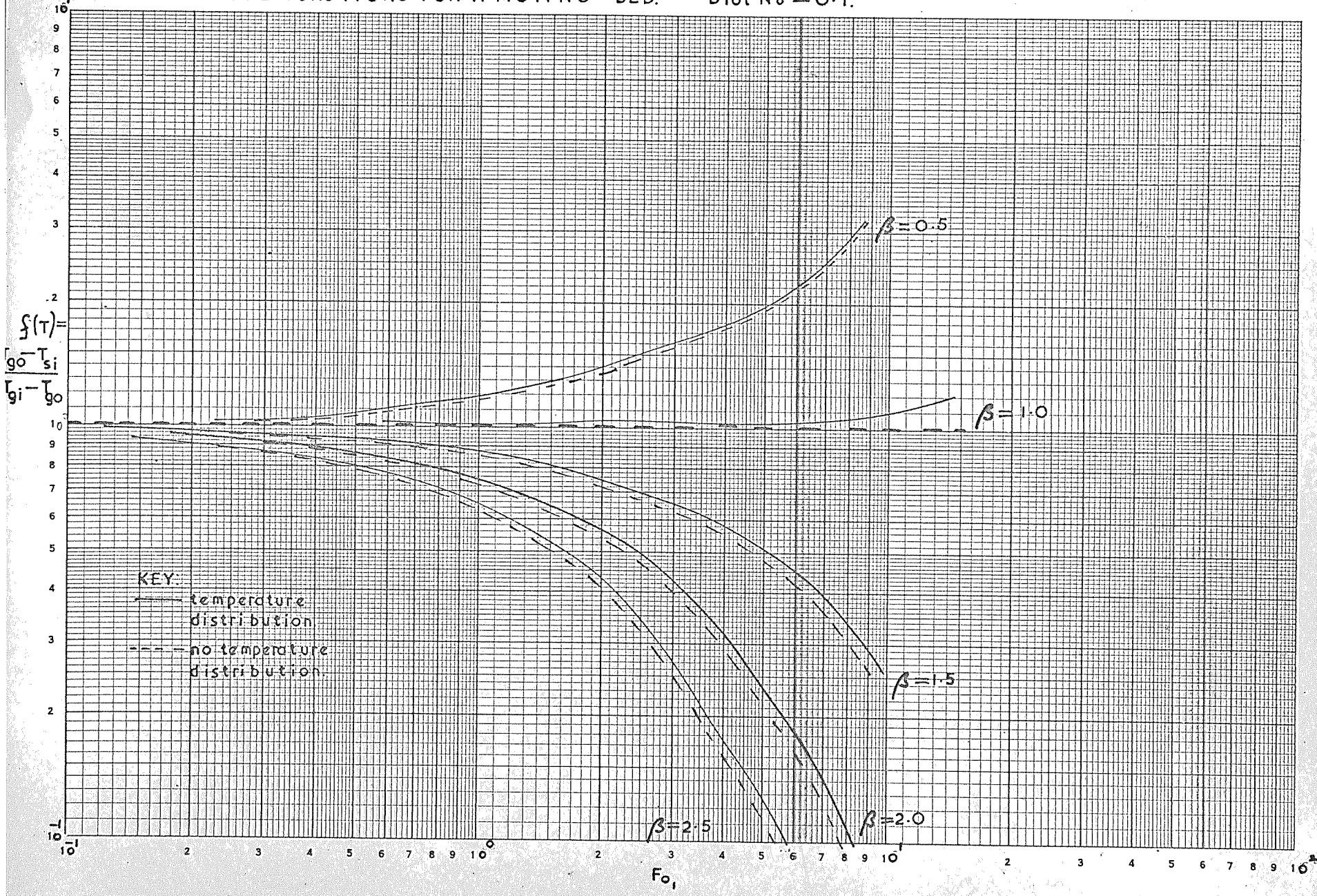

N O M E N C L A T U R E

Nomenclature

a	heat transfer area/unit volume of bed	ft^{-1}
a_n	eigenvalue	-
a_T	total heat transfer area	ft
A_s	specific surface of particles	ft^2/lb
A_x	cross sectional area	ft^2
bi	eigenvalue	-
Bi	Biot number $h_g d_p/k_s$	-
c_1, c_2	glass heat capacities at temperatures T_1 and T_2	Btu/lb°F
c_f	fluid heat capacity	"
c_L	liquid heat capacity	"
c_g	gas heat capacity at constant pressure	"
c_s	solids heat capacity	"
c_{sm}	mean glass heat capacity	"
$C_1 C_2$	constants in equations A4 and A5	-
d_c	heating coil diamter	ft
d_j	heating jacket diameter	"
d_o	outside diameter of a tube	"
d_p	equivalent spherical particle diameter	"
d_{pv}	$3\sqrt{\frac{6}{\pi}\frac{\text{volume of particles}}{\text{number of particles}}}$	"
d_v	diameter of vessel	"
e	void fraction	-
$E(G_s c_s)$	$\frac{\Delta h}{h} \Big/ \frac{\Delta G_s c_s}{G_s c_s}$	-

$E(\theta_{so})$	$\frac{\Delta h}{h} \Big/ \frac{\Delta\theta_{so}}{\theta_{so}}$	-
f	parameter for rotameter chart	-
Fc_l	Modified Fourier number $\frac{k_s(1-e)\,\ell}{G_s c_s R_o^2}$	-
F_T	fiducial flow	lit/min
g	acceleration due to gravity	ft/hr^2
G	flow rate	$lb/hr\ ft^2$
h	heat transfer coefficient	Btu/hr ft^2 °F
h_c	coil heat transfer coefficient	"
h_J	jacket heat transfer coefficient	"
h_L	heat transfer coefficient for solids melting in a liquid	
$h_g a$	gas film heat transfer coefficient/unit volume of bed	Btu/hr ft^3 °F
$h_m a$	melt film heat transfer coefficient/unit volume of bed	"
H	length of inclined plane	ft
j_h	$St\left(Ps^{2/3}\right)$	-
j_d	$Sh\ Sc^{2/3}$	-
J_1	Bessel function of the first order	-
k	thermal conductivity	Btu/hr ft °F
K_1, K_2	rotameter constants	-
ℓ	height from top of bed	ft
L	total bed height	ft
n	exponent and number of stages	-
N	stirrer speed	hr^{-1}
Pe	Peclet number RePr	-
Pr	Prandtl number $\mu c/k$	-

Pu	upstream pressure	cm Hg
Q	total heat flux	Btu/hr ^{o}F
Q	flow rate at operating conditions	lit/min
Q_F	flow rate at calibration conditions	"
r	radius of spherical shell	ft
r_v	column radius	ft
Re'	Reynolds number $G_g d_p/(1 - e)\mu_g$	-
Re_p	Reynolds number $G_g d_p/\mu_g$	-
Re_s	Reynolds number $V_s \rho_g d_p/\mu_g$	-
R_o	outside radius of sphere	ft
Sc	Schmidt number	-
Sh	Sherwood number	-
St	Stanton number $h_g/G_g c_g$	-
t	time	hr
T	temperature	h
T_m	melting point temperature	$^{o}C, ^{o}F$
T_m'	melt interface temperature	"
T_{sm}	mean solids outlet temperature	"
T_w	temperature of hot surface	"
$f(T)$	$\dfrac{T_{go} - T_{si}}{T_{gi} - T_{sm}}$	-

$(\Delta T_g')_{l.m.}$ log mean temperature difference between the gas, solid, and melt interface

$$\frac{(T_{gi} - T_m') - (T_{go} - T_{si})}{\ln\left[\dfrac{T_{gi} - T_m'}{T_{go} - T_{si}}\right]} \qquad ^{o}C, ^{o}F$$

$(\Delta T_{g,s})_{l.m.}$ log.mean temperature difference between the gas, solid, and melt

$$\frac{(T_{gi} - T_m) - (T_{go} - T_{si})}{\ln \frac{T_{gi} - T_m}{T_{go} - T_{si}}}$$ $^{o}C, ^{o}F$

ΔT_m	arithmetic average of inlet and outlet gas-solid temperature differences	$^{o}C, ^{o}F$
U	overall heat transfer coefficient	Btu/hr ft^2 ^{o}F
Ua	overall heat transfer coefficient per unit volume of bed	Btu/hr ft^3 ^{o}F
$(Ua)_{lim.}$	$0.8\ h_g a$	"
V	bulk volume of particles per stage	ft^3
V	velocity	ft/hr
V_g	superficial gas velocity	"
W	solids feed and melt rate	lb/hr
x	exponent	-
x	r/Ro^2	-
y	exponent	-
Y	$h_f a \ell / G_f c_f$	-
z	ℓ / L	-
Z	$h_f\ a\ t / c_s \rho_s (1 - e)$	-

α	thermal diffusivity, $k_s/\rho_s c_s$	ft/hr
β	$G_s c_s / G_g c_g$	-
γ	h_m/h_g	-
θ	dimensionless temperature $(T - T_{si})/(T_{gi} - T_{si})$	-
θ_i	imaginary dimensionless temperature	-
θ_m	dimensionless mean temperature	-
θ_n	dimesnionless increment temperature	-
λ	latent heat of fusion	Btu/lb
μ	viscosity	lb/hr ft
ν	kinematic viscosity, μ/ρ	ft/hr
ρ	density	lb/ft^3
σ	pressure gradient in molten film	lb/ft^3
σ	rotameter float density	gm/cc.
τ	Fourier number $\dfrac{k_s t}{c_s \rho_s Ro^2}$	-
ϕ	angle of inclined plane to vertical	-
ψ	shape factor	-
ω	rotameter float weight	gm

Subscripts

f	fluid
g	gas
i	inlet
L	liquid
m	melt, mean
n	increment number
o	outlet
p	particle
s	solid
v	vessel

B I B L I O G R A P H Y

Bibliography

* Actual references not consulted

1. Ross, T.K., International Developments in Heat Transfer, A.S.M.E.,(5),919,(1961)
2. Hixon, A.W., Baum, S.J., Ind.Eng.Chem.,33,1433,(1941)
3. Chilton, T.H., Drew, T.B., Jebens, R.H., Ind.Eng.Chem.,36,510,(1944)
4. Ross, T.K., Chem.Eng.Sci., 1,212,(1952)
5. Watson, D., Glen, C.G., Inst.Gas.Eng.J.,3,17,(1963)
6. Glen, C.G., Ibid.,4,27,(1964)
* 7. Nusselt, W., Z.Ver.Deut.Ing.,60,541,569,(1916)
8. Colburn, A.P., Hougen, O.A., Ind.Eng.Chem.,26,1178,(1934)
9. Skelland, A.H.P., Can.J.Chem.Eng.,44,64,(1966)
10. Palmer, A.G.C., "Some Aspects of Continuous Crystallisation,"Ph.D.Thesis, University of Birmingham, 1960.
11. Trollope, G.A.R., "Studies of an Oslo Cooling Crystalliser,"Ph.D.Thesis, University of Birmingham, 1962.
12. Knight, S.J., Manuel, K., Randle, R.G., "Non-Ferrous Metal Melting,"The Midland Junior Gas Association, 9/2/66
13. Glen, C.G., Personal Communication, 31/10/66, Royal School of Mines, Imperial College of Science and Technology, London.
14. Norton, C.L., J.Am.Ceram.Soc.,29,187,(1946)
15. Kilpatrick, M.O., Dean, L.E., Hall, D.S., Seed, K.W., Oil and Gas J.,53,(1),162,(1954)
16. Idem, Petroleum Refiner,33,171,(1954)
17. Idem, Petroleum Processing, 903,(1954)
18. Bowers, T.G., Reintjes, H., Chem.Eng.Prog.,Symp.Ser.,57,69,(1961)
19. Löf, G.O.G., Hawley, R.W., Ind.Eng.Chem.,40,1061,(1948)
20. Gamson, B.W., Thodos, G., Hougen, O.A. Trans.Am.Inst.Chem.Eng.,39,1,(1943)
21. Ramaswamy, S.R., Gerhard, E.R., Brit.Chem.Eng.,11,1210,(1966)
22. Smith, D.M., Eng.,138,479,606,(1934)
23. Johnstone, H.F., Pigford, R.L., Chapin, J.H., Trans.Am.Inst.Chem.Eng.,37,95,(1941)
* 24. Boussinesq, J., J.Math.Pures et Appl.,1,285,(1905)

* 25.	Frösling, N.,	Gerlands Beiträge zur Geophysik,52, 170,(1938) U.K.A.E.A.translation,MaP32740,1964)
26.	Adamski, T.,	Brit.Chem.Eng.,11,118,(1966)
27.	Gurney, H.P., Lurie, J.,	Ind.Eng.Chem.15,1170,(1923)
28.	Schumann, T.E.W.,	J. Franklin Institute,208, 405,(1929)
29.	Young, P.A.,	Symp.Chem.Eng.in Metallurgical Ind., Inst.Chem.Eng.,33,(1963)
30.	Furnas, C.C.	Trans.Am.Inst.Chem.Eng.,24,142,(1930)
31.	Idem,	Ibid,22, 721,(1930)
32.	Denton, W.H.,	Proc.Gen.Disc.Heat Transfer,Inst. Mech. Eng.,370,(1951)
33.	Denton, W.H., Robinson, C.H., Tibbs, R.S.	A.E.R.E.,R4346,(1963)
34.	Saunders, O.A., Ford, H.,	J.Iron and Steel Inst.,141,291P,(1940)
35.	Gamson, B.W.,	Chem.Eng.Prog.,47,19,(1951)
36.	Coppage, J.E., London, A.L.,	Chem.Eng.Prog.,52, (2),57,(1956)
37.	Bell, J.C., Katz, E.F.,	"A Method for Measuring Surface Heat Transfer using Cyclic-temperature Variations," Heat Transfer and Fluid-Mechanics Inst.,Berkley,California. A.S.M.E.,May 1949.
38.	Dayton R.W., Fawcett, S.L., Grimble, R.E., Sealander, C.E.,	"Improved Measurements of Surface Heat Transfer by the Method of Cyclic-temperature Variations," Battelle Memorial Inst.,Columbus,Ohio. B.M.I.-747,May 1952.
39.	Meek, R.M.G.,	Int.Developments in Heat Transfer, A.S.M.E. (5),770,(1961)
40.	Idem,	"Measurement of Heat Transfer Coefficients in Randomly packed Beds by the Cyclic Method," National Engineering Laboratory,Report No.54, 1962.
41.	Dingee, D.A., Chastain,J.W.	"A Study of Error Effects in Measuring Cyclic-temperature Heat Transfer Coefficients,"Battelle Memorial Institute,Columbus,Ohio.B.M.I.-1167
42.	Martin, J.J. McCabe, W.L., Monrad, C.C.,	Chem.Eng.Prog.,47,(2),91,(1951)

43.	Wadsworth, J.,	"Experimental Examination of Local Processes in Packed Beds of Homogeneous Spheres," N.R.C. Report MT-41,(Feb.1960)
44.	Idem,	"Int.Developments in Heat Transfer," A.S.M.E.Part 5,760,(1961)
45.	Rowe, P.N., Claxton, K.T.,	Trans.Inst.Chem.Eng.,43, T321,(1965)
46.	Cornish, A.R.H.,	Ibid.,43,T332,(1965)
47.	Wilke, C.R., Hougen, O.A.,	Trans.Am.Inst.Chem.Eng.,41,445, (1945)
48.	Bird, R.B., Stewart, W.E., Lightfoot, E.N.,	Transport Phenomena,1st.Ed., Hall,Wiley, New York,(1960)
49.	Munro, W.D., Amundson, N.R.,	Ind.Eng.Chem.,42,1481,(1950)
50.	Leung, P.K. Quon, D.,	Can.J.Chem.Eng.,43,45,(1965)
51.	Grober, H., Erk, S., Grigull, U.,	"Fundamentals of Heat Transfer," McGraw Hill, New York,(1961)
52.	Boelter, L.M.K., Cherry, V.H., Johnson, H.A., Martinelli, R.C.,	"Heat Transfer Notes," University of California Press, (1948)
53.	Fourier, J.,	"The Analytical Theory of Heat," Dover Publications Inc., New York, (1955)
54.	Mickley, H.S., Sherwood, T.K., Reed, C.E.,	"Applied Mathematics in Chemical Engineering," McGraw Hill,New York, (1957)
55.	Schneider, P.J.,	"Conduction Heat Transfer," Addison-Wesley Publishing Co.Inc.,Mass.(1955)
56.	Lovell, C.L., Karnofsky, G.,	Ind.Eng.Chem.,35,391,(1943)
57.	McAdams, W.H.,	"Heat Transmission,"3rd Ed., McGraw Hill, New York, (1954)
58.	Lapidus, L.,	"Digital Computation for Chemical Engineers," McGraw Hill, New York, (1962)
59.	Wiggins Electrical Resistance Materials, Henry Wiggins & Co.Ltd.,Wiggin Street, Birmingham,?	
60.	Reynolds, J.H.,	Personal Communication,4/10/64, Midlands Electricity Board Research Centre, Mucklow Hill,Halesowen.
61.	Personal Communication,	Berry's Furnaces, 1 Regina Drive, Birmingham, 22B.
62.	Sutherland, W.,	Phil.Mag.,36,507,(1893)
63.	Roeser, W.F., Dahl, A.I., Gowens, G.J.,	J.Research Nat.Bureau Standards,14,(3), 242,(1935)

64. Knacke, O., Pohl, H., Chem.Ing.Tech.,31,50,(1959)

65. Jaffe, J., Foss, N.E., J.Am.Pharm.Ass.Sci.Ed.,48,26,(1959)

66. Windheuser, J.J., Misra, J., Higuchi, T., J.Pharm.Sci.,52,767,(1963)

* 67. Yamamoto, P., Baba, M., Ann.Repts.Shionogi Res.Lab.,1,315, (1953)

68. Train, D., Trans.Inst.Chem.Eng.,35, 258,(1957)

69. Wilson, R., Proc.Royal Soc.,A212,450,(1952)

70. Brophy, J.E., Zisman, W.A., Ann.N.Y.Acad.Sci.,53,836,(1951)

71. Tabor, D.A., Proc.Royal Soc.,A212,498,(1952)

72. Strickland, W., Higuchi, T., Busse, L.W., J.Am.Pharm.Ass.,49,35,(1960)

73. Payne, J.F., Personal Communication,20/8/65, Boots Chemists, Beeston Works, Nottingham.

74. Hargrove, K.W., Personal Communication,20/8/65, Manesty Machines Ltd.,Speke, Liverpool,24.

75. Personal Communication, 20/8/65, Burroughs Wellcome and Co.Man Chem.,Wellcome Chemical Works, Dartford.

76. Siegel, S., Hanus, E.J., Carr, J.W., J.Pharm.Sci.,52,604,(1963)

77. Little, A., Mitchell, K.A., "Tablet Making", The Northern Publishing Co.Ltd.,Liverpool.(1949)

78. Kuong, J.F., Brit.Chem.Eng.,8,572,(1963)

79. Pilpel, N., Brit.Chem.Eng.,11,699,(1966)

80. Denton, W.H., "The Packing and Flow of Spheres," A.E.R.E.,E/R 1095,(1957)

81. International Critical Tables McGraw Hill,N.Y.,5,85,(1926)

82. Wilkes, G.B., J.Am.Ceram.Soc.,15,72,(1932)

83. Searle, A.B., Grimshaw, R.W., "The Chemistry and Physics of Clays," Ernest Benn Ltd., (1959)

84. Goldsmith, A., Waterman, T.E., Hirshhon, H.J., Handbook of Thermophysical Properties of Solid Materials, Macmillan,London, (1962).

85. Ginnings, D.C., Corruccini, R.J., — J.Res.Nat.Bur.Stand.,38, 593,(1947)

86. Powell, R.W., — Research,7,492,(1954)

87. Popper, P., — "Special Ceramics."Proceedings of a Symposium by the British Ceramics Research Association,Heywood and Co. Ltd., London,(1960)

88. Smoke, E.J., Koenig, J.H., — Engineering Res.Bulletin No.40, Rutgers State University,(1958)

89. Personal Communication,8/3/66,Physical Characteristics of High Alumina Regalox,Royal Worcester Industrial Ceramics Ltd.,Tonyrefail, Glamorgan.

90. Abbott, J.S., — Personal Communication,29/6/66, English Glass Co.Ltd.,Leicester.

91. Sharp, D.E., Ginther,L.B., — J.Am.Ceram.Soc.,34,260,(1951)

92. Ratcliffe, E.H., — Class Technology,4,113,(1963)

93. Personal Communication,22/8/66,Messrs. Dragon-Werke,Georg Wild, Bayreuth,Germany.

94. Bastick, R.E., — Personal Communication,9/8/66,Chance Bros.Ltd.,Glassworks,Smethwick,40, Birmingham.

95. Johnstone, H.F., Plaurtz, D.A., — A.I.Ch.E.J.,1,193,(1955)

96. Seidel, H.P., — Chem.Ing.Tech.,37,1125,(1965)

* 97. French patent, — 1,328,284,(1963)

* 98. Sakato, M., — Ozo Butsuri,25,305,(1956)

99. Huggins, M.L., Sun, K.H., — J.Am.Ceram.Soc.,26,4,(1943)

100. Keenan, J.H., Kaye, J., — Gas Tables,Wiley and Sons Inc.,N.Y., (1945)

101. Schwartz, C.E., Smith, J.M., — Ind.Eng.Chem.,45,1209,(1953)

102. Knudsen, J.G., Katz, D.L., — Fluid Dynamics and Heat Transfer, McGraw Hill,N.Y.,(1958)

103. Happel, J., — Ind.Eng.Chem.,41,1161,(1949)

104. Rowe, P.N., — Trans.Inst.Chem.Eng.,41,C.E.69.,(1963).

105. Bishoff, K.B., Levenspiel, O. — Chem.Eng.Sci.,17,245,(1962)